Forschungszentrum Karlsruhe
in der Helmholtz-Gemeinschaft

Wissenschaftliche Berichte
FZKA 7207

Magnetostriction and Thermal Expansion of the High-Temperature Superconductor $YBa_2Cu_3O_7$

P. Popovych

Institut für Festkörperphysik

Mai 2006

Forschungszentrum Karlsruhe
in der Helmholtz-Gemeinschaft

Wissenschaftliche Berichte
FZKA 7207

Magnetostriction and thermal expansion of the high-temperature superconductor $YBa_2Cu_3O_7$

Pavlo Popovych

Institut für Festkörperphysik

von der Fakultät für Physik
der Universität Karlsruhe (TH) genehmigte Dissertation

Forschungszentrum Karlsruhe GmbH, Karlsruhe
2006

Forschungszentrum Karlsruhe GmbH
Postfach 3640, 76021 Karlsruhe

Mitglied der Hermann von Helmholtz-Gemeinschaft
Deutscher Forschungszentren (HGF)

ISSN 0947-8620

urn:nbn:de:0005-072072

Magnetostriktion und thermische Ausdehnung des Hochtemperatur-Supraleiters $YBa_2Cu_3O_7$

Zur Erlangung des akademischen Grades eines
DOKTORS DER NATURWISSENSCHAFTEN
von der Fakultät für Physik
der Universität Karlsruhe (TH)

genehmigte

DISSERTATION

von

Pavlo Popovych, Dipl.-Ing.-Phys.(Ukraine)
aus Uzhgorod (Ukraine)

Tag der mündlichen Prüfung: 03.02.2006
Referent: Prof. Dr. Hilbert von Löhneysen
Korreferent: Prof. Dr. Elmar Dormann

Magnetostriction and thermal expansion of the high-temperature superconductor $YBa_2Cu_3O_7$

Abstract

In this work the anisotropic magnetostriction and thermal expansion of fully oxygenated untwinned $YBa_2Cu_3O_7$ single crystals have been studied for magnetic fields $H||c$ up to 10 T along all three crystallographic directions. Due to the high crystal quality, the measurements are reversible over a large part of the $H-T$ region studied, making a thermodynamical analysis of the data possible. By carefully measuring the thermal expansion in a restricted temperature interval, it was also possible to obtain a thermodynamic signal in the irreversible low temperature region. The magnetostriction of a classical superconductor is related to the pressure dependencies of T_c, H_{c0}, and of the Sommerfeld constant, and an analysis of the reversible magnetostriction using a classical model without thermal fluctuations was made in order to obtain these pressure dependencies for $YBa_2Cu_3O_7$. It was found that this thermodynamical model describes the magnetostriction data very well up to the vortex melting transition, which marks the onset of strong fluctuations, and that the uniaxial normalized pressure dependence of T_c is much larger than the normalized pressure dependencies of H_{c0}. In conventional superconductors, these values are closely related. By carefully measuring the thermal expansion in a restricted temperature interval, it was also possible to obtain the thermodynamic signal in the irreversible low temperature region. An alternative method to describe the magnetostriction based on 3D XY scaling was also investigated.

Magnetostriktion und thermische Ausdehnung des Hochtemperatur-Supraleiters $YBa_2Cu_3O_7$

Kurzfassung

Im Rahmen dieser Arbeit wurde die Thermodynamik entzwillingter $YBa_2Cu_3O_7$ - Einkristalle im Magnetfeld ($H||c$) bis 10 T mittels Messungen der anisotropen Magnetostriktion und thermischen Ausdehnung entlang allen drei krystallographischen Richtungen untersucht. Die sehr hohe Probenqualität ermöglichte die Bestimmung des reversiblen thermodynamischen Signals über einen weiten Temperatur- und Magnetfeldbereich. Thermodynamische Beziehungen zeigen, dass die Magnetostriktion mittels einer Summe von gewissen Druckabhängigkeiten (der kritischen Temperatur, des kritischen Felds, der Sommerfeld Konstante usw.) beschrieben werden kann. Eine Analyse der reversiblen Magnetostriktion wurde mit Hilfe von einem klassischen Model ohne Fluktuationen gemacht, um diese Druckabhängigkeiten herauszufinden. Die Messungen der thermischen Ausdehnung im magnetischen Feld stellen eine zusätzliche Methode zur Messung der Magnetostriktion dar, die es ermöglicht, das thermodynamische Signal auch im irreversiblen Zustand zu erhalten. Bis zu dem Feld des Vortexschmelzüberganges, der durch starke Fluktuationen gekennzeichnet ist, entsprechen die aus diesem Modell berechneten Kurven unseren Messergebnissen für alle drei Kristallrichtungen in dem gesamten gemessenen Temperaturbereich. Die normierten uniaxialen Druckabhängigkeiten von T_c sind mehrmals größer als die H_{c0}. Dies ist überraschend, weil bei den klassischen Supraleitern diese Werte stark korreliert sind. Als Alternative zu dem thermodynamischen Modell im Rahmen einer Ginzburg-Landau-Theorie wurde daher auch eine 3D-XY-Skalierung getestet.

Contents

Deutsche Zusammenfassung

In der vorliegenden Arbeit wurde die Thermodynamik entzwillingter $YBa_2Cu_3O_7$-Einkristalle im Magnetfeld ($H||c$) bis $\mu_0 H$=10 T mittels Messung der anisotropen Magnetostriktion und der linearen thermischen Ausdehnung in allen drei krystallographischen Richtungen untersucht. Die sehr hohe Probenqualität ermöglichte die Bestimmung des reversiblen thermodynamischen Signals über einen weiten Temperatur- und Magnetfeldbereich. Die vorliegende Arbeit stellt die erste systematische Untersuchung der thermodynamischen Magnetostriktion in $YBa_2Cu_3O_7$-Einkristallen dar.

Thermodynamische Methoden (Wärmekapazität usw.) wurden seit der Entdeckung der Supraleiter zur Untersuchung von deren grundlegenden Eigenschaften benutzt. Da die Thermodynamik klassischer Supraleiter gut verstanden ist, sind solche Experimente auch für Hochtemperatursupraleiter (HTSL) von großem Interesse.

Thermodynamische Beziehungen zeigen, dass die Magnetostriktion mittels einer Summe von gewissen Druckabhängigkeiten (der kritischen Temperatur T_c, des kritischen Felds H_c usw.) beschrieben werden kann. Die uniaxialen Druckabhängigkeiten der kritischen Temperatur sind für das $YBa_2Cu_3O_7$-System gut untersucht. Ein einfaches Modell auf der Basis druckinduzierter Ladungsumverteilung kann diese Abhängigkeiten nicht erklären. Die Untersuchung der Druckabhängigkeiten weiterer Parameter ist daher von großem Interesse, aber es ist schwierig diese direkt zu messen.

Da zuverlässige Magnetostriktionsdaten für diese Arbeit nötig waren und die gemessenen Längenänderungen nur ein paar Angstrom groß sein können, waren Verbesserungen der Messapparatur und der Datenanalyse erforderlich. Es wurde gezeigt, dass die Messungen der thermischen Ausdehnung im magnetischen Feld eine zusätzliche Methode zur Messung der Magnetostriktion darstellt, die es ermöglicht, das thermodynamische Signal im irreversiblen Zustand zu erhalten. Weiterhin wurden Wärmekapazitäts- , Magnetisierungs- und magnetokalorische[1] Messungen durchgeführt. Die uniaxialen Druckabhängigkeiten der Schmelzübergangstemperatur wurden nach der Clausius-Clapeyron-Beziehung aus den magnetokalorischen und magnetostriktiven Daten berechnet, in Übereinstimmung mit den schon veröffentlichten Daten.

Die uniaxialen Druckabhängigkeiten der kritischen Temperatur dT_c/dp_i wur-

[1] Diese Messungen wurden in der Universität Genf gemacht

den nach der Ehrenfest-Beziehung berechnet. Sie spielen bei der Magnetostriktion die wichtigste Rolle, andere Druckabhängigkeiten sind von geringerer Bedeutung. Eine Druckabhängigkeit des Ginzburg-Landau-Parameters κ wurde aufgrund einfacher Modellannahmen ausgeschlossen. Bis zu dem Feld des Vortexschmelzüberganges, der durch starke Fluktuationen gekennzeichnet ist, entsprechen die aus diesem Modell berechneten Kurven unseren Messergebnissen für alle drei Kristallrichtungen in dem gesamten Temperaturbereich.

Die dT_c/dp_i sind für die b-Achse positiv, für $a-$ und $c-$ Achsen negativ. Die uniaxialen Druckabhängigkeiten des thermodynamischen Felds dH_{c0}/dp_i, die einer direkten Messung noch immer nicht zugänglich sind, konnten aus den Ergebnissen unserer Messungen abgeleitet werden. Die dH_{c0}/dp_i sind positiv sowohl für die $a-$ als auch für die $b-$ Achse, im Widerspruch zu dem Verhalten von klassischen Supraleitern, bei denen die dT_c/dp_i und dH_{c0}/dp_i das gleiche Vorzeichen haben. $1/T_c \cdot dT_c/dp_i$ ist jeweils um ein Vielfaches größer als $1/H_{c0} \cdot dH_{c0}/dp_i$. Dies ist überraschend, weil bei den klassischen Supraleitern diese Werte stark gekoppelt sind. Dieses Resultat führt auch zu zwei anderen stark vom Fall für klassische Supraleiter abweichenden Extrapolationen. Zum Einen sind die abgeleiteten uniaxialen Druckabhängigkeiten des Sommerfeld-Koeffizients $d\gamma/dp_i$ um ein Vielfaches größer und haben ein anderes Vorzeichen als es bei den thermischen Ausdehnungsdaten bis zu 500 K zu erwarten wäre. Zum Anderen ergibt die Subtraktion der extrapolierten Magnetostriktion zwischen normalleitendem und supraleitendem Zustand von den Null-Feld-Daten der thermischen Ausdehnung nicht den erwarteten glatten Normalzustandsuntergrund. Dies könnte ein Hinweis darauf sein, dass die Magnetostriktion von $YBa_2Cu_3O_7$ sich nicht völlig durch das auf der Thermodynamik klassischer Supraleiter basierende Modell beschreiben lässt.

Als Alternative zu dem thermodynamischen Modell im Rahmen einer Ginzburg-Landau-Theorie wurde daher eine 3D-XY-Skalierung getestet. Die Idee hier war hierbei, das Skalierungsgebiet zu höheren Feldern jenseits des Vortexschmelzübergangs und auf diese Weise zu tieferen Temperaturen hin zu extrapolieren. Erstaunlicherweise ergibt diese Skalierung einen glatten Untergrund. Dies lässt vermuten, dass das 3D-XY-Modell eine bessere Beschreibung der zugrundeliegenden Physik liefert als das klassische thermodynamische Modell. Für das zu erwartende obere kritische Feld wird mit $\mu_0 H_{c2}(0) = 255$ T bei beiden Modellen aber der gleiche Wert abgeleitet. Der Grund für die unterschiedliche Modellierung der Längenänderung als Funktion der Temperaturänderung liegt in der Vernachlässigung von Fluktuationen im klassischen thermodynamischen Modell.

In unseren Messungen war es nicht möglich H_{c2} direct zu bestimmen auch nicht bei $T \approx T_c$ an Übergang vom supraleitenden zum normalleitenden Zustand. In diesem Temperaturbereich könnte daher der Phasenübergang bedingt durch Fluktuationen zu einem "Crossover"-Verhalten ohne scharfe Phasengrenze modifiziert werden.

Schlißlich wurde auch die durch die Flussverankerung verursachte irreversible Magnetostriktion untersucht. Einige Signale zeigen Temperatur- und Feldänderung-

skalierungsverhalten. Diese konnten aber bei Magnetisierungs- noch bei Wärmekapazitäts-Messungen gefunden werden und konnten bei einem erneuten Einbau der Probe nicht völlig reproduzieren werden. Die Signale zeigten keine Abhängigkeit von der magnetischen Feldänderung-Rate. Deshalb könnten diese Signale ein Nachweis eines möglichen Übergangs zwischen verschiedenen Vortexphasen sein: Das Vortexphasendiagramm könnte somit komplizierter sein als bislang erwartet, und die Magnetostriktion könnte eine Technik sein, um dies zu untersuchen.

Chapter 1

Introduction

The history of superconductivity started very shortly after the procedure of liquefying He was discovered by Kamerling-Onnes in 1908. Only three years later he reported the effect of total loss of electrical resistance of mercury at 4 K. As time passed by, more and more striking behaviors were found: the ideal diamagnetism (Meissner-Ochsenfeld effect, 1931), quantization of the magnetic flux in a superconducting ring, Josephson effects, high temperature superconductivity in cuprates (Bednorz -Müller [Bed86]) and so on.

It is widely accepted that this phenomenon is caused by paired electrons, which build up a macroscopic quantum state - the condensate. This thrilling behavior of matter was understood only almost 50 years after its discovery [Bar57]. The phonon-mediated coupling in classical superconductors creates the Cooper pairs below a critical temperature T_c (usually less than 20 K). Increasing of the temperature or applying a magnetic field disturbs the pair correlation; they split up, the condensate finally disappears and the superconductor becomes again a normal metal.

After the discovery of the high temperature superconductors (HTSC), a new turn started. These substances behave in some ways as the old ones do, but the underlying mechanism(s) seems to be rather different. Not only is the T_c increased (up to 135 K in Hg1223 at ambient pressure [Gao94]), the "host" substances now are doped insulators, the density of charge carriers is small, and the thermal and quantum fluctuations play a much higher role than in classical superconductors [Var99, Ull90, Car99].

One of the pictures to explain the high temperature superconductivity is based on the "preformed pair" scenario [Eme95], where instead of a single critical temperature T_c, the system is characterized by two temperatures: T^*, the pairing temperature, when the formation of bosons starts, and T_c ($T_c < T^*$), when the pairs condense, phase coherence appears, and the substance becomes superconducting. However, the mechanism of the coupling is still unclear, and, furthermore, this picture is not universally accepted.

Previous dilatometric studies of $YBa_2Cu_3O_{7-\delta}$, which is probably the best studied high-temperature cuprate superconductor, have shown a variety of interesting effects in the thermal expansion [Mei91, Mei01, Nag00, Pas98, Lor02b, Lor03]. This material is nearly ideally suited for these types of measurements because:

1. it is possible to grow fairly large and high-quality single crystals [Ryk96],

2. the thermal expansion anomalies at T_c and the oxygen ordering glass transition are quite large in comparison to the phonon background.

$YBa_2Cu_3O_{7-\delta}$ [Wu87] has an orthorhombic structure (see Fig. 1.1); it is characterized by CuO_2 planes and CuO chains running along the b-axis. The expansivity anomalies at T_c are related to the uniaxial pressure dependence of T_c [Mei91], which was found to be quite large and very anisotropic. The origin of this pressure dependence is not fully understood; however, both a pressure induced charge transfer [Pic97], which is similar to doping, and an intrinsic effect which directly couples to the pairing mechanism, are believed to play a role [Mei96]. The anomalies at T_c along the a- and b-axes have nearly the same magnitude but opposite sign. This was found to be quite useful for further increasing the relative size of the anomaly at T_c by subtracting the expansivity curves from each other. Using this difference curve in $\alpha_{(b-a)}$, convincing evidence was found for the 3D XY character of the superconducting phase transition both in zero magnetic field [Pas98, Pas00, Mei01] and in fields up to 12 T [Lor02a, Lor03].

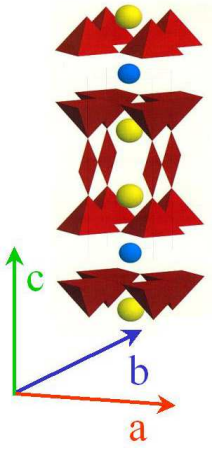

Figure 1.1: The crystal structure of $YBa_2Cu_3O_{7-\delta}$.

These previous studies concentrated mostly on the expansivity around the superconducting phase transition. Further interesting information about the superconducting state (e.g. the pressure dependence of the thermodynamic critical field H_c, the pressure dependence of the Sommerfeld constant and the pressure dependence of the Ginzburg-Landau parameter κ) can in principle be obtained by studying the thermal expansivity between T=0 and $T > T_c$ and in fields up to the upper critical field H_{c2} [Bra70]. The pressure derivatives dT_c/dp_i and dH_{c0}/dp_i are usually coupled in classical superconductors [Roh60, Lor06a], and have the same sign. Such an analysis has not been performed on any HTSC material. It is the subject of this thesis to perform precise thermal expansion and magnetostriction measurements in order to undertake such an analysis of the thermal expansion data. Fully oxygenated $YBa_2Cu_3O_7$ was chosen because previous studies had shown that the quality of these crystals had improved to such a point that the reversible thermodynamic properties could be studied over a large part of the superconducting phase

region [Lor02a]. It would be impossible to study these effect in "normal" samples due to the irreversibility introduced by flux pinning.

The structure of this thesis is as follows: In Chapter 2 a short introduction to the thermodynamics of a superconductor and to the magnetostriction is given. Chapter 3 is devoted to the measurement technique and the details of data treatment in order to account for different backgrounds and undesired signals. The investigated samples and their characterization with thermal expansion, magnetization, specific heat and magnetocaloric measurements are presented in Chapter 4. In Chapter 5 we present our main experimental results and explain a treatment for accessing the reversible magnetostriction signal in the irreversible region. An analysis of our results is given in Chapter 6. The possibility to describe the solid vortex phase in the framework of classical thermodynamics is discussed. The summary of this work is given in Chapter 7. Some interesting results from irreversible measurements, which were not the main focus of this thesis, are given in the Appendix.

Chapter 2

Magnetostriction of superconductors - Thermodynamic approach

In this Chapter we briefly present the necessary thermodynamics to describe the magnetostriction and thermal expansion of superconductors in a magnetic field. We start with a short introduction to the phenomenon of superconductivity.

The thermodynamics of the superconducting state is widely discussed in textbooks [Tin75, Buc04], but the magnetostriction - due to the very small signal (relative length change 10^{-8} - 10^{-7}) - usual is out of scope of these works. That is why we will discuss it here in some detail. The magnetostriction in type-I superconductors was first time treated by Shoenberg in [Sho65]. Type-II material contains several other terms [Bra70]:

1. the *real* thermodynamic magnetostriction, given as the pressure dependence of the magnetization, $\frac{\partial M}{\partial p}$, this term exists in all solids;
2. signal due to the expelled field (also exist in type-I);
3. pinning at the surface; (effect of Bean-Livingston),
4. pinning in the bulk;
5. demagnetization effect (also exist in type-I).

The goal of our work is to analyze the first term, which gives insight into the thermodynamics of the superconductor, and compare it with that of classical superconductors. Just below T_c the signal contains almost exclusively the thermodynamic response of the system (first term), here there is no hysteresis between field increasing and decreasing loops. Decreasing the temperature increases the role of pinning, leading to a hysteresis in measurement. In our case, the range of this thermodynamic behavior is (55 - 88 K), at lower temperatures irreversibilities (third and fourth) quickly outweigh the first term. The second and fifth terms play almost no role in our measurements.

2.1 Type-I and type-II superconductors

Along with zero electrical resistance (below the critical current) in the superconducting state, the superconductor exhibits perfect diamagnetism caused by screening currents,

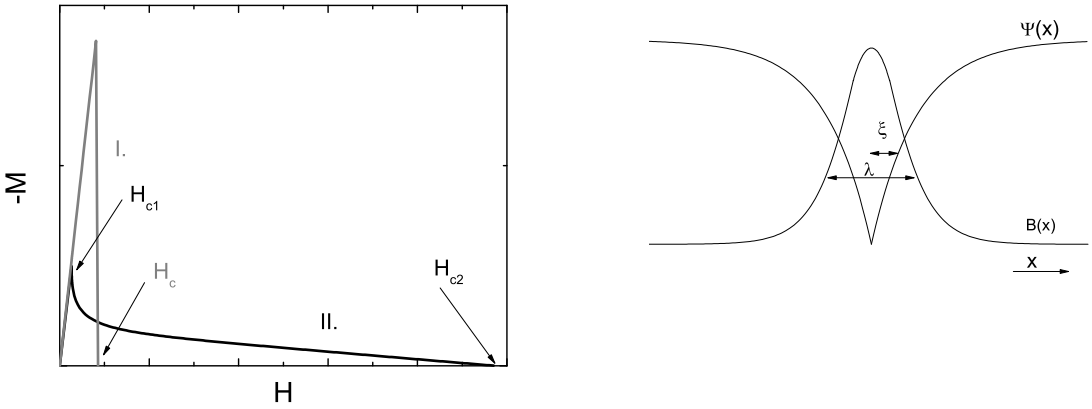

Figure 2.1: *Left:* Magnetization curve for type-I and type-II superconductors. *Right:* Superconducting order parameter Ψ and magnetic field B variation in a single vortex.

generated by magnetic field (Meissner-Ochsenfeld effect). This shielding current flows in a thin surface layer of thickness λ^L (the London penetration depth)[1]. There are two kinds of superconductors, depending on the sign of the interface energy, which describes how the sample reacts on field: either the interface energy is positive, then it costs energy for system to create boundaries between normal and superconducting regions, or this energy is negative, and the system wins energy with every created interface between phases (Fig. 2.1).

In type-I superconductors (mostly found in clean metals, e.g. In, Pb etc) the interface energy is positive. When the magnetic field approaches a certain critical magnetic field, H_c, the perfectly screened state is no more favorable for the superconductors, the magnetic field destroys the superconducting state[2].

In type-II superconductors (the majority of superconducting materials) the situation is different, because the interface energy is negative. In this case, after reaching of the lower critical field, H_{c1}, the fully screened state is destroyed and the increasing applied magnetic field generates magnetic vortices inside the superconductor (Abrikosov state), each containing a normal state core, shielded by supercurrents. Increasing magnetic field produces an increasing number of vortices up to upper critical field H_{c2} where sample becomes normal[3]. In an ideal crystal these vortices moves freely. Due to Lorentz force they repel each other, so they tend to build up an ordered lattice (Abrikosov lattice).

For a phenomenological description of superconductivity, one can use the Ginzburg-

[1]Note that we use a somehow unusual notation for the London penetration depth in order to avoid confusion with the magnetostriction coefficient, noted as λ.

[2]We consider an infinitely long sample parallel to the applied field, thus we can neglect the intermediate state, which describes the coexistence of superconducting and normal domains, caused by the local increase of magnetic field due to demagnetization effect.

[3]We neglecting the surface superconductivity, which survives after reaching of H_{c2} up to the third critical field H_{c3}.

Landau theory [Gin50] for phase transitions of second order. The order parameter Ψ can be viewed as the density of the superconducting pairs. The surface energy depends on the Ginzburg-Landau parameter $\kappa = \lambda^L/\xi$, where ξ is the correlation length of superconducting wavefunction. The phase transition of high-temperature superconductors at the upper critical field H_{c2} is of second order, with Ginzburg-Landau parameter $\kappa \gg 1$, so the transition itself and the Abrikosov state can be well described down to lower critical field H_{c1} by this theory. There are two equations and two boundary conditions on the surfaces, which do not have analytical solutions, so one should use variational methods to solve them. Nevertheless, these solutions differ slightly, depending on the used trial function and simplifications, but all of them coincide well with the approximate Abrikosov solution [Abr57a] for high fields ($H_{c1} \ll H < H_{c2}$).

2.2 Thermodynamics

It is natural to describe superconductor with the Gibbs free energy and its differential, defined as:

$$G(T, \mathbf{H}) = U - TS + pV + \mu_0 V \mathbf{H}\mathbf{M}, \tag{2.1}$$
$$dG = -SdT + pdV + \mu_0 V \mathbf{M} d\mathbf{H},$$

where T is the temperature, $\mathbf{H}$ the magnetic field, U the total internal energy, S the entropy, p the pressure, V the volume, $\mathbf{M}$ the magnetization per unit volume. The following relations can be derived for volume at constant temperature and entropy at constant pressure,

$$V = \left.\frac{\partial G}{\partial p}\right|_T \tag{2.2}$$

$$S = -\left.\frac{\partial G}{\partial T}\right|_p \tag{2.3}$$

For a type-I superconductor the Gibbs energy difference between the normal and superconducting state at constant temperature and volume is given as [Sho65]:

$$G_n(T) - G_s(T) = G_s(T, H_c) - G_s(T, 0) = \int dG = -\mu_0 \int_0^{H_c} V \mathbf{M} d\mathbf{H} \tag{2.4}$$

where H_c is the thermodynamical critical field, above which the superconducting state is suppressed. For type-I superconductors the Meissner-Ochsenfeld effect occurs below $H_c(T_c)$, where $\mathbf{M} = -\mathbf{H}$. Therefore equation 2.4 can be written as:

$$G_s(T, H_c) - G_s(T, 0) = \mu_0 V \frac{H_c^2}{2} \tag{2.5}$$

For a type-II superconductor, the superconducting state extends up to H_{c2}, so equation 2.4 now reads

$$G_n(T) - G_s(T) = G_s(T, H_{c2}) - G_s(T, 0) = \int dG = -\mu_0 \int_0^{H_{c2}} V \mathbf{M} d\mathbf{H}. \tag{2.6}$$

The thermodynamic critical field is still defined by 2.5. The quantity $\mu_0 \frac{H_c^2}{2}$ is the **condensation energy**, strictly speaking, energy per unit volume. H_c is now only an energy measure; nothings happen at this field. The thermodynamic critical field is related to H_{c1} and H_{c2} as $H_c \approx \sqrt{H_{c1} H_{c2}}$ [Par69].

If we keep the field constant and sweep the temperature, the measured length change is given by the **thermal expansion** (or contraction) of the sample. The volumetric thermal expansion coefficient β is defined as

$$\beta = \frac{1}{V}\frac{\partial V}{\partial T}\bigg|_p = \frac{1}{V}\frac{\partial^2 G}{\partial p \partial T}\bigg|_T = -\frac{1}{V}\frac{\partial S}{\partial p}\bigg|_T . \tag{2.7}$$

In case of an orthorhombic crystal, the linear thermal expansion α is

$$\alpha_i = \frac{1}{L_i}\frac{\partial L_i}{\partial T}\bigg|_p , \tag{2.8}$$

where the crystallographic axes i=a, b, c. The volume expansion coefficient β is,

$$\beta(T) = \sum_{i=1}^{3} \alpha_i(T) \tag{2.9}$$

One can also keep the temperature constant and sweep the magnetic field - then the length change is given as the **isothermal magnetostriction**. One defines the volumetric magnetostriction coefficient λ as:

$$\lambda = \frac{1}{\mu_0 V}\frac{\partial V}{\partial H}\bigg|_T = \frac{1}{\mu_0 V}\frac{\partial^2 G}{\partial p \partial H}\bigg|_H = \frac{1}{V}\frac{\partial MV}{\partial p}\bigg|_T = \frac{\partial M}{\partial p}\bigg|_{T,V} \tag{2.10}$$

In case of an orthorhombic crystal, the uniaxial magnetostriction coefficients λ_i are

$$\lambda_i = \frac{1}{\mu_0 L_i}\frac{\partial L_i}{\partial H}\bigg|_T \tag{2.11}$$

where i=a, b, c. The volumetric magnetostriction coefficient λ is:

$$\lambda(T) = \sum_{i=1}^{3} \lambda_i(T) \tag{2.12}$$

If one has a first-order phase transition, the relation between the length change and entropy yields the uniaxial pressure dependence of critical temperature T_c as given by the Clausius-Clapeyron equation (e.g.[Adk87]):

$$\frac{dT_c}{dp_i} = \frac{\frac{L_i - L_{0i}}{L_i} V_{mol}}{\Delta S}. \tag{2.13}$$

$\frac{L_i - L_{0i}}{L_i}$ is the relative length change at the phase transition, ΔS is the entropy discontinuity, and V_{mol} is the molar volume.

In case of a second order phase transition, the Ehrenfest relation [Ehr33] gives:

$$\frac{dT_c}{dp_i} = \frac{\Delta\alpha_i T_c V_{mol}}{\Delta C_p} \tag{2.14}$$

where $\Delta\alpha$ and ΔC_p are the discontinuities of the linear thermal expansion and the heat capacity (at constant pressure) at the phase transition. The heat capacity at constant pressure, is defined as:

$$C_P = T\left(\frac{\partial S}{\partial T}\right)_P \tag{2.15}$$

Of interest is also the **magnetocaloric coefficient** at constant temperature, which is the measure of the energy change of the solid in magnetic field:

$$M_T = \left.\frac{\partial Q}{\mu_0 \partial H}\right|_T = \left.\frac{\partial^2 G}{\mu_0 \partial T \partial H}\right|_T = -TV\left.\left(\frac{\partial M}{\partial T}\right)\right|_T. \tag{2.16}$$

2.3 Thermodynamic magnetostriction

Let us consider a type-I superconductor in the form of a long rod parallel to the applied magnetic field H, bigger than H_c. The magnetic field destroys the superconducting state, and the material is now in the normal state. The difference of the Gibbs energy between the normal[4] state and the superconducting state is given by (2.5). Using relation (2.2) we can derive the volume change between these two states [Sho65]:

$$V_s(H_c) - V_s(0) = V_n(H_c) - V_s(0) = V_s\mu_0 H_c \left.\frac{\partial H_c}{\partial p}\right|_T + \mu_0 \frac{H_c^2}{2}\left.\frac{\partial V_s}{\partial p}\right|_T \tag{2.17}$$

The last term in equation (2.17) represents the change of the size of the superconductor due to pressure of the expelled magnetic field. This pressure exists also in type-II superconductors in the mixed state. In the case of a BCS superconductor [Bed86], there is a scaling law for thermodynamic critical field $H_c = H_{c0} * g(t)$, where g is the function describing the critical field change with temperature, and approximately equal to $(1 - t^2)$, t is the reduced temperature (T/T_c). The critical field H_c is coupled to the critical temperature T_c

$$\mu_0 H_{c0}^2 \, g''(t)|_{t=0} = T_c^2 \gamma^\star, \tag{2.18}$$

where $\gamma^\star$ electronic specific heat per unit volume, one can find the relative volume change [And62][5]:

$$\frac{V_n - V_s}{V_s} = -\mu_0 H_0^2 \kappa \left[s(1-t^4) + \frac{g}{2}(1-t^2)^2\right]. \tag{2.19}$$

Here $\kappa = -1/V\partial V/\partial p$, $s = dlnT_c/dlnV$, $g = ln\gamma/lnV$ and $\gamma = C_{el}/T$, i.e. the electronic specific heat coefficient per mole.

The above equations describe the volume change between the superconducting and normal state. For a type-II superconductor, when one is also interested in the volume

[4] We assume that there is no magnetic response of the normal state.

[5] The equation given in cited article is mistyped.

(length) change as a function of field, one starts by defining the magnetization M [Bra70] as:

$$M = -VH_c f(H/H_c, \kappa), \tag{2.20}$$

where V is the volume of the superconductor, H_c the critical field, and f the function which gives the shape of the magnetization curve, which can be obtained from the solution of the Ginzburg-Landau equation or experimentally from magnetization measurements. Following equation 2.10 [Bra73] one can find the length change of the superconductor in a magnetic field H:

$$l(H) - l(0) = -\frac{1}{A}\frac{\partial}{\partial p}\int_0^H VMdH, \tag{2.21}$$

where $l(H)$ and $l(0)$ are the length of sample in the magnetic field H and with no magnetic field ($H||l$), A the area of sample perpendicular to the field. If we substitute (2.20) to (2.21) and consider that the volume of sample is $V = lA$, we obtain:

$$\frac{l_i(H) - l_i(0)}{l_i(0)} = \frac{1}{l_i}\frac{\partial l_i}{\partial p_i}\mu_0 H_c \int_0^H f dH + \mu_0 \frac{\partial H_c}{\partial p_i}\int_0^H \left(f - H\frac{\partial f}{\partial H}\right) dH + \frac{\partial \kappa}{\partial p_i}\mu_0 H_c \int_0^H \frac{\partial f}{\partial \kappa} dH \tag{2.22}$$

There are three terms, introducing three different pressure dependencies. First of all, the pressure dependence of the volume, which is by definition equal to the negative compressibility $-k$. The second term describes the length change due to the pressure dependence of the critical field. The third term is proportional to the pressure dependence of κ. This term does not contribute to the total $L_n - L_s$, since the integral

$$\int_0^{H_{c2}} \frac{\partial \kappa}{\partial p_i} dH = 0$$

[Bra73], so the whole equation transforms to (2.17).

Let us consider the length change in field, if there was no difference in length between superconducting ($H = 0$) and normal state ($H > H_{c2}$). We calculated this case neglecting the contribution of the third term (Fig. 2.2).

It is easy to see that the contribution of the compressibility term should be canceled by the pressure dependence of the critical field at H_{c2}. But if the magnetic field is smaller than H_{c2}, one will detect some signal, even if very small. It means, that even for the case $l(H_{c2}) = l(0)$ the pressure dependence of the condensation energy would be zero, $dE_c/dp = 0$, but $dH_c/dp \neq 0$.

2.4 Magnetostriction from flux pinning

The applied magnetic field B influences not only the thermodynamics of the material, but also generates a Lorentz force $F_L = J \times B$, where J is the induced current density. This force directly acts on the vortex lattice while the motion of vortices is opposed by pinning

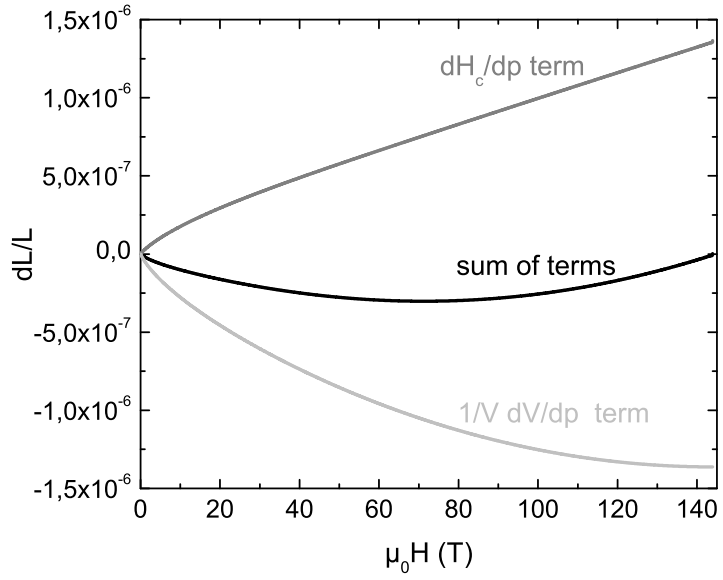

Figure 2.2: Expected magnetostriciton at T=0 of a type-II superconductor with zero pressure dependence of the condensation energy per mole. The compressibility $(1/VdV/dp)$ and dH_c/dp terms cancel each other at H_{c2} (145 T), but surprisingly, a finite magnetostriction remains between $0 < H < H_{c2}$.

centers. The maximum of this pinning force is given by $F_p = J_c \times B$, where J_c is the critical current density, the limit of dc current which can flow through the superconductor without loss of zero resistance. The critical current strongly depends on the amount of pinning. The pinning force can be quite large, resulting in a large *non-thermodynamic* magnetostriction. This magnetostriction is irreversible, i.e. the hysteresis between loops in increasing and decreasing field appears, which also contains impact from critical state, governed by pinning. Magnetostriction becomes even more complex, if the geometrical effects are taken into account [Schl02, Joh98, Joh99a, Joh99b] - the bending and shape distortion of the sample detected as a magnetic field induced length change.

Here three different energies play a vital role: first of all the repulsion energy which tries to distribute vortices spatially homogeneously and builds up the Abrikosov lattice; the second one is the pinning energy which hinders the motion of the fluxons and the last one is the thermal activation energy which causes the random motion of the vortices. Depending on the relations between energies a very complicated phase diagram can arise. We will discuss the critical state in more detail in Appendix.

2.5 Conclusions

In this Chapter we gave a short introduction to the thermodynamics of superconductors. We explained also, which part of the magnetostrictive signal is of main interest

to us, and how one can gather information about the pressure dependencies of different thermodynamic parameters without actually applying pressure.

Chapter 3

Capacitance dilatometry

There are several techniques to measure the length change of solids: e.g. X-ray and neutron scattering, strain gauges and capacitance dilatometry. In case of the HTSC, where in the region of the interest (0 - 300 K) the relative length change due to thermal expansion is about 10^{-3}, the most suitable method is the last one.

The expected relative magnetostriction signal in our measurements is around $10^{-8}..10^{-5}$, which is up to thousand times smaller than in case of ferromagnets, heavy-fermion compounds etc. That is why the very accurate signal measurement and treatment is inevitable in order to gather useful data for our analysis.

3.1 Capacitance cell

All length change measurements of this work were performed with a capacitance dilatometer, installed in a gas-flow cryostat (Oxford Instruments). The cell is thermally coupled to a variable temperature insert (VTI) by ^{4}He exchange gas at 4-5 mbar (400-500 Pa) pressure. The temperature range is (1.4 - 260 K), the magnetic field can be swept up to 1 T/min to $\pm$10 T. The VTI controlling unit senses temperature with a *Lake Shore* Cernox© thermometer and manipulates it by changing the heater voltage and altering the gas flow by an electronically controlled needle valve.

The basic design of the cell (Fig. 3.1) follows the one of Pott and Schefzyk [Pot83], with several modifications [Mei91]. The holder of the cell was designed in a way that it is possible to rotate it parallel and perpendicular to the magnetic field (Fig. 3.2). The working principle of this kind of dilatometry is based on measuring the change of the gap between two capacitor plates, one of which is movable and coupled to the sample. This plate with its holder is fixed by Cu-Be springs to the frame in such way that the plates are always parallel to each other. The plates and the protecting rings are electrically isolated by epoxy. All parts of the dilatometer except the springs are crafted from copper. The Eichhorn und Hausmann capacitance bridge was used to measure the capacitance signal. The main advantage of this bridge, in comparison with other commercially available devices is its speed of measurement. The signal from the bridge is measured by a digital voltmeter, which is connected to the computer with GPIB.

There are two resistance thermometers installed on the cell: a platinum and a Cernox© thermometer. Each of them is measured by 4-contact method with digital voltmeter,

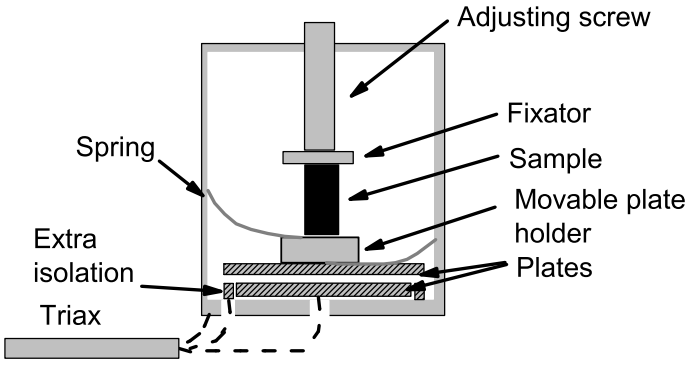

Figure 3.1: Schematic view of the dilatometer cell.

which are connected to the computer also by GPIB. The magnetic field is controlled by an Oxford Instruments IPS-120 device, the value of the field is measured using a special shunt and a digital voltmeter.

Concluding, the whole measuring system contains 4 digital voltmeters, which are controlled by a computer program, written in LabWindows©.

The gap between plates is around 12-30 μm depending on the size of the expected signal. In order to have higher resolution, two different preamplifiers with maximal possible gaps of 20 and 40 μm were used. The usual resolution is 0.05 Å ($0.5 * 10^{-11}$ m). Worthwhile to notice is that the capacitance dilatometry gives only the *length change*, and is not suitable to measure the *absolute length* of the sample. We used an electronic micrometer screw to find the length of the samples at room temperature.

The installation of the sample is done as follows - the sample is put between the frame of the movable plate and the fixator (Fig. 3.1), which is coupled to a screw, allowing us to change the gap between the plates at room temperature.

Our measurement technique is dynamic instead of the commonly-used step-by-step quasi-static method [Lan91], which means that the temperature or the magnetic field is changed at a constant rate (up to 15 mK/sec or 1 T/min). The usual point density is around one point every 0.7 second in thermal expansion (it means one point every 0.1 K - a mean value is taken to suppress the noise), and is 170 points per Tesla in magnetostriction for the usual 0.5 T/min sweep rate. The main advantages here are the possibility to measure kinetic effects and that it is less time consuming. Also, the drift of electronics plays a smaller role in comparison with usual static measurements.

We also found that our preamplifiers are slightly field dependent, and we used a special μ-metal pot to screen them from the stray magnetic field of our 10 T magnet. Test measurements showed that this eliminated this problem.

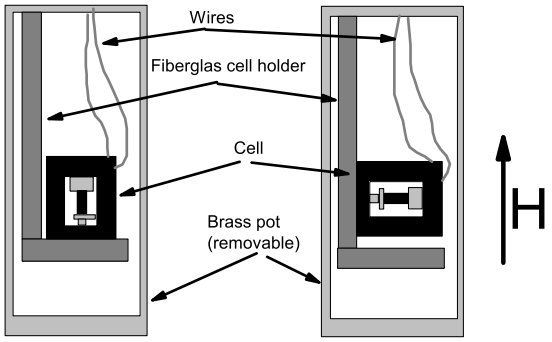

Figure 3.2: The two possible positions of the cell.

3.2 Calibration of the cell

In thermal expansion or magnetostriction measurement not only does the sample change its size but also the dilatometer has an own response. As we measure the copper capacitance, the resulting signal also has a part, caused by copper expansion, which is the material of the dilatometer.

To calibrate the dilatometer cell, pure Cu measurements were used, the thermal expansion of which is published [Kro77]. Cu data measured with different heating rates were used as background, and were subtracted from experimental data.

There are two preamplifiers with different amplification ratio. This ratio is expected to be linear and constant in the working range of preamplifier. Two main reasons can disturb it: overrange and non-linear response of the cell. The distance between the plates is expected to follow

$$d = \epsilon_0 \frac{S}{C},$$

where d is the distance between plates, S their area and C the capacitance. It is easy to see, that if we have some missaligment of plates or rough surface, at some point the signal would not be inversely proportional to the distance. Now, if we measure a silicon single crystal, and then compare it with literature data [Lyo77], the scaling coefficient between them gives the amplification ratio. Also we can find the minimal gap between plates, where we have constant amplification ratio - this distance is the same for both amplifiers, and usually - depending on how good the plates were polished and readjusted - is around 12 μm.

All this means that we need two measurements (Cu and Si) to find out two unknown parameters: background and sensitivity.

3.3 Isothermal magnetostriction

The biggest advantage of a magnetostriction measurement in comparison with a thermal expansion measurement is the absence of the phonon background, since the temperature

is kept constant. The exchange gas pressure is kept at 5 mbar (500 Pa), which was found to be the smallest value where the sample is still coupled to VTI sufficiently well, and the thermal mass of the cell is enough to damp the temperature oscillations produced by control mechanism. Also the lower pressure requires less helium, which means longer operation time of cryostat between the refillings.

The Cernox driven mode is used to reach and stabilize the desired temperature for magnetostriction measurement, then it is changed to a Capacitance Temperature Sensor driven mode to make the measurements. Knowing the magnetoresistance of Cernox© thermometer at the cell gives the temperature change during the measurement, which is used to correct the small thermal expansion effect. Due to the big relaxation time at temperatures of interest, usually after reaching thermal drift as small as 2-3 mK/min the measurements were done, the obtained thermal expansion effect on magnetostrictive data was easily corrected.

Magnetic field is swept using a rate of 0.5 T/min, which was considered quick enough to not be affected by electronics drift, but slow enough to allow the whole system to cool down after heating caused by eddy currents. We also did several 1 T/min, 0.1 T/min and 0.05 T/min measurements to try to find kinetic effects, mainly in the irreversible region (the temperature is usually less than 60 K).

3.4 Analysis of the different effects on the measured magnetostrictive signal

In the case of a magnetostrictive measurement, the signal, measured by dilatometry, contains, in addition to the desired magnetostrictive part, the thermal expansion signal due to the slow drift of the cell, the eddy current effects due to the field sweeping and also the background of the cell.

The Cernox© sensors used in our system, have a magnetic field dependence, which lead to an error in the measured temperature, that is why we built in the Capacitance Sensor option from Oxford Instruments. The original Cernox-driven mode was used to achieve the desired temperature, but during the magnetostriction measurement the temperature was controlled by Capacitance Sensor. The main advantage of this thermometer is the almost unmeasurable magnetic dependence of the measured and controlled temperature, on the other side, the Capacitance Sensor has bigger temperature drift with time than Cernox, but this small thermal expansion signal could be easily corrected.

Eddy currents are generated during the magnetic field sweeps. They are symmetric with respect to field inversion, but have different signs for the up and down sweeps. If there is no other hysteresis producing effect, then the magnetostriction can be corrected by taking the mean value.

To present these different effects we use the same magnetostriction measurement, taken on SRLW sample at 87.7 K ($\approx T_c$)[1], where the magnetostriction signal is smallest and the undesired effects play a vital role.

[1]This $YBa_2Cu_3O_7$ single crystal will be presented in more detail in Chapter 4.

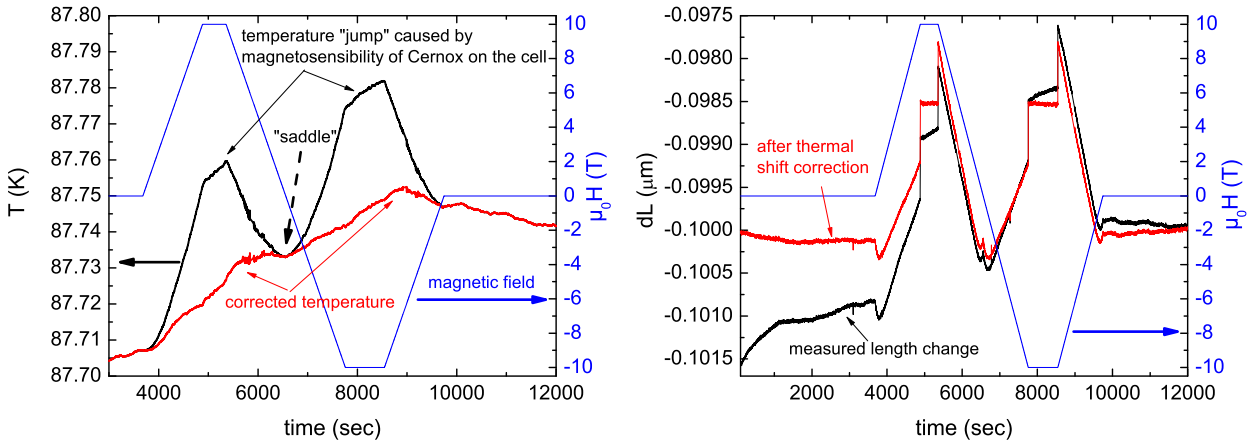

Figure 3.3: *Left:* Correction of the temperature reading of the Cernox thermometer on the cell in magnetic fields. Black line: change with time of the measured temperature on the Cernox thermometer; red: temperature after correction of the magnetoresistance of Cernox; blue: change of applied magnetic field with time. *Right:* Correction of the thermal drift. The black line denotes the measured length change, the red line the length change after subtracting of thermal drift effect, and the blue line the change of applied magnetic field with time.

3.4.1 Thermal drift

Our system is controlled by the Cernox© thermometer (or Capacitance Sensor), which is located in the VTI insert in the copper block (or on the shielding pot of the measuring stick) and decoupled from the cell. This means that we always have a thermal gradient between our controlling point and the sample. This gradient changes depending on the level of the liquid Helium in the cryostat, the pressure of the helium backline, temperature of the VTI walls etc. In the Capacitance Sensor driving mode exists also a drift of the sensor itself, which amounts to around +10 mK/hour temperature change. So, we have different thermal drifts which affect the temperature of the sample, and are difficult to get rid of, but we can easily correct these undesired effects. For the correction we use the thermal expansion data; as temperature where we take the dL/dT is a middle point of the sweep (saddle), which is usually also the middle of the temperature change (Fig. 3.3).

Subtracting this calculated expansion of the sample from measured signal gives almost symmetric length change in field (Fig. 3.4).

3.4.2 Eddy currents modeling

The changing magnetic field generates eddy currents in metallic parts of dilatometer. These currents produce field, opposite to applied, the interplay between them generate a stress in dilatometer. The movable plate of cell is the only part which shifts due to this effect, one detects a signal change from dilatometer (Fig. 3.5), which linearly proportional to the sweep rate (Fig. 3.6, left). In order to investigate this parasitic signal, we measured

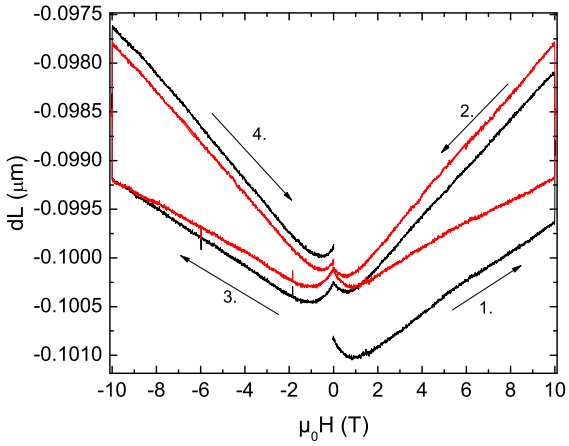

Figure 3.4: Typical magnetostriction curve for increasing and decreasing field. There is a length drift in the raw data (black curve) due to a temperature drift of the cell, which has been corrected (red curve).

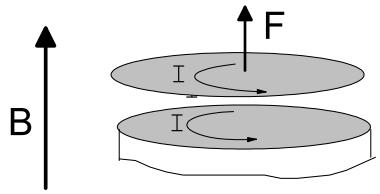

Figure 3.5: The changing applied magnetic field B generate shielding current I in the plates, but only the upper (movable) one can move due to force F.

a needle from silicon - material where no magnetic signal is expected. We also measured other materials (copper, silicon, SRLW and SRL Genf-A[2]), and found that the impact of eddy currents does not depend on the sample or its length. This signal wholly comes from the cell itself. Even in superconductors, this part of length change was the same as for other materials at the same temperature. We defined the apparent jump in length at the end of a field sweep at 10 T, $dL_{Eddy}(10\mathrm{T})$, as a measure for this signal. Our results are presented in Fig. 3.6, right. In both positions of the cell the temperature dependence of $dL_{Eddy}(10\ \mathrm{T})$ follows a similar curve, only in longitudinal position the jump is always negative and smaller than in transverse position.

For this positional dependence we have two reasons: first, the profile of cell in longitudinal position to field is smaller; second, the movable plate in transverse position can be misaligned from the parallel position due to gravitation force. The eddy current effect on the length change, which is tightly coupled to magnetoresistance of copper, can be

[2]This $YBa_2Cu_3O_{7-\delta}$ single crystal will be presented in more detail in Chapter 4.

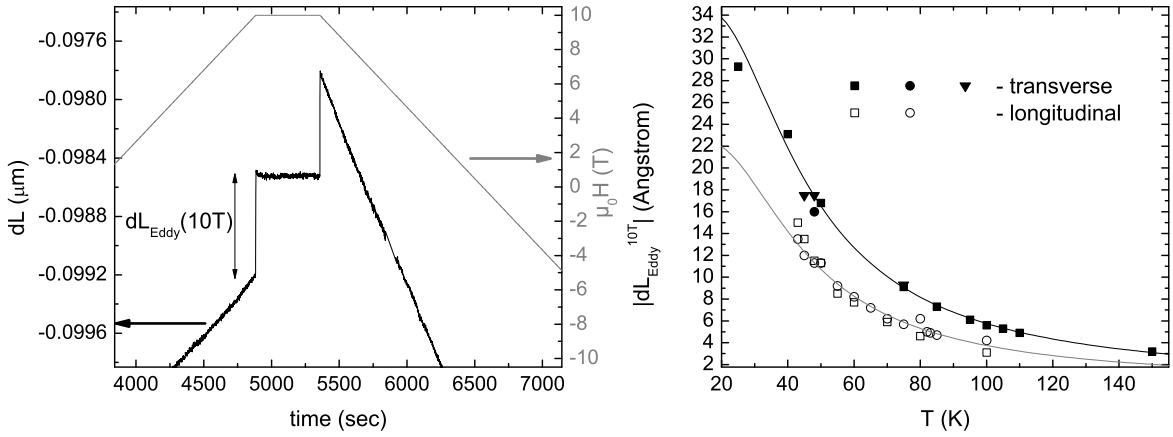

Figure 3.6: Typical length change versus time during a magnetostriction experiment showing the length "jumps" due to eddy currents where the field ramping is stopped and started at 10 T (*left*). The right part of the Figure shows the temperature dependence of the absolute value of this "jump" in both longitudinal and transverse position.

approximated as follows:

$$dL_{Eddy}(B) = \frac{A * B}{1 + 200A * B}$$

where B is the applied magnetic field in Tesla, A is a temperature dependent coefficient, experimentally found as

$$A = \frac{dL_{Eddy}(10\text{ T})}{10 - 2000 * dL_{Eddy}(10\text{ T})}.$$

The $dL_{Eddy}(B)$ curve, calculated from the known 10 T jump, should be subtracted from magnetostriction measurement in order to correct the effect of eddy currents. For the region where sample has no hysteresis, the eddy current length change can be corrected simply by:

$$L_{real}(H) = \frac{L\uparrow(H) + L\downarrow(H)}{2} \qquad L_{eddy}(H) = \frac{L\uparrow(H) - L\downarrow(H)}{2}$$

where $L\uparrow(H)$ and $L\downarrow(H)$ are the length change in increasing field and decreasing field respectively, $L_{real}(H)$ is the real length change without eddy current effect, and $L_{eddy}(H)$ the eddy current caused length change. If one investigates the irreversible temperature region (in our case, below 65 K), the eddy current effect, calculated in the aforementioned manner, should be subtracted.

3.4.3 Cell drift

Our cell has several drifts. First of all, if we change the temperature of the VTI, it takes some time until the dilatometer reaches the desired temperature, the relaxation time depends on the temperature gradient and temperature itself. This kind of drift can

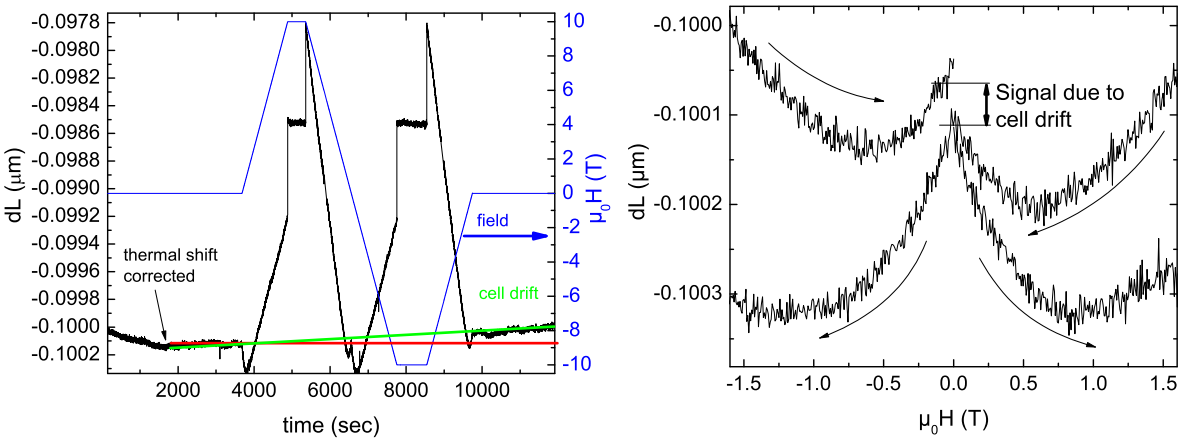

Figure 3.7: *Left:* Correction of the cell drift (the thermal shift is already corrected, eddy current impact is not). The black line is the length change with temperature, the green one is the modeled cell drift, the blue line is the field change with time. *Right:* Magnetostriction signal due to cell drift is shown, in this particular case it is around 0.5 Å. Arrows show the direction of the field change.

be corrected by subtracting the thermal expansion effect. We have already described this thermal drift in Section 3.4.1. The second kind of drift is caused by mechanical relaxations. Due to epoxy glue we always have some stress between parts of the cell if the temperature changes. This drift could be approximated as a smooth curve from begin and end of the magnetostriction measurement (Fig. 3.7), usually it is a straight line. The correctness of this procedure can be checked by the intersection of the starting and the ending points of the field sweep, in other words, the lengths of the sample is the same at zero magnetic field. The value for this error is around ±2 Å. This error did not directly depend on the temperature change, so could not be corrected by a thermal drift treatment.

3.4.4 Cell background

Magnetostriction measurements of copper samples with different lengths have shown that our dilatometer has its own signal, which is around 2-3 Å, depending on temperature. When measuring a sample from the same material as the cell itself, the expected response should be zero. For samples with different length the signal is almost the same, so we attribute this signal to the background of the cell and not to the possible magnetostriction of copper. In Fig. 3.8 one can see two measurements at 50 and 100 K, done for the longitudinal and transverse positions of the cell. One can see that this background has different signs depending on position. A sharp peak of unknown origin appears in longitudinal measurements in the region from -2 to +2 T, but it is not crucial due to the fact that most of the measurements (all *a*- and *b*-axis) were done in transverse position.

This background was subtracted from our magnetostriction measurements.

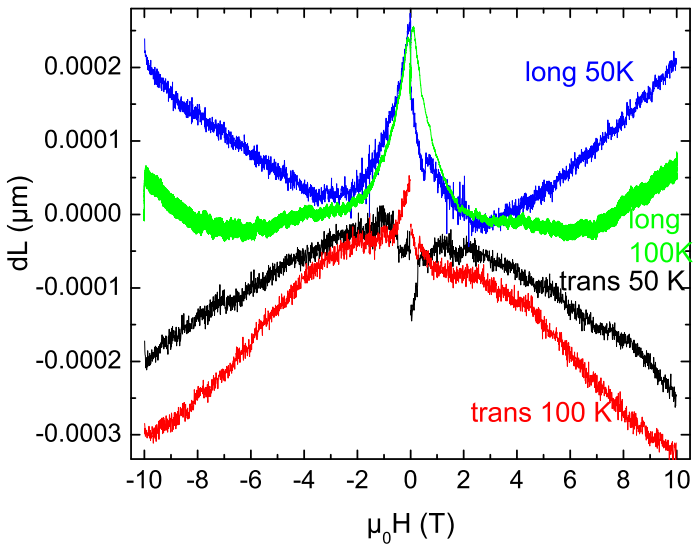

Figure 3.8: Background magnetostriction of the cell from copper measurements at 50 K and 100 K, for longitudinal and transverse positions of the cell.

3.4.5 Comparison of different undesired signals

We have discussed four different undesired contributions in our magnetostriction measurements. In order to clarify the importance of each we give a brief overview:

- a thermal drift can amount to several tens of Å, it decreases with decreasing temperature, caused by thermal expansion of the sample due to not properly controlled temperature;

- the eddy currents contribute 20-30 Å at low temperatures (with a standard sweep rate). This number quickly decreases with increasing temperature. It is fully produced by the cell itself, it does not depend on the sample, being proportional to the magnetic field sweep rate;

- the cell background is about 2-3 Å, being almost independent of temperature. It is the response of the cell to an applied magnetic field, and does not depend on the sample;

- the cell drift is caused by the slow relaxation of the cell, probably due to epoxy glue used as insulator between its parts. It can be up to 1-2 Å per hour.

One can see that the biggest signal is produced by the thermal drift, which is the only one depending on the sample; all other impacts are purely cell effects.

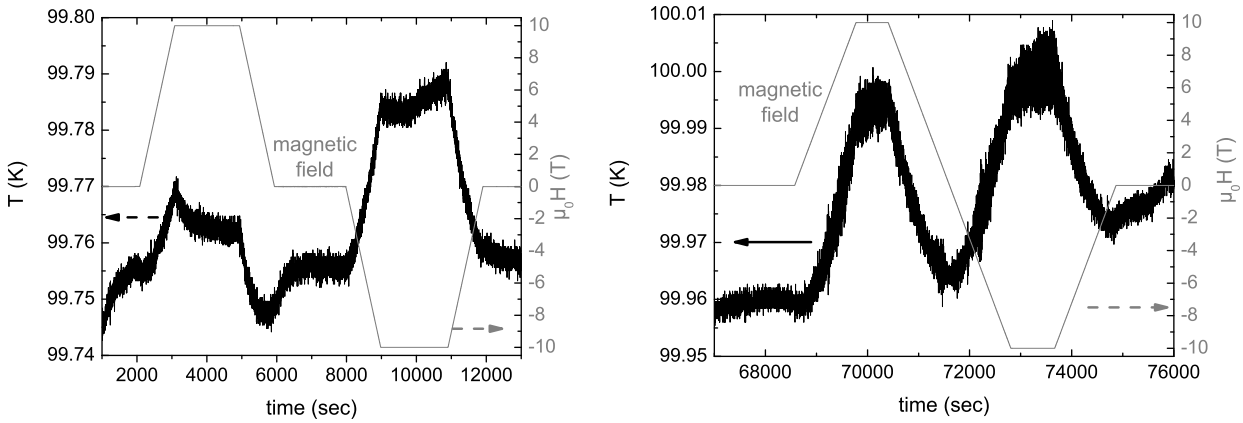

Figure 3.9: Time dependence of the cell Cernox temperature reading before (*left*) and after (*right*) installing the capacitance temperature sensor, during field ramping to ±10 T at 100 K. *Left:* Before improvement of our setup the temperature peak in positive field is smaller than in negative field by a factor of almost two. *Right:* After installation of the capacitance sensor driven mode both peaks in temperature reading are equal.

3.5 Capacitance Temperature Sensor

A Cernox and a platinum thermometer are used for measuring the temperature of the dilatometer cell. The main sensor is Cernox, which is *almost* magnetic field independent at high temperatures, and is well suited for thermal expansion experiments, both with and without field. Another Cernox sensor is used to control the temperature of the VTI, which also has some error in magnetic field - tens of mK at 10 T. As this Cernox is used to control the temperature of the VTI, the applied magnetic field generates an error in the sensor reading leading to an imperfect control of the temperature. Instead of a smooth temperature change of the sample rapid changes correlating with field changes, were detected. These "peaks" are presented in Fig. 3.9, left.

The magnetic field dependence of the Cernox thermometer at low temperatures is known, e.g. [Hei98]. To investigate this problem in detail, several Si magnetostriction measurements at different temperatures were done. Pure silicon was taken as a material without any measurable magnetostriction. The capacitance sensor was used as a thermal sensor - the whole length change, measured in magnetic field, is the expansion of the silicon due to a change of temperature. The capacitance cell readings dL show the real temperature change, $dT = dL\frac{\partial T}{\partial L}$, where the $\frac{\partial T}{\partial L}$ is known from a usual thermal expansion measurement, so the temperature error of VTI Cernox in magnetic field can be easily found (Fig. 3.10). Two sets of errors in Cernox-driven mode are presented: the temperature error estimated as the temperature change on Cernox of the cell, and calculated in aforementioned way. The first set of data shows the difference of error between VTI and cell Cernox thermometers, the second one shows the real error of the VTI Cernox. We also plotted the experimental data for slightly different Cernox from [Hei98], where we approximated the 10 T data by interpolating between the 8 and 12 T data.

The reason for these "peaks" is the magnetoresistance of Cernox. The strong asymme-

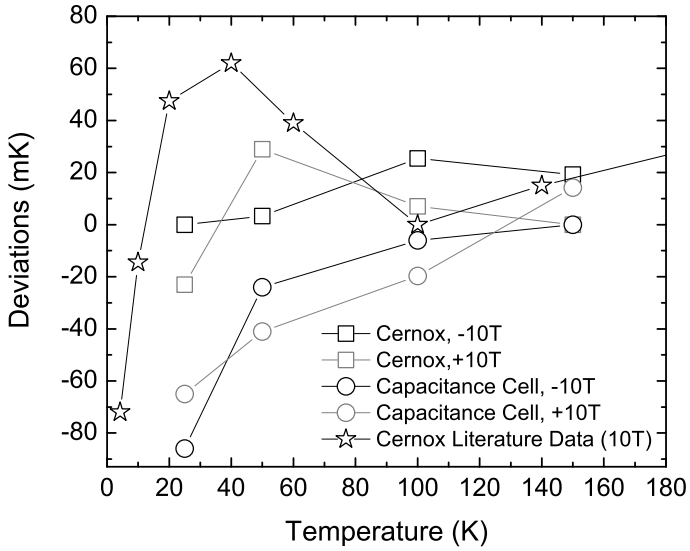

Figure 3.10: Temperature dependence of deviation from correct temperature reading of Cernox caused by magnetic field of ±10 T. Details in text.

try between positive and negative field "peaks" is caused by *sum* of magnetodependence of two different sensors (on the cell and on the VTI).

Our first attempt to avoid this effect was to do a magnetostriction measurement without temperature controlling, but the results were even worse. As the possibility to change the controlling program of VTI is limited, we installed a Capacitance Sensor Controller from Oxford Instruments to our VTI controlling unit and the capacitance temperature sensor (CTS) on the brass shielding pot covering our cell. There are two reasons to install the CTS on the pot: first, in order to have reliable temperature control the distance between thermometer and heater should be as small as possible; second, the installing of CTS on the cell is technically complicated. This kind of temperature sensor is actually a commercially available capacitor with high sensitivity in the range below 100 K. It could not be used as a primary thermometer due to instability with thermal cycling. Also we had to check the suitability of this kind of sensor in our temperature region of interest (up to 100 K) which is two times higher than mentioned by the producer. Using again silicon as magnetostriction-free substance we found that using of capacitance sensor to control the temperature of VTI, the peaks are symmetric in field (Fig. 3.9, right), and also we calibrated this error of the Cernox of the cell for different temperatures. The obtained correction dependence $T_{error} = f(T, H)$ is similar to those published [Bra99]. The equation, used to correct the temperature reading of Cernox on cell is:

$$T_{real}(H) = T_{measured} - C(T)H^2$$

where $C(T)$ is the temperature dependent correction coefficient, which was estimated from our Si measurements.

The signals before and after installation of the CTS are compared in Fig. 3.9. In the Cernox driven mode the reading of the Cernox on the cell (left) depends on the direction

of the field, which is not the case after our improvement in CTS driven measurement (right). As in the second type of measurement the Cernox of the VTI is not involved, it means that the whole discrepancy comes from sensor on the cell.

The heating of the cell in magnetic field due to eddy currents cannot be the reason for peaks in temperature. In this case one should expect a relaxation of the temperature in static field, which is not observed.

With this knowledge we can now calculate the temperature of the sample in magnetic field, correcting the temperature reading of the Cernox sensor on the cell by the estimated dependence on field at different temperatures, thus correcting for the undesired thermal expansion signal in magnetostriction measurements. In detail this correction presented in Subsection 3.4.1.

The capacitance sensor is not intended to be used as a primary thermometer in case of a temperature sweep, i.e. for thermal expansion measurements. Here we still use Cernox sensor, where the error introduced by a constant field is small and almost independent of temperature.

3.6 Thermal expansion

Our usual thermal expansion measurement starts at 5 K, where we adjust the pressure inside of VTI to 4 mbar (400 Pa), which was found to be the best value to keep the heating rate constant over the whole temperature range [Lor02a]. The temperature of VTI is swept with 10 or 20 mK/sec, but due to the thermal mass of the cell the temperature of the sample changes with a rate about 7 or 15 mK/sec. This is not constant but well reproducible between different runs, which is essential in order to analyze accurately our data.

Due to the finite relaxation time of the system and different heating and cooling rates, there is a hysteresis in measured signal, which comes from the temperature gradient between sample and thermometer, installed in cell. This hysteresis can be found out taking the phase transition between normal and superconducting state, which does not change with sweep rate. The obtained shifts between maxima of the peaks are around 750 mK for sweep rate of 15 mK/sec and 250 mK for 7 mK/sec. The mean values on two samples SRLW and SRL Genf (see Chapter 4) coincide with T_c^{SRLW}= 87.5 K and $T_c^{SRLGenf}$= 88.0 K (Fig. 3.11).

The measured length change $dL(T)$ is analyzed in the following way. The background (copper measurement at the same heating rate) is subtracted, and the obtained data set $dL_{noBG}(T)$ differentiating with respect to temperature, and finally the standard copper thermal expansion added [Kro77], which gives the linear thermal expansion coefficient α_i of the investigated sample, where i=(a, b, c).

We also introduced a more accurate way of measuring the length change at low temperatures. As we saw from our previous measurements, there are some discrepancies at very low temperatures, caused by friction or thermal relaxation of the epoxy glue. With up to 10 temperature sweeps in a comparatively small temperature "window" (5-100 or 5-40 K) and VTI heating rate of 10 mK/sec, the difference between subsequent loops became very small (0.5 to 150 Å over 100 K, i.e. less that 0.5 percent of the whole change!).

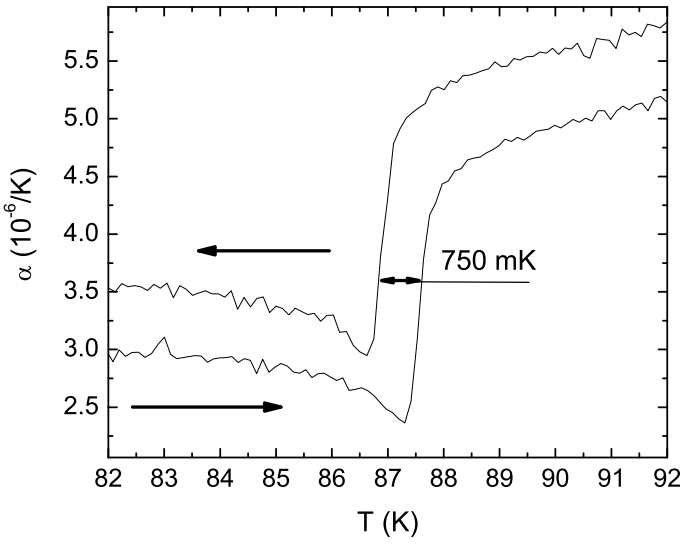

Figure 3.11: Thermal expansion data for SRLW sample (a-axis) for heating and cooling at 15 mK/sec exhibits a small temperature hysteresis due to the "dynamic" measuring technique.

The discrepancy between the first and second loop at 6 K gives us a good measure of the inaccuracy in case of "only one shot" measurements. In Fig. 3.12 one can see the series of measurements, taken on a SRLW sample along the b-axis, temperature window is (5-45 K), VTI swept with 10 mK/sec. The very first loop lies well below all the others. All following loops have a high reproducibility. We have also done these repeated experiments with and without magnetic field, the very good reproducibility gives us confidence in our measurement procedure and our data.

As a first experiment, we always performed a thermal expansion measurement without field in the whole temperature range (5-260 K) in order to find the correct minimal gap between the plates of the capacitance cell. In order to optimize our magnetostrictive measurements we would like to have the smallest gap at which we still have a linear response of the voltage to the length change, but on the other hand we should not have too small a gap to avoid that the plates touch which can destroy the sample. If the initial gap gave us too small values, we had to change it at room temperature. Also we use the collected thermal expansion data to correct the thermal drift in our magnetostriction measurements, in detail presented in Subsection 3.4.1.

We always did several thermal expansion measurements without field to check their reproducibility. Also several experiments were done during night, which gave us the possibility to get a feeling about the noise, provided by other equipment (computers, other measuring devices etc), switched off during night time. We found out that the signal did not change, and concluded that our experimental setup is well isolated.

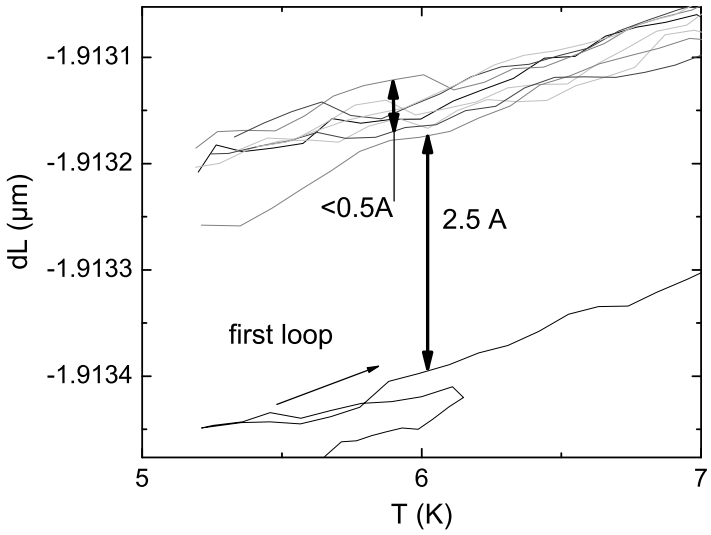

Figure 3.12: Comparison of scattering of the different heating loops, taken on the SRLW crystal in b-axis (5-40 K cycles, 7 mK/sec)

3.7 Conclusions

In this Chapter we presented our measurement technique and showed the calibrations we have done. It was found that the built-in temperature controller unit was not accurate enough in magnetic field, that is why we installed a Capacitance Temperature Sensor. We also explained the treatment of four parasitic signals, appearing in magnetostriction, and compared their effect on the measured length change.

Chapter 4

Samples and their characterization

The $YBa_2Cu_3O_{7-\delta}$ untwinned single crystals used in this work were grown by S. Tajima and A. Rykov at the Superconductor Research Laboratory, International Superconductivity Technology Center, Tokyo, Japan. Three samples have been studied: SRLW (4.3x4.1x1.3 mm^3, T_c = 87.5 K, m = 123 mg), SRL-Genf A (2.97x2x1 mm^3, T_c = 88 K, m = 33.7 mg) and SRL-Genf B (2.97x1.2x0.89 mm^3, m = 15.2 mg). The last two are pieces from same single crystal, which broke into two parts during the length measurement with micrometer. The critical temperatures of these samples are almost the same, the transitions are very sharp (width less than 0.5 K) so we assume that the doping of the samples is uniform. The SRLW sample was oxygenated over 167 hours at 450 °C and 773 bar pressure of O_2. From equation, which connect these parameters [Hong91] we expect to have $\delta \approx 0.001$. The SRL Genf was treated at 400 °C in 90 bar O_2 pressure for 200 hours. From the difference of T_c we expect $\delta \approx 0.005$ for SRL Genf samples.

The crystals have been characterized using thermal expansion, specific heat, magnetization and magnetocaloric measurements. A particularly good indicator of the sample quality is the presence of a first-order vortex melting transition, which is observed in the very best single crystals only. In the following we will show that our samples exibit a very prominent vortex melting transition in the specific heat, thermal expansion and magnetocaloric effect. The magnetization does not show a reversible jump at the melting transition, however the hysteretic behavior is quite low. Because of their relatively large size and nearly reversible behavior, these crystals are ideally suited for the present magnetostriction and thermal expansion studies.

4.1 Thermal expansion

In order to compare our two samples we performed thermal expansion measurements with and without magnetic field. Our results are presented in the Fig. 4.1. One can see that the measured thermal expansion coefficient is almost the same, indicating that the samples are both detwinned to a high degree[1]. The small difference between T_c-s may be due to experimental uncertainties, a small difference in the O-content or a slight degree of twinning in the SRL-Genf sample. The difference between the temperature of the vortex

[1]By volume <1%, investigated by inelastic neutron scattering by Dr. P. Schweiss, IFP, FZK.

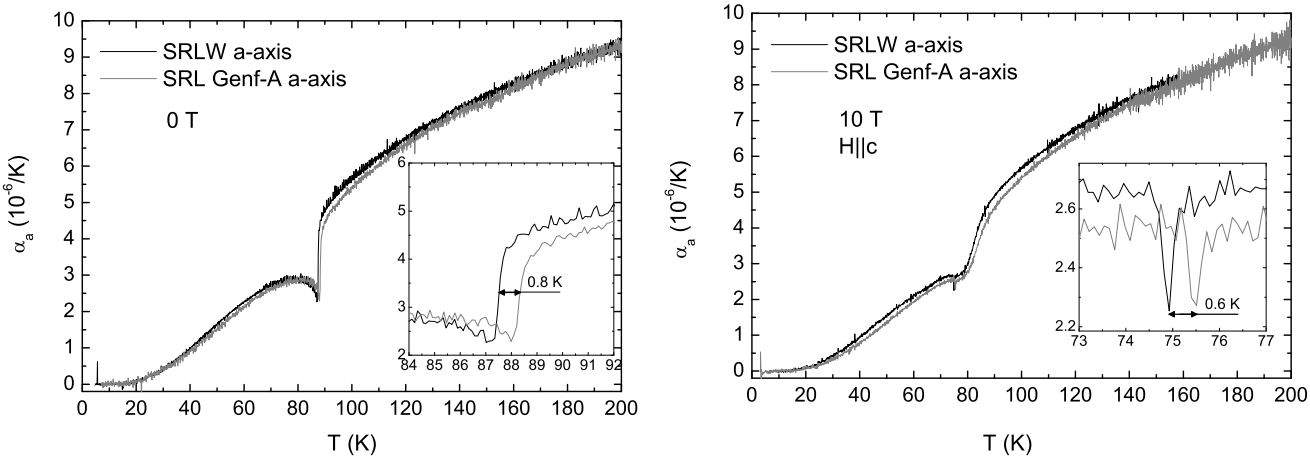

Figure 4.1: Comparison of the thermal expansion coefficients of the SRLW and SRL Genf-A samples, measured in a-direction, without field (*left*) and with 10 T (*right*). Sweep rate is 15 mK/sec. The inserts show close-ups of the superconducting (*left*) and vortex melting transitions (*right*).

melting transition at 10 T of both cuprates (0.6 K) is almost the same as that of T_c (0.8 K). The vortex melting transition in both crystals is visible as a very sharp peak, which proves the quality of our samples.

4.2 Specific heat

The specific heat of these crystals was measured in magnetic fields up to 8 T,[2] as explained in detail [Schi97]. Sharp peaks at the transition from the vortex solid to the vortex liquid were found. In fact, the entropy jump at the transition of these crystals is larger than that of any other samples measured by Dr. A. Schilling (private communication). We have also done measurements of the thermal expansion at similar magnetic fields and obtained peaks at similar temperatures (Fig. 4.2, right).

4.3 Magnetization

Magnetization measurements were performed using a Vibrating Sample Magnetometer (VSM, Oxford Instruments)[3] or the extracting magnetometer option of a Physical Properties Measuring System (PPMS, Quantum Design). Magnetization curves give the starting point to calculate the length change, based on Eq. 2.22.

The main problem of these measurements is the hysteresis, which already appears at low fields, and which prevents the accurate determination of the thermodynamical magnetization. The usual procedure is to take the mean value between up and down

[2]We appreciate kindly help of Prof. Dr. A. Schilling (University Karlsruhe).

[3]We appreciate the help of Dr. H. Küpfer and Dr. M. Uhlarz (University Karlsruhe).

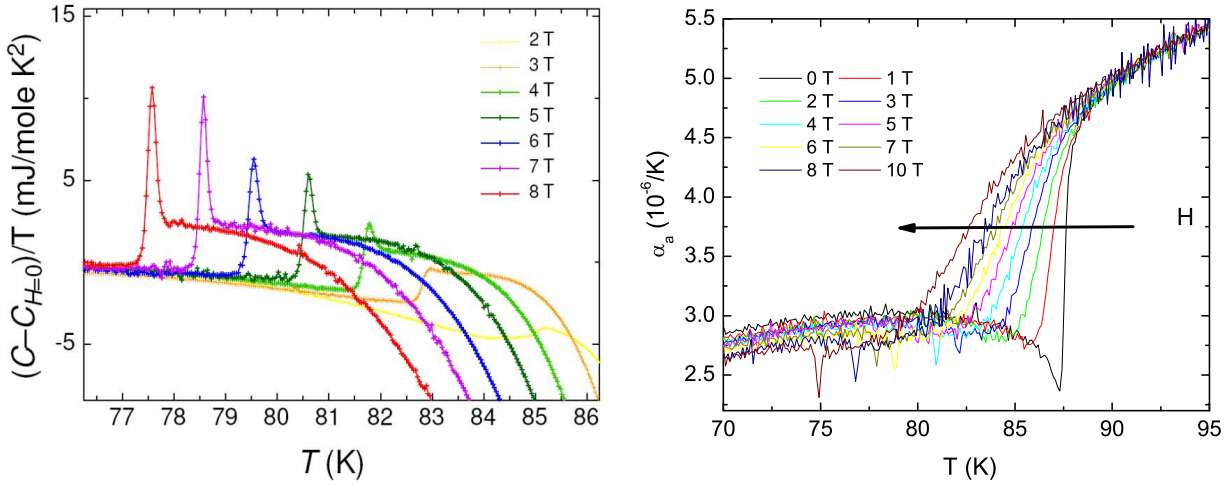

Figure 4.2: *Left:* Vortex melting transition measured using heat capacity under magnetic field. The measurements were made by Dr. A. Schilling. *Right:* Thermal expansion coefficient at different magnetic fields for the a-axis (SRLW). The arrow indicates increasing fields.

sweeps. However, this procedure gives improper results for the low field region. In order to compare the magnetization and magnetostriction we did the measurements at the same temperature; these curves are shown in Fig. 4.3. One can see that the magnetization curves, measured with the extraction magnetometer option of the PPMS, have some hysteresis up to 5 T; for higher fields, the increasing and decreasing field curves collapse. On the other hand, the magnetostriction measurements show nearly no hysteresis[4], which is an argument to use magnetostriction instead of magnetization to investigate the thermodynamics of $YBa_2Cu_3O_{7-\delta}$.

In the low temperature region the measurements are more strongly influenced by flux pinning, which means that the irreversible signal is significant in comparison with the thermodynamic signal. We used different approaches to measure the magnetization in order to distinguish between effects caused by the measuring process. If one has a superconducting sample with flux pinning, then the moving sample will "shake" the vortices; the distribution of the trapped magnetic flux will be changed [Avr01], depending on the amplitude and frequency of the movement of the sample in the magnetic field. These parameters which are different in VSM and PPMS. A more detailed analysis of the magnetization is given in the Appendix, where the vortex matter is considered more carefully.

As it was not possible to get reversible magnetization curves from these measurements, indeed we used the theoretical magnetization, calculated from approximated solution of the Ginzburg-Landau equations. Also, one can use the experimental magnetization curve only up to vortex lattice melting transition. This is discussed in more detail in Section 6.6.

[4]We would like to stress that magnetostriction measurement were treated without taking the mean value of the increasing and decreasing curves. Indeed, some hysteresis is always present, but at this temperature it is orders of magnitude smaller than in magnetization.

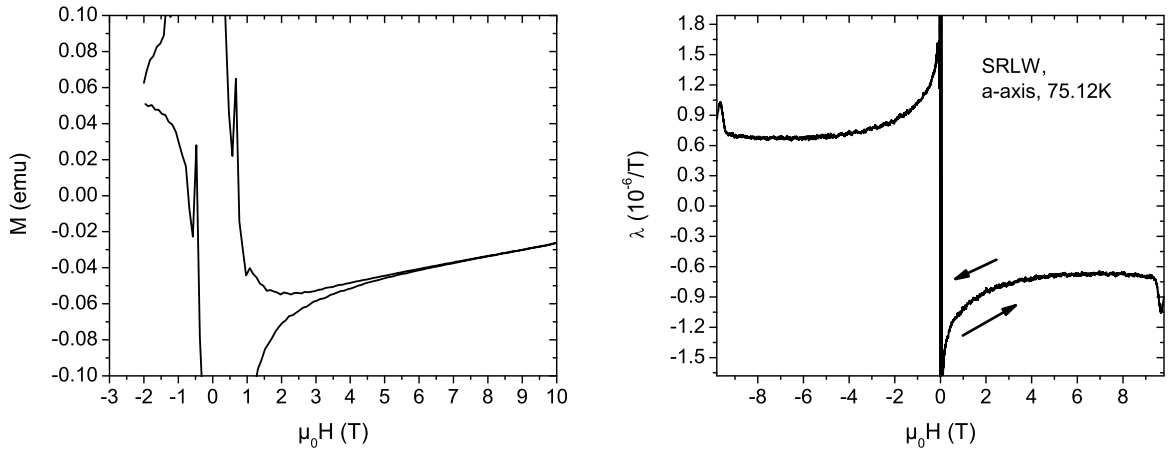

Figure 4.3: Comparison of magnetization (75 K, 0.3 T/min, *left*) and magnetostriction (75.12 K, 0.5 T/min, *right*) measurements on the SRLW sample. There is almost no hysteresis in the low field region of the magnetostriction.

4.4 Magnetocaloric effect (MCE)

Magnetocaloric measurements were done by the Geneva group[5]. In Fig. 4.4 are shown four magnetocaloric coefficients M_T measurements (see Eq. 2.16) for temperatures below T_c. The vortex melting transition is very well defined, as we observed in the thermal expansion and specific heat measurements. At lower temperature, M_T also shows irreversibility due to flux pinning.

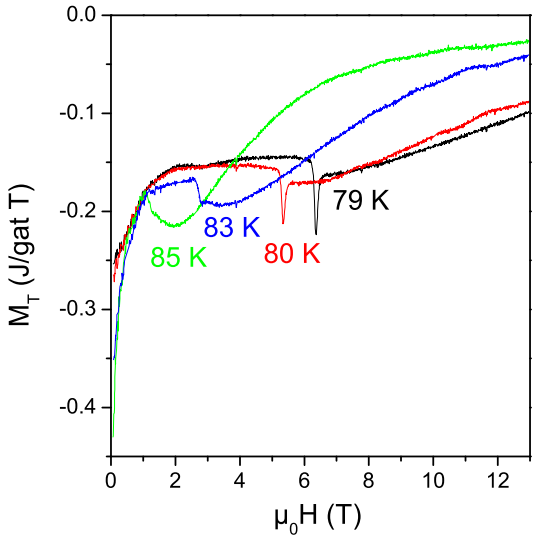

Figure 4.4: Magnetocaloric effect coefficient for temperatures 79, 80, 83 and 85 K for sample SRL Genf. The measurements were made by Dr. R. Lortz, Dr. T. Plackowski, Prof. Dr. A. Junod in Geneva.

[5]Dr. R. Lortz, Dr. T. Plackowski, Prof. Dr. A. Junod.

Chapter 5

Results of magnetostriction and thermal expansion measurements

Since $YBa_2Cu_3O_{7-\delta}$ is an orthorhombic material, we measured its thermal expansion and magnetostriction along the three primary axes (a, b and c). The magnetic field was applied along the c-axis, because the superconducting order is most easily destroyed along this direction. We could not fully suppress the ordered state due to high values of the upper critical field H_{c2} at temperatures $T << T_c$ (extrapolated to more than 100 T at $T = 0$). In this Chapter we report our results gathered in magnetostriction and thermal expansion measurements. We explain also the methods used to avoid the undesired irreversible signal due to flux pinning at $T \leq 50$ K.

5.1 Magnetostriction for different axes

In Figures 5.1-5.3 are shown the magnetostriction curves obtained for temperatures between 43 and 120 K. The relative length change is plotted with an offset for clarity for the three different axes. The curves have been corrected for the thermal drift, the eddy current effect, the cell background and the cell drift. Let us check the evolution of the magnetostriction with decreasing temperature on the a-axis data (Fig. 5.1). For $T > T_c$, there is almost no signal. Below the critical temperature the signal becomes bigger with decreasing temperature. This signal is maximal at 79 K, and for T <79 K the magnetostriction becomes smaller again. At 65 K a hysteresis appears, which becomes larger with decreasing temperature; one can see also several structures in the hysteresis curves. This will be discussed in more detail in the Appendix. Magnetostriction measurements were done only down to 43 K in order not to destroy the sample due to the large pinning forces. As shown in Figures 5.1-5.3, the qualitative response from the three axes is very similar, the a- and b-axis response is of similar magnitude, but of opposite sign, and the c-axis response has the same sign as the a-axis one, but is about a factor of 4 smaller in magnitude. The irreversibilities appear at the same temperatures for all axes.

The analysis of these curves is done in detail in Chapter 6. The next section is devoted to the estimation the reversible signal from the irreversible measurements. We did also similar measurements on the SRL Genf-A sample, the results being presented in Fig. 5.4

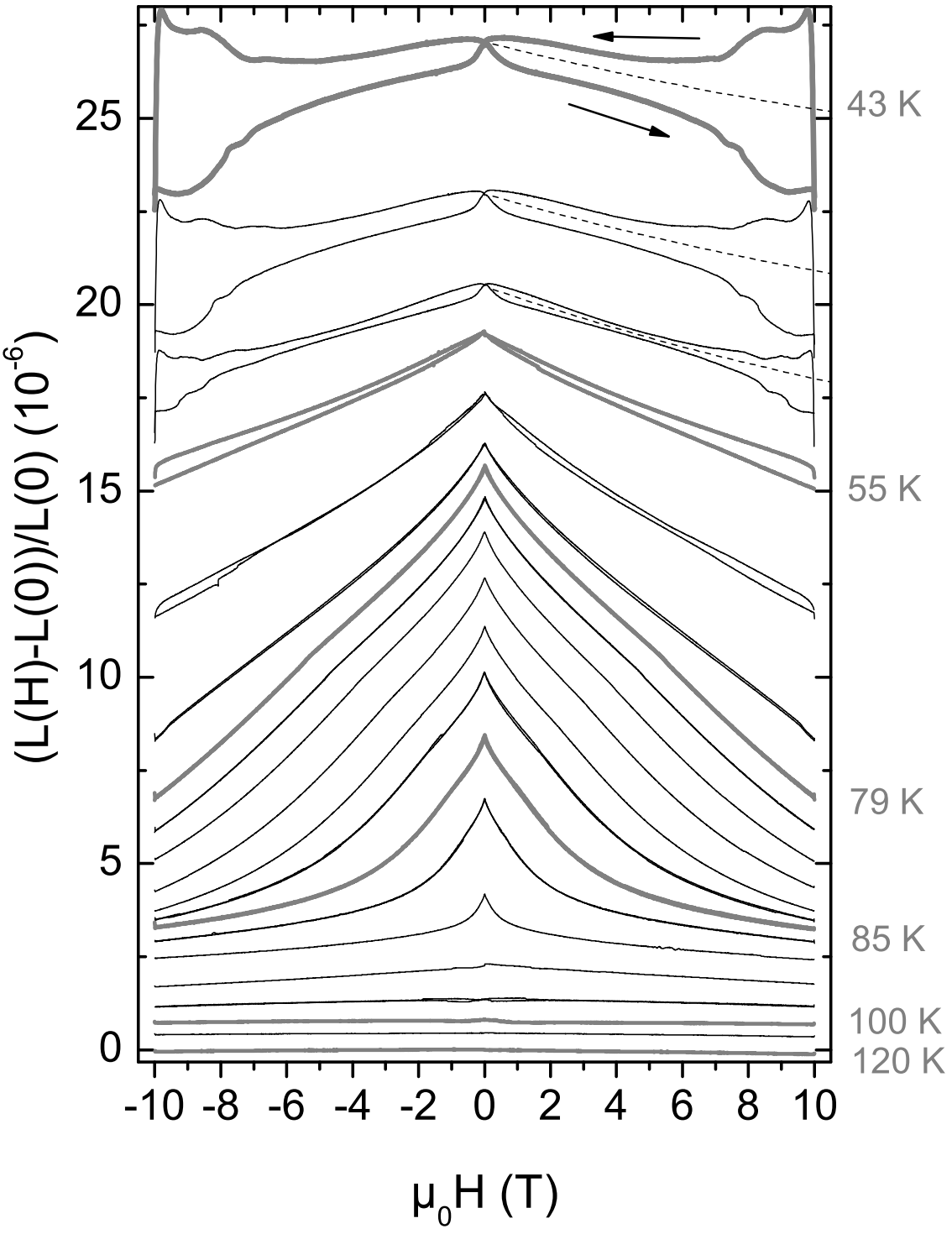

Figure 5.1: *a*-axis magnetostriction for different temperatures for the SRLW sample. The data have been offset for clarity. Temperatures are: 43, 45, 48, 55, 65, 75, 79, 80, 81, 82, 83, 84, 85, 86, 87, 87.5, 90, 100 and 110 K. The dashed lines show the approximated reversible signal for the hysteretic curves (see text).

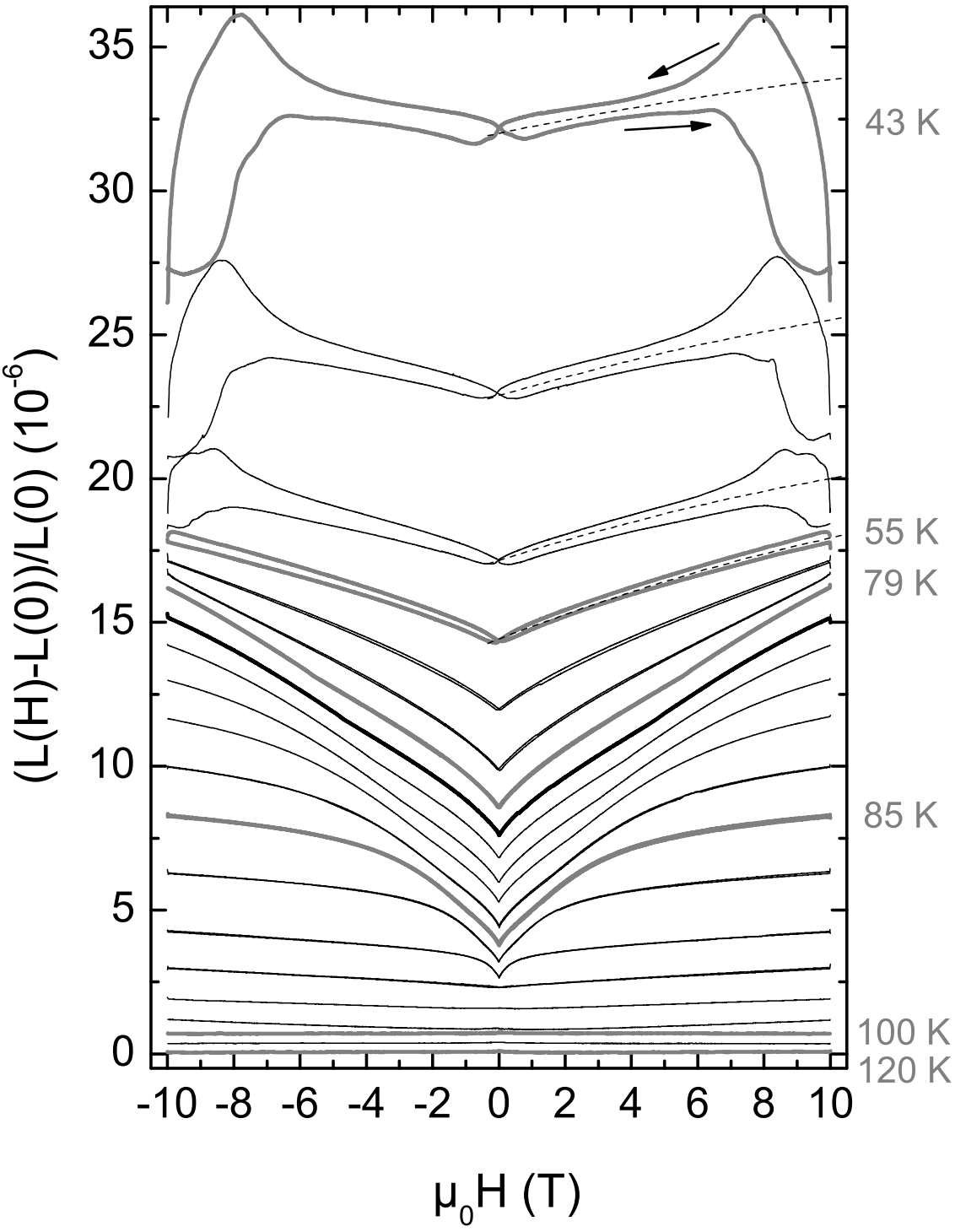

Figure 5.2: *b*-axis magnetostriction for different temperatures for the SRLW sample. The data have been offset for clarity. Temperatures are: 43, 45, 48, 55, 65, 75, 79, 80, 81, 82, 83, 84, 85, 86, 87, 87.5, 90, 100 and 110 K. The dashed lines show the approximated reversible signal for the hysteretic curves (see text).

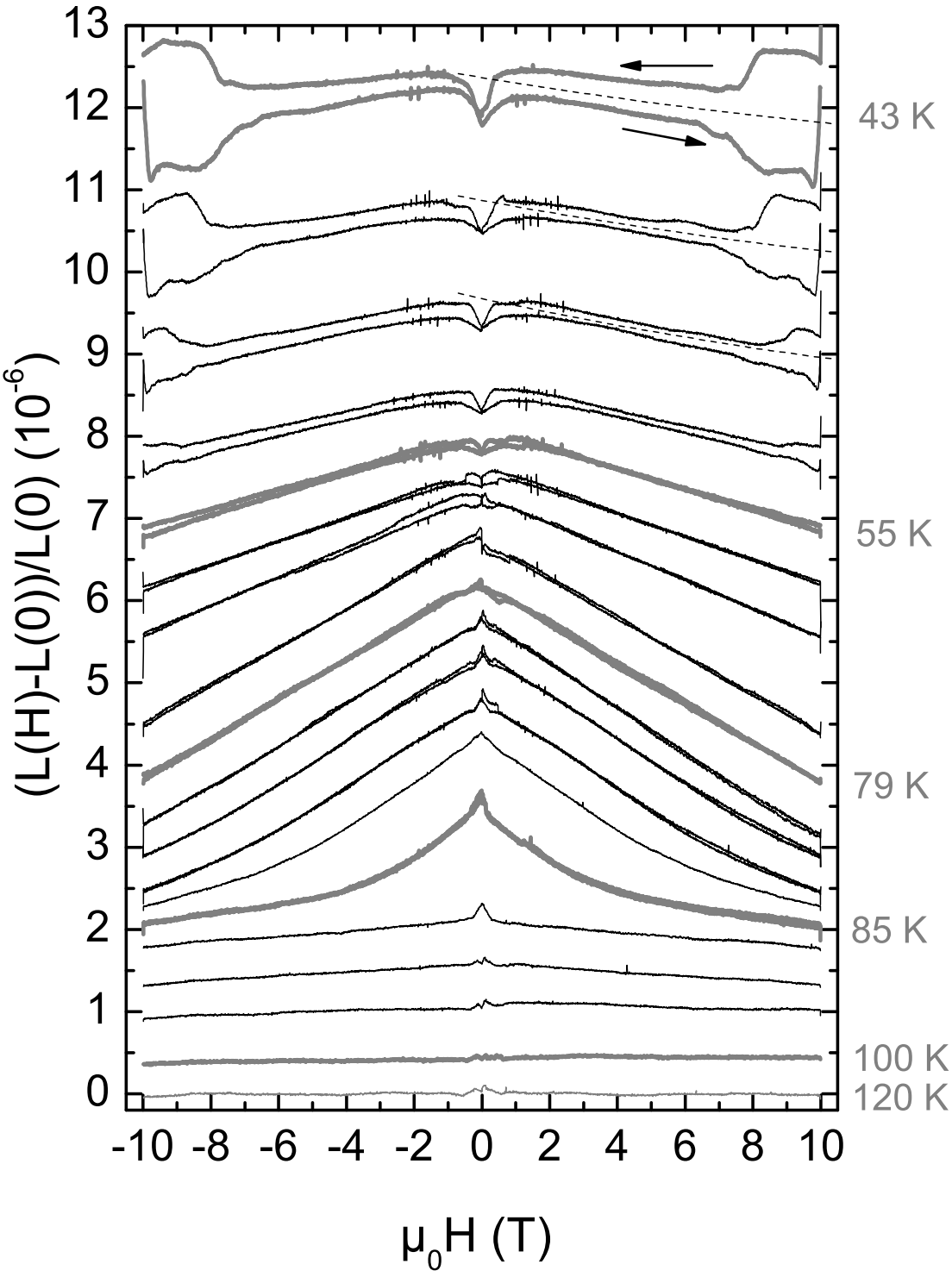

Figure 5.3: *c*-axis magnetostriction signal for different temperatures for the SRLW sample. The data have been offset for clarity. Temperatures are: 43, 45, 48, 50, 55, 60, 65, 75, 80, 81, 82, 85, 87, 90, 100 and 120 K. The dashed lines show the approximated reversible signal for the hysteretic curves (see text).

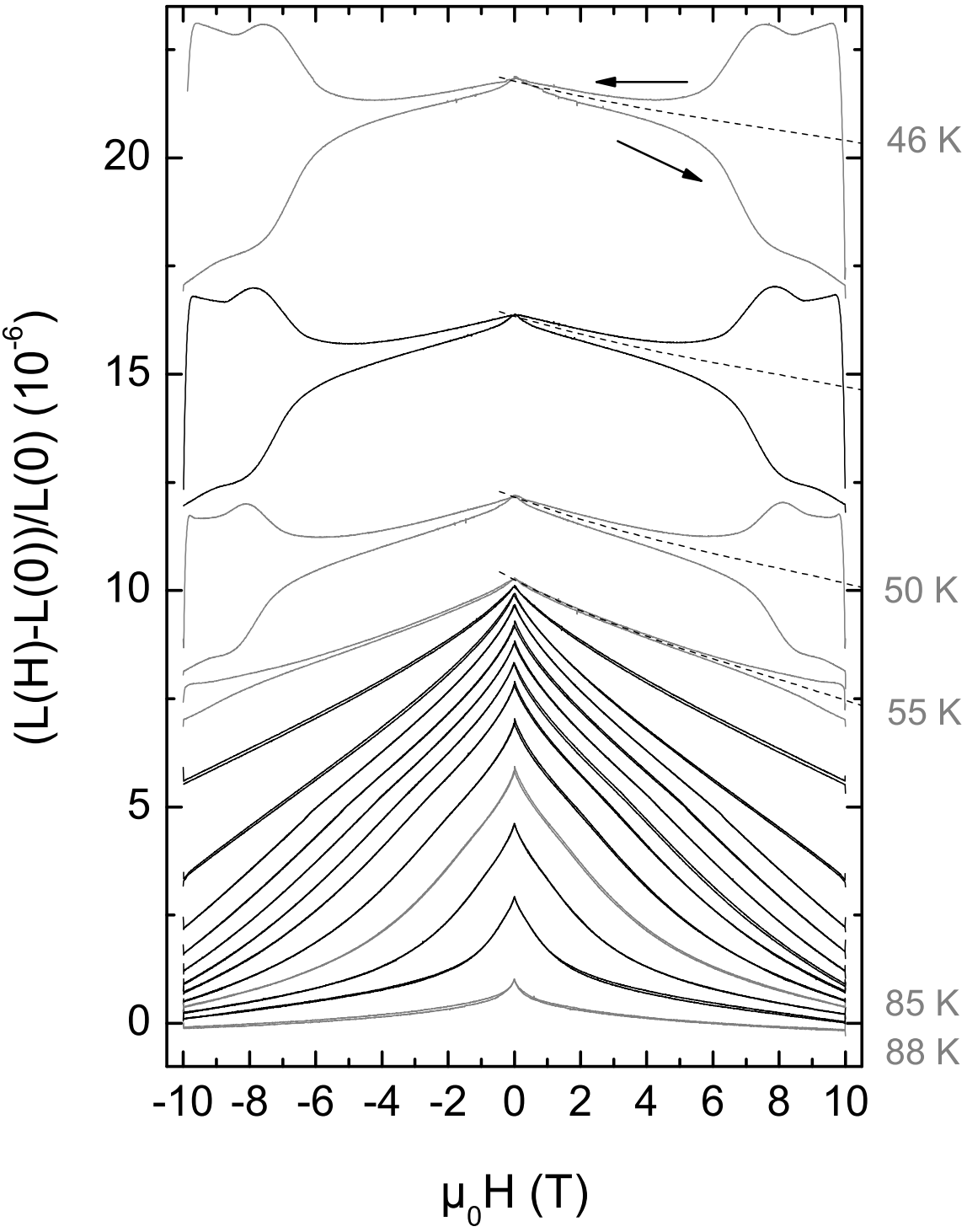

Figure 5.4: *a*-axis magnetostriction signal for different temperatures for the SRL Genf-A sample. The data have been offset for clarity. Temperatures are: 46, 48, 50, 55, 65, 75, 79, 81, 82, 83, 84, 85, 86, 87 and 88 K. The dashed lines show the approximated reversible signal for the hysteretic curves (see text).

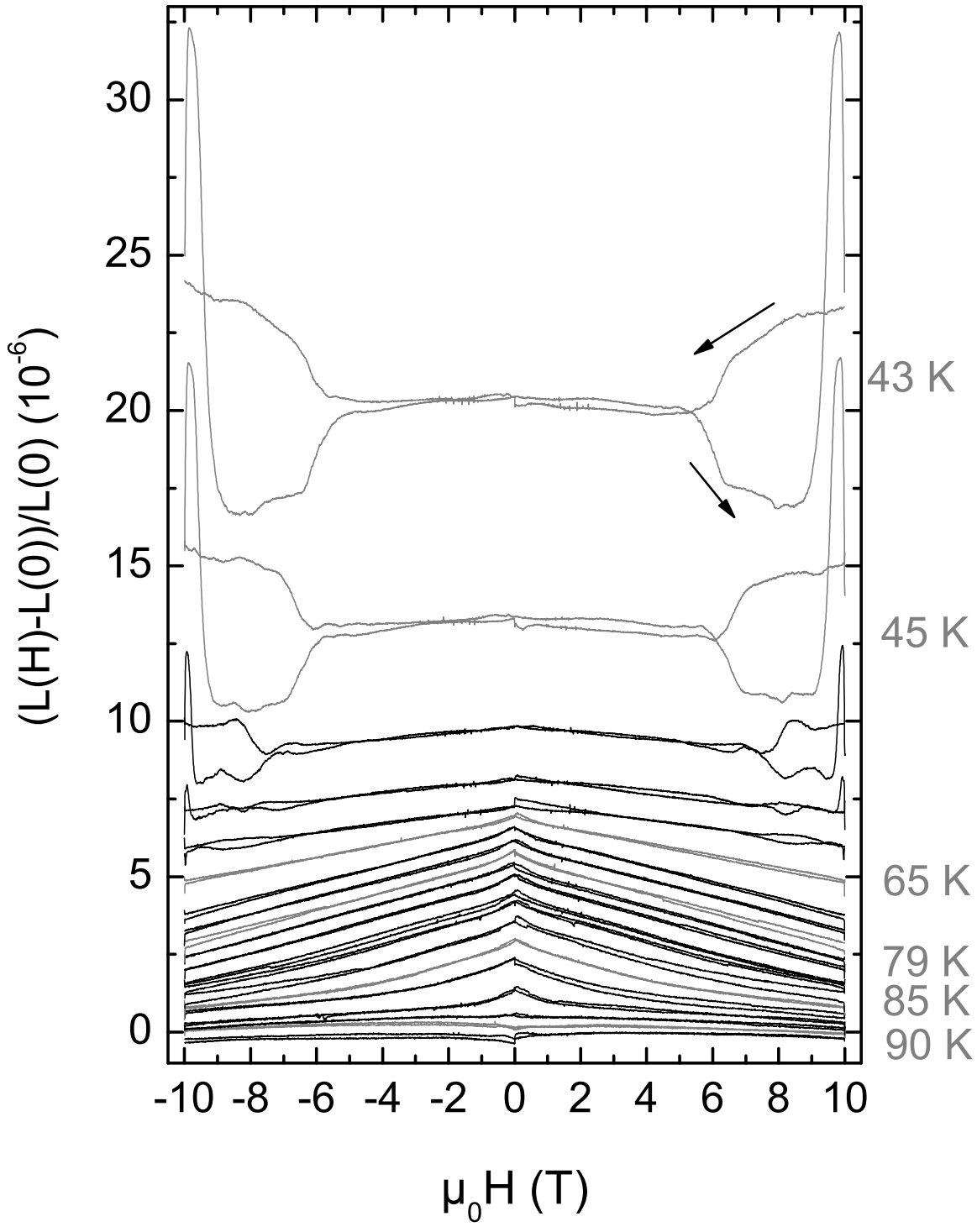

Figure 5.5: *c*-axis magnetostriction signal for different temperatures for the SRL Genf-A sample. The data have been offset for clarity. Temperatures are: 43, 45, 55, 65, 77, 78, 79, 80, 81, 82, 83, 84, 85, 86, 87, 88, 90 and 95 K (see text).

and Fig. 5.5. The behavior in magnetic field of the different axes is similar in different samples in the reversible region. However, the hysteresis appears more quickly at low temperatures for the SRL Genf-A crystal, which is probably due to a larger density of the pinning centers compared to the SRLW sample.

5.2 Reversible signal obtained from irreversible measurements

As the temperature decreases, the measured magnetostriction becomes more and more irreversible. Changing the temperature from 45 to 43 K (Fig. 5.1) leads to a two times bigger hysteresis of the magnetostriction curve along the a-axis. On the other hand, the reversible part of the signal decreases with decreasing temperature. This means that the reversible thermodynamic magnetostriction, which interests us, becomes quickly overwhelmed by the irreversible response as temperature is decreased. Knowing the temperature dependence of the eddy current signal (Section 3.4.2) permits us to correct the measured signal such as not to loose the valuable information about the hysteresis coming from the sample[1].

In order to obtain the thermodynamic signal in the irreversible region, we proceeded as follows: first, we averaged the increasing and decreasing field curves to eliminate a large irreversibility and then scaled the last reversible curve (at 55 K) by an appropriate factor to these averaged curves between 1 T and 5 T, where the hysteresis is the smallest. This temperature dependent factor was found to be the same at given temperature for different axis of the same sample, which is ensure the correctness of our procedure.

In Figure 5.6 we show that with this scaled curve (red line) leads to a rather good fit of the "mean values" (open circles), obtained from the fully corrected magnetostriction curves (black lines), up to 7 Tesla. This scaling gives us the value for the thermodynamic signal higher than 7 T, for instance, between 10 and 0 T we expect to have around 77 Å reversible magnetostrictive signal (Fig. 5.6) if there were no irreversibilities caused by pinnings. The small discrepancy between the fitted curve and the mean signal in the low field region (up to 1 T) is attributed to the non-symmetric irreversibilities, caused by the establishment and destruction of the critical state. The thermodynamic signal obtained with this procedure for temperatures corresponding to the irreversible region, is indicated in Figures 5.1-5.4 by a dashed black line (a-, b- and c-axis for the SRLW sample, and a-axes for SRL Genf-A sample).

5.3 Thermal expansion

As seen in the previous section, the reversible thermodynamic signal at 43 K, which is only the half of T_c, is already difficult to obtain. Does it mean that with our measuring

[1] Averaging over the increasing and decreasing curves of the magnetostriction would lead to the loss of the information about the irreversible signal caused by vortex pinning etc. All curves, already presented in Figures 5.1-5.5 were corrected as presented in Section 3.4.2. In the reversible region only eddy current effects lead to a hysteresis in magnetostriction measurement which is easy to accounted for.

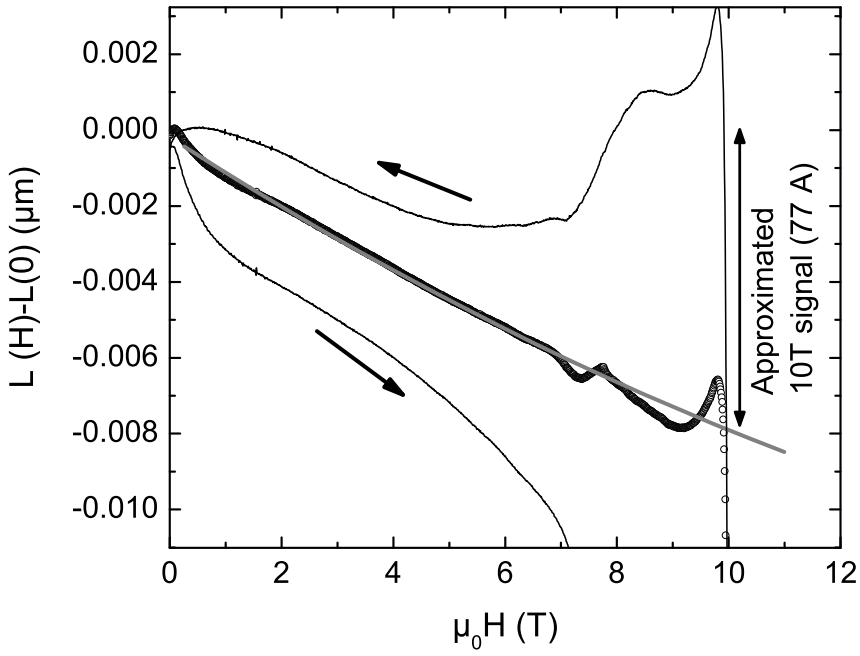

Figure 5.6: Irreversible magnetostriction signal for the a-axis of SRLW sample at 43 K. The arrows shown the direction of the field sweep. The open circles show the mean value between increasing and decreasing field curves; the gray line is the reversible magnetostriction curve measured at 55 K, scaled by an appropriate factor to fit the mean value.

technique we could not gather more information about the reversible magnetostriction for lower temperatures? The answer is *yes* for the direct magnetostriction experiment, and *no* if we make some very simple considerations. As we measure the length change with altering either the magnetic field or the temperature, our experimental data can be seen as the surface $dL(H,T)$ in a three dimensional space (dL,H,T). In order to calibrate our results we assume $dL(0,0) \equiv 0$. In a magnetostriction measurement the temperature is kept constant and the magnetic field is tuned from -10 T to +10 T. In the case of a thermal expansion measurement in field we tune the temperature from 4 to 300 K, keeping the field constant. The same length change $dL(H,T)$ is measured either in magnetostriction measurement at constant temperature T for a field H, or for a thermal expansion experiment at constant field H for a temperature T. In the first case $dL(H,T)$ is the difference between the length measured at the field H and the length measured at $H = 0$. In the second case, $dL(H,T)$ is the difference between two curves measured at magnetic field H and at $H = 0$ for the same temperature T. Consequently, from thermal expansion measurements made at different fields applied before cooling through T_c, we can obtain the reversible magnetostrictive signal down to 4 Kelvin. As the field does not change, no critical state is induced, so one obtains less irreversibilities.

We have therefore done a set of thermal expansion measurements along a-, b- and c-axes for the SRLW sample and along the a- and c-axes for the SRL Genf-A sample. The magnetic field was almost always applied at temperatures higher than T_c to avoid

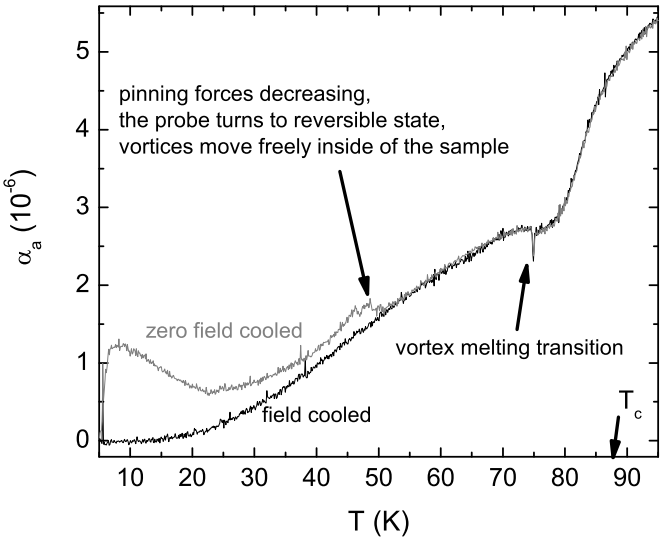

Figure 5.7: Thermal expansion coefficients along the a-axis of sample SRLW at $\mu_0 H$=10 T. The black curve is the usual measurement with the field applied above T_c, and the gray one is the the zero-field-cooled measurement, in which the field was applied at 5 K. Both curves were obtain upon heating.

the trapping of vortices. The thermal expansion measurements were done with 7 or 15 mK/sec sweep rates with a constant applied field.

Only once have we done a thermal expansion experiment with increasing magnetic field up to 10 T (sweep rate 0.5 T/min) at 5 K. The reason was the very high risk to damage the sample. The penetrating magnetic vortices are trapped by pinning centers, the increasing field pushes them further, causing a tension on the sample, and leading to microcracks. If the pinning forces are big enough (they have their maximum at zero K) the magnetic field sweep would pulverize the crystal. In our case the jump at 5 K was 1100 Å, $dL/L = 2.6 \cdot 10^{-4}$ which is equal to the thermal expansion of the sample over a temperature interval of more than 50 K! This signal of more than thousand Å is actually the magnetostriction, caused by pinning forces, which is almost three times bigger than the maximum measured thermodynamic signal on the same sample for this axis (around 360 Å at 80 K).

In Figure 5.7 are shown the field cooled (black) and zero field cooled (gray) thermal expansion measurements. In the zero field cooled curve there is a jump around 5 K, due to flux induced magnetostriction: the vortices build up a critical state inside the superconductor with increasing magnetic field. There is some gradient in the vortex density, which is decreasing toward the middle of the sample, the simplest shape of this decrease is linear, which is described by the Bean model [Bea62]. Upon heating the sample the pinning forces decrease, the mobility of pinned vortices rises, allowing a smaller gradient, there is less and less difference between field cooled and zero field cooled curves. At the temperature of around 50 K this gradient disappears, showing the crossover from irreversible to reversible state at this field. Based on this measurement we would expect almost reversible behavior of magnetostriction above 50 K. For lower values of applied magnetic field the temperature of this crossover will decrease.

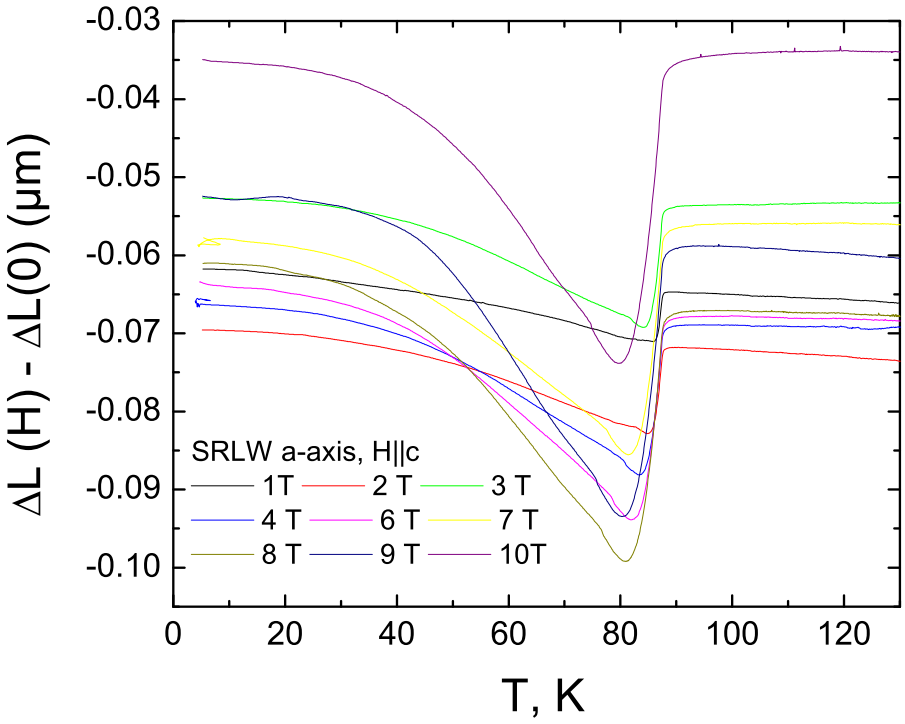

Figure 5.8: Length difference between field and zero-field thermal expansion measurements as a function of temperature for SRLW sample (a-axis). The temperature was cycled between 4 K and 260 K. The data do not vary in a consistent manner due to the non-reproducibility of the cell.

5.4 Combining of thermal expansion and magnetostriction measurements

In this part we will use the quantity $\Delta L(H,T)$, defined as the difference between thermal expansion measurements with a magnetic field H and without magnetic field at a same temperature T:

$$\Delta L(H,T) = L(H,T) - L(0,T), \tag{5.1}$$

The variation with T of $\Delta L(H,T)$ for different applied fields is plotted in Fig. 5.8. Despite using the same $dL(0,T)$ measurement, there is a scatter between different $\Delta L(H,T)$ curves, caused by dissaligment of the plates, caused by thermal cycling over long time - these measurements cover more than one month. This is a known issue (Chapter 3.6), in order to avoid it one can measure in a smaller temperature range with lower temperature sweep range.

$\Delta L(H,T)$, obtained from magnetostriction measurements[2] was used to shift the thermal expansion curves vertically until coincidence was obtained. The results for 10 T for different axes are plotted in Fig. 5.9, 5.10 and 5.11.

[2]Note that magnetostriction measurement have no background problems, i.e. $\Delta L(0,T) \equiv 0$.

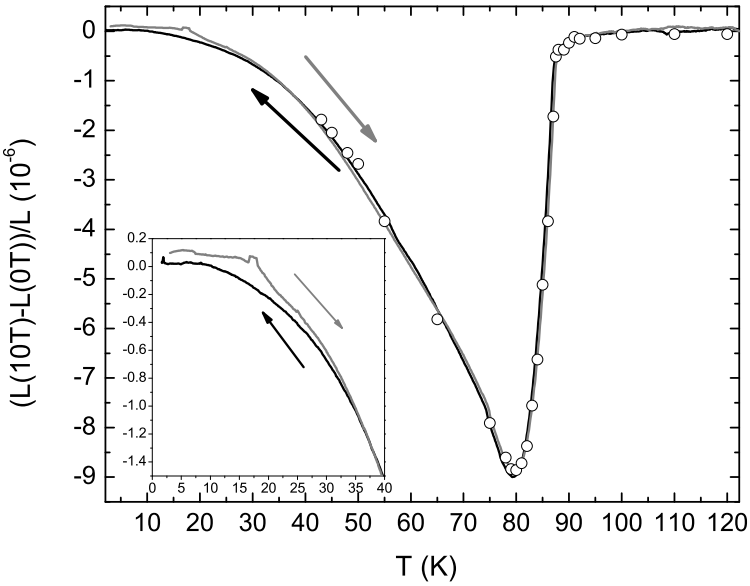

Figure 5.9: Length difference between 10 T and 0 T thermal expansion data (solid lines), obtained by repeating cycling of the temperature in a limited temperature interval (2-150 K), which considerably reduces the non-reproducibility of the cell (see Fig. 5.8.). The open circles are from the 10 T magnetostriction data. The good coincidence between the results of these two measurement techniques allow us find the thermodynamic reversible magnetostriction down to 5 K. The cooling curves are black, the heating ones are gray. SRLW sample, *a*-axis. *Insert:* Low temperature part.

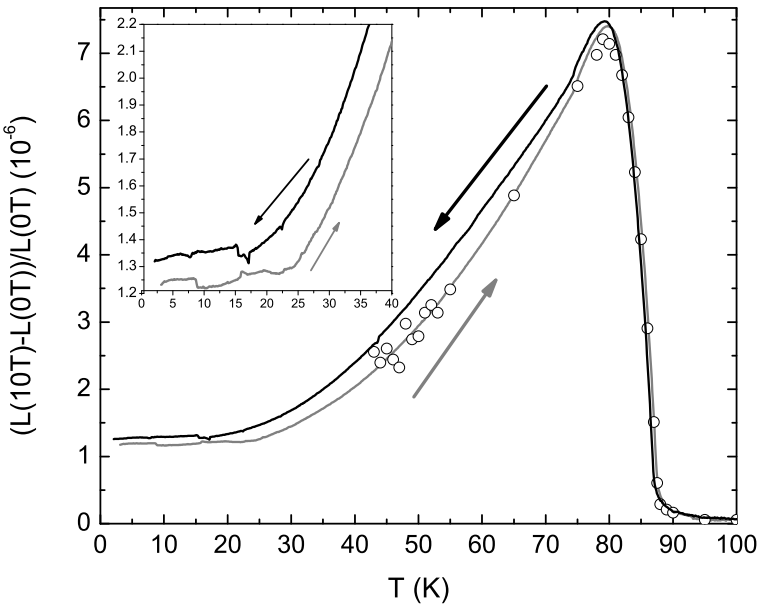

Figure 5.10: Length difference between 10 T and 0 T thermal expansion data (solid lines), obtained by repeated cycling of the temperature in a limited temperature interval (2-150 K), which considerably reduces the non-reproducibility of the cell (see Fig. 5.8.). The open circles are from the 10 T magnetostriction data. SRLW sample, *b*-axis. The good coincidence between the results of these two measurement techniques allow us find the thermodynamic reversible magnetostriction down to 5 K. The cooling curves are black, the heating curves are gray. *Insert:* Low temperature part.

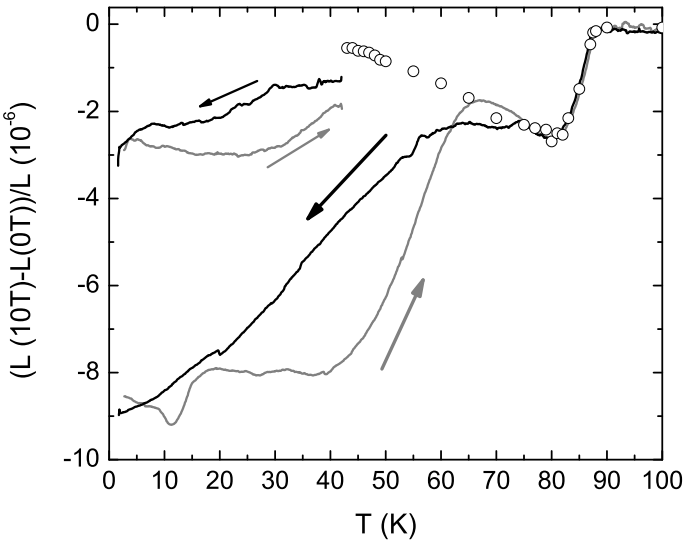

Figure 5.11: Length difference between 10 T and 0 T thermal expansion data (solid lines), obtained by repeating cycling of the temperature in a limited temperature interval (2-150 K), which considerably reduces the non-reproducibility of the cell (see Fig. 5.8.). The open circles are from the 10 T magnetostriction data. The cooling curves are black, the heating ones are gray. Also measurements up to 40 K are shown, done in slow mode. In contrast to the a- and b-axes data (Fig. 5.9 and Fig. 5.10.), no reliable data could be obtained for the $c-$axis due to small thermodynamic signal and small length of the c-axis. SRLW sample, c-axis.

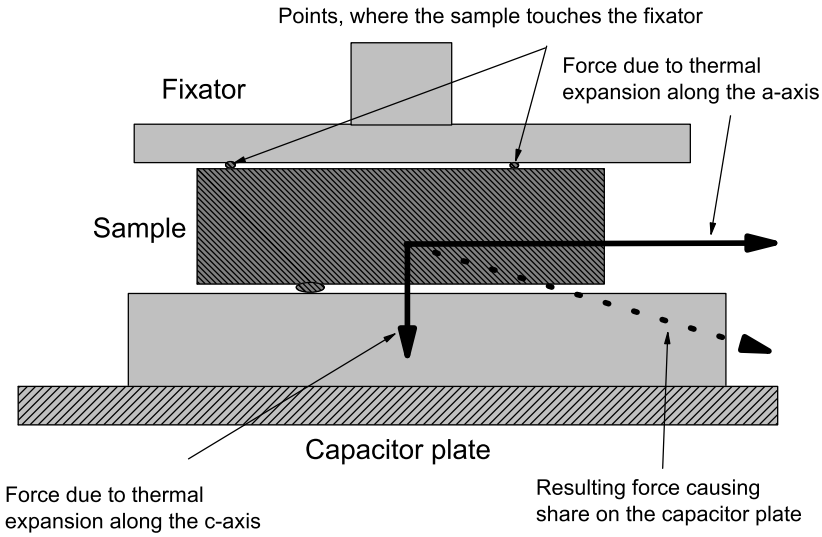

Figure 5.12: c-axis measurement problem. The thermal expansion along the $a-$ and $b-$axes along with small dimension of $c-$axis causes a shear on capacitor plates. This parasitic signal can be much higher than the thermal expansion along the $c-$axis. This is the reason for discrepancy between magnetostriction and thermal expansion 10 T - 0 T in Fig. 5.11.

With this procedure, a good coincidence of the thermal expansion curves and magnetostriction points is obtained over the whole T range where both measurements overlap, although a discrepancy between them develops at low fields, which is attributed to the experimental error. For the data measured along the c-axis, the large discrepancy is due to fact that the length change is small, which leads to a big error. Also a thermal expansion along the a and b axes can generate a shear on the fixators, which is detected as a signal along c-axis (Fig. 5.12.).

5.5 Hysteresis in the length change

Figures 5.9, 5.10 and 5.11 present a hysteresis between heating and cooling curves.

This hysteresis is believed to be an intrinsic property of the sample, caused by irreversibilities. The a-axis shows less irreversibility than the b-axis, a good agreement being obtained with the irreversible magnetostriction measurements (Chapter 5.1). For the measurements along the c-axis the thermal expansion data below $T = 60$ K do not match with the magnetostriction points, because of the hysteresis - magnetostriction measurements lead to better data than thermal expansion measurements.

5.6 Conclusions

We have presented our main results and a way to correct the undesired irreversible signal. We also introduced a method to combine thermal expansion and magnetostriction measurements in order to obtain the low temperature reversible signal. However, some hysteresis between heating and cooling curves remains even in our best quality thermal expansion measurement in magnetic field, which is attributed to the pinning forces.

Chapter 6

Analysis of the reversible magnetostriction

The expression for the magnetostriction of a classical superconductor, Eq.(2.22) in Chapter 2, is repeated here for discussion purposes. As can be seen, $\Delta L(H)$ has four different contributions resulting from the pressure dependence of the volume, the zero-temperature thermodynamical critical field, T_c and of κ. It is goal of this Chapter to investigate to what extent the magnetostriction curves from Chapter 5 can be described using this equation. In the first part of this Chapter (Sections 6.1-6.3) it is argued that the primary term governing the magnetostriction comes from the third term proportional to dT_c/dp_i. Then using values of H_c and compressibility derived from field dependent specific heat measurements [Lia04], the magnetostriction curves will be fitted in order to obtain quantitative values of dH_{c0}/dp_i. This information is then used to extrapolate the length changes up to H_{c2} and to estimate the uniaxial pressure dependence of the Sommerfeld constant. The plausibility of these results is checked by comparing the results to the zero-field thermal expansion data. Finally, an attempt is made to converge these results, which is based on a classical (non-fluctuation) state, with the strong 3D XY fluctuation dominated regime near T_c.

$$\begin{aligned}\frac{\Delta L_i(H)}{L_i(0)} = \frac{L_i(H) - L_i(0)}{L_i(0)} &= \frac{1}{L_i}\frac{\partial L_i}{\partial p_i}\mu_0 H_{c0} g(T) \int_0^H f dH + \\ &+\mu_0 \left(\frac{\partial H_{c0}}{\partial p_i} g(T) + H_{c0}\frac{T}{T_c}\frac{dg(T)}{dT}\frac{dT_c}{dp_i} \right) \int_0^H \left(f - H\frac{\partial f}{\partial H} \right) dH + \\ &+\frac{\partial \kappa}{\partial p_i}\mu_0 H_c \int_0^H \frac{\partial f}{\partial \kappa} dH \end{aligned} \tag{6.1}$$

The first term gives the response of the sample to the expelled field, which is proportional to the compressibility, the second one is the signal from pressure dependencies of critical field and critical temperature. The third term in equation 6.1 is responsible for the shape

change of the magnetostriction curve, but this term is reported to be small and the integral over the field range $(0 - H_{c2})$ is zero [Bra73]:

$$\frac{\partial \kappa}{\partial p_i} \mu_0 H_c \int_0^{H_{c2}} \frac{\partial f}{\partial \kappa} dH \equiv 0.$$

6.1 Calculation of the pressure dependence of the critical temperature from Ehrenfest relation

From all pressure dependencies presented in equation 6.1 the most often investigated ones are the pressure dependencies of the critical temperature, also for different oxygen contents. There are several possibilities to find out these values, i.e. using the direct measure of the magnetization under pressure [Wel92],[Wel94] or the jump at the critical temperature [Mei91],[Pas00] or the vortex melting transition [Lor02a] in thermal expansion experiment. As these values are strongly dependent on the crystal quality - twinning will decrease the difference between pressure dependencies along *a*- and *b*- direction - and oxygenation, we have done the calculation of this parameter based on our data.

The heat capacity of the SRL Genf crystal was measured by an adiabatic calorimetry method by Dr. Y. Wang at Geneva, and the data were given to us prior to publication. As molar volume we used value $V_{mol} = 1.04 * 10^{-4}$ m^3/mol calculated from crystal lattice parameters [Kru97]. We followed the graphical method, described by V. Pasler in his PhD thesis, to obtain the jumps in the α_i, obtaining on heating. Using the Ehrenfest relation, given by Eq. 2.14, we obtain the values of the pressure dependencies of the critical temperature for different axes. Calculated values are presented in Table 6.1 together with data of V. Pasler for fully doped YBCO.

axis	SRLW, $\delta \approx 0.001$	SRL Genf, $\delta \approx 0.005$	$\delta < 0.001$[Pas00]
dT_c/dp_a (K/Pa)	$(-2.97 \pm 0.2) * 10^{-9}$	$(-2.91 \pm 0.1) * 10^{-9}$	$-3.41 * 10^{-9}$
dT_c/dp_b (K/Pa)	$(2.48 \pm 0.2) * 10^{-9}$	*n.a.*	$2.991 * 10^{-9}$
dT_c/dp_c (K/Pa)	$(-0.86 \pm 0.2) * 10^{-9}$	$(-0.75 \pm 0.1) * 10^{-9}$	$-0.87 * 10^{-9}$

Table 6.1: Uniaxial pressure dependence of the critical temperature of different samples calculated using the Ehrenfest relation for different axes.

6.2 Scaling of magnetostriction curves for different axes

The magnetostriction data of the axes in Figures 5.1-5.3 all have very similar field-dependent shapes; what differs is the magnitude and sign of the effect. This suggests

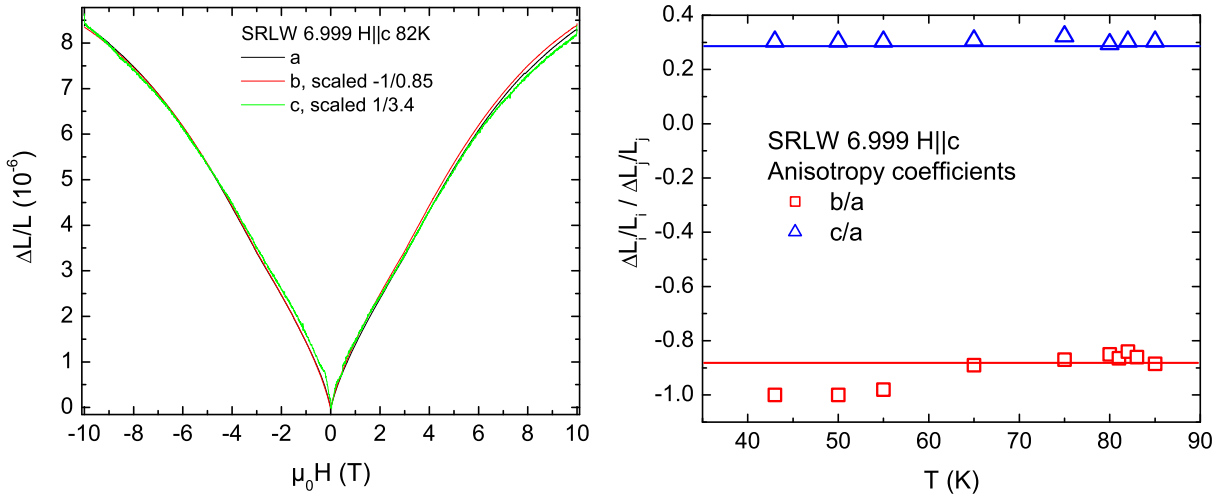

Figure 6.1: *Left:* Scaling of the magnetostriction signal for different axes, SRLW sample, at 82 K,. *Right:* Temperature dependence of the scaling coefficient. The lines show the ratios between the corresponding uniaxial pressure dependencies.

that one can scale the ΔL curves along the different directions with a constant factor. Fig. 6.1, *left*, shows that this type of scaling in fact works quite well for sample SRLW at $T = 82$ K, and the scaling ratios obtained are presented as a function of the temperature in Fig. 6.1, *right*. For temperatures near T_c we found that the scaling coincides with the relation between pressure dependence of critical temperature of the corresponding axes, calculated from the Ehrenfest relation at a second order transition:

$$\frac{\lambda_b}{\lambda_a} = -0.85 \approx \frac{\frac{dT_c}{dp_b}}{\frac{dT_c}{dp_a}} = -0.84 \qquad \frac{\lambda_c}{\lambda_a} = 0.29 = \frac{\frac{dT_c}{dp_c}}{\frac{dT_c}{dp_a}} = 0.29$$

This result implies that the driving force of the magnetostriction is the pressure dependence of the critical temperature, at least, in the region between 65 and 88 K. The discrepancy between measurement along c-axis and the pressure dependence along this direction is due to the small size of the crystal in this dimension, and the expected signal is also much smaller than along the other directions[1]. This simple scaling between axes does not hold at lower temperature, where another pressure dependence influences the length change.

6.3 Comparison of the magnetocaloric and magnetostriction coefficients

Fig. 6.2 shows that the magnetostriction coefficient λ of the a-axis (SRL Genf-A) and the magnetocaloric coefficient M_T can also be scaled at three different temperatures using a

[1]Three times smaller signal and more than three times smaller dimension, which gives us circa 10 times smaller measured signal.

simple scaling factor $4.60 \cdot 10^{-6}$ (g $\cdot$ at/J) for the a-axis[2]. Very good scaling is obtained over the whole field range; the size of the anomaly at the melting transition does not scale well, which is attributed to the differing degrees of averaging of the two methods. In order to better understand this scaling, the ratio:

$$\frac{\lambda}{M_T} = \frac{\frac{dM}{dp}\Big|_H}{-\frac{dM}{dT}\Big|_H TV_{molar}} \tag{6.2}$$

is considered. Taking this relation exactly at critical temperature T_c, and making the assumption $dT_c/dp = dT/dp$ at this point we obtain:

$$\frac{\lambda}{M_T} = \frac{\frac{dM}{dp}\Big|_H \frac{dp}{dT_c}}{-\frac{dM}{dT}\Big|_H T_c V_{molar} \frac{dp}{dT_c}} = \frac{\frac{dM}{dT}\Big|_H}{-\frac{dM}{dT}\Big|_H T_c V_{molar} \frac{dp}{dT_c}} = -\frac{\frac{dT_c}{dp}}{T_c V_{molar}} \tag{6.3}$$

These two coefficients are tightly coupled by virtue of a simple thermodynamic relation, so knowing the scaling factor allows us to calculate the pressure dependence of T_c. Taking atomar volume $V_{g\cdot at} = 1.035/13 \cdot 10^{-4}$ m^3, we got $dT_c/dp_a = -3.22 \cdot 10^{-9}$ K/Pa, which is in good agreement with our aforementioned result ($-2.97 \cdot 10^{-9}$ K/Pa) from the Ehrenfest relation. The discrepancy can be due to both the measurement error and the approximation itself, which is accurate only for $T = T_c$. Anyway, one can see that $\lambda(H)$ and $M_T(H)$ can be well scaled together for the same temperature. This is an another indication that the pressure dependence of T_c is the driving force of the length change in magnetic field near the critical temperature[3].

6.4 Calculating the pressure dependence of the temperature of the vortex melting transition from magnetostriction and magnetocaloric effect

The melting transition from the solid vortex phase to the vortex liquid is first order, based on resistivity [Saf92, Saf94, Kwo92], magnetization [Wel96, Wel94, Schi00] and thermal expansion [Lor02a]. One can therefore use the Clausius-Clapeyron equation to calculate the pressure dependence of the transition temperature by combining thermal expansion and heat capacity data [Lor02b]. We can also calculate this pressure dependence based on the magnetostriction and magnetocaloric measurements.

Integrating the coefficient of the magnetocaloric effect M_T (Fig. 4.4) over magnetic field one gets the change of the heat of the sample[4]. As the magnetocaloric effect was

[2]We acknowledge the help of Dr. R. Lortz, who pointed out that these two values have the same shape, did the preliminary scalings and gave us this data prior to publication. We chose the *a*-axis due to the high level signal here, the signal along *c*-axis is much smaller, and so the error is bigger.

[3]Since there is no pressure dependent term in the magnetocaloric coefficient, the dT_c/dp term comes exclusively from magnetostriction.

[4]One might be confused by the negative value of M_T, expecting also a negative change of the energy, but indeed, based on definition of the coefficient of the magnetocaloric effect, it means the flow of heat *into* the sample [Pla02]. Hence the jump in entropy is *positive* by melting transition.

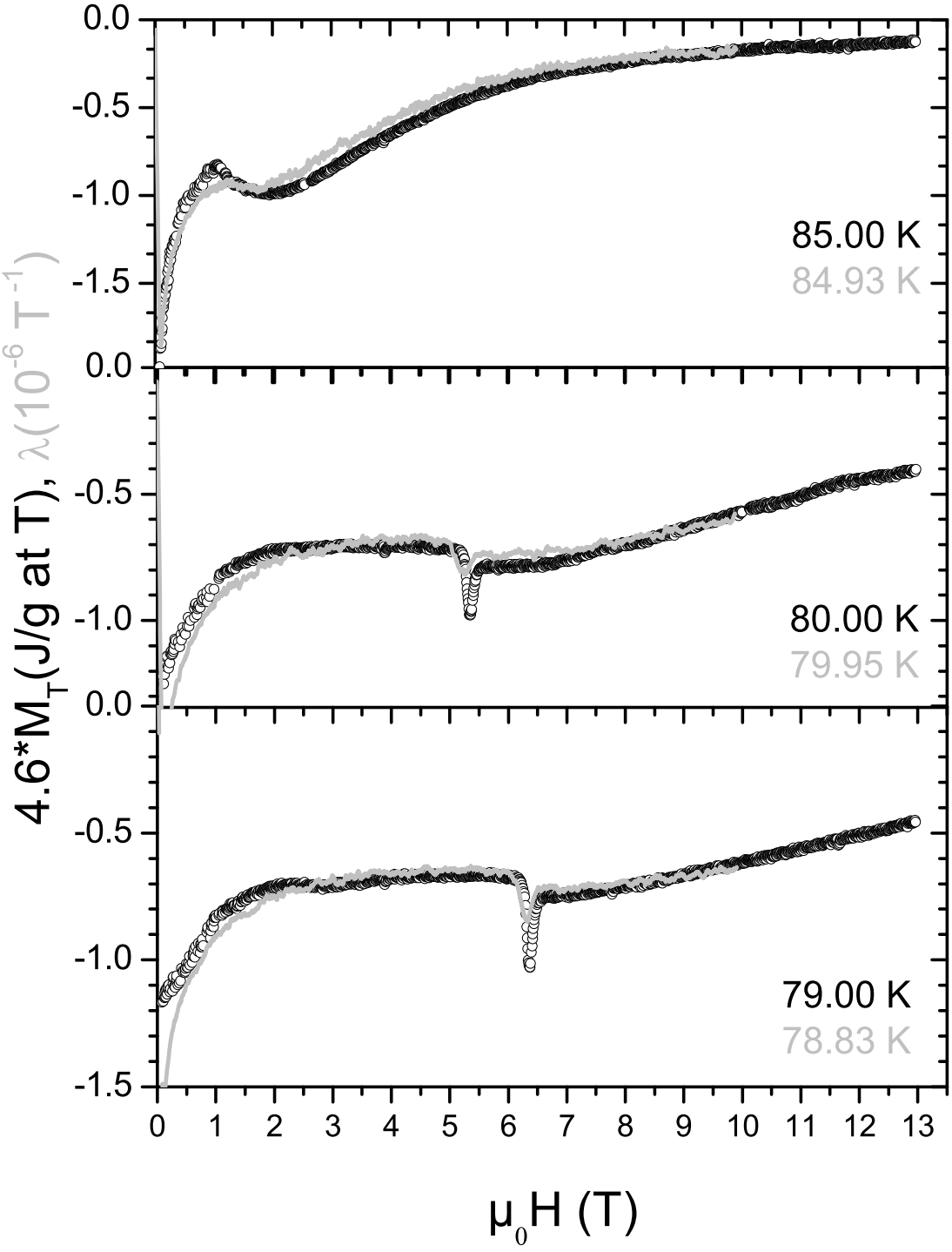

Figure 6.2: Scaling of the magnetostriction coefficient along the a-axes with magnetocaloric constant for 79 K, 80 K and 85 K (SRL Genf-A sample). The small discrepancies are caused by slightly different temperatures between different kinds of measurements, and also due to the smoothing procedure, which we used to reduce the noise in magnetostriction. The magnetocaloric data were obtained by Dr. T. Plackowski, Dr. R. Lortz, Prof. Dr. A. Junod in Geneva.

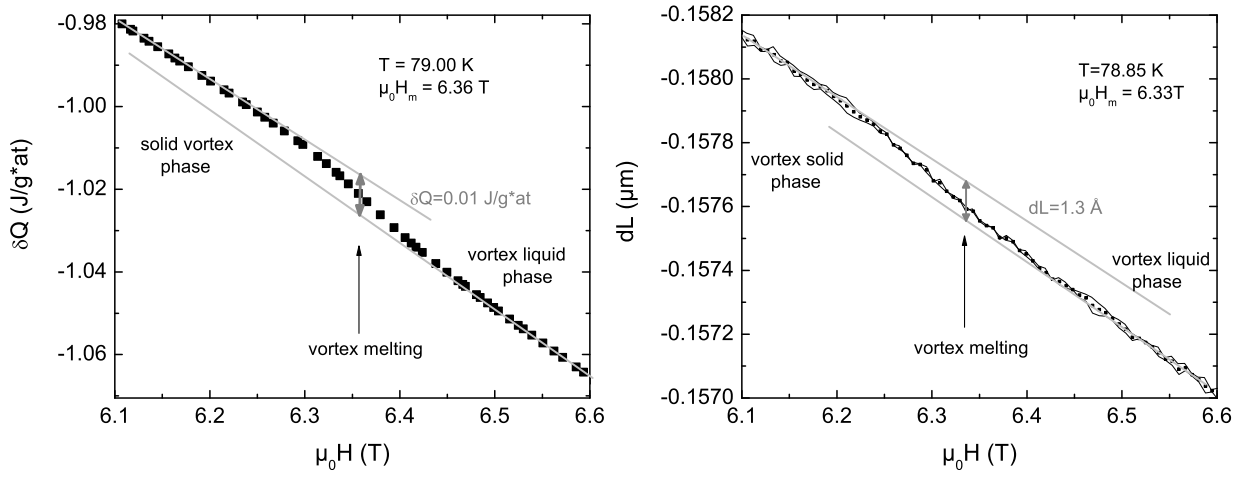

Figure 6.3: The heat jump δQ (*left*) by integrating M_T and length jump dL (*right*) at the vortex melting transition.

measured in isothermal condition, one can find the entropy jump at the melting transition:

$$\Delta S(T) = \left.\frac{\delta Q}{T}\right|_T$$

To find this jump, first of all, we need the exact field where it happens so we took the peak in M_T at the melting transition. There is no sharp jump of δQ at the melting point, so we took the integrated M_T, approximated the jump by the difference between two straight lines (Fig. 6.3), modeling vortex solid and vortex liquid phases. Using a similar procedure we found out the jump in length dL. For this case the Clausius-Clapeyron relation is:

$$\frac{dT_m}{dp_i} = \frac{\frac{dL_i}{L_i} V_{mol}}{\Delta S} \tag{6.4}$$

From $\delta Q = 0.01$ J/g·at and $dL_a/L_a = -1.3 \cdot 10^{-10}/2.97 \cdot 10^{-3}$ we found $dT_m/dp_a = -(2.78 \pm 0.3) \cdot 10^{-9}$ K/Pa, again very close to dT_c/dp_a, as expected [Lor02b]. We should mention that this method is not accurate enough due to very small changes, used in the calculation, but anyway, it is another proof of the first order transition of the melting of vortex lattice.

In order to get reliable data from the c-axis length measurements, we put two pieces of the SRL Genf sample on top each other, so we gathered for T= 80 K next values: $dL_a/L_a = -0.22 \cdot 10^{-10}/1.89 \cdot 10^{-3}$. With magnetocaloric data for this temperature, $\delta Q = 0.009$ J/g·at, we found the $dT_m/dp_c = -(0.94 \pm 0.2) \cdot 10^{-9}$ K/Pa. This shows for the first time that T_c and T_m remain coupled for c-axis pressure, something which was not clear in the earlier investigation [Lor03, Lor02a].

6.5 Toy model

Having established that dT_c/dp_i is the primary factor in the magnetostriction, it is useful to consider a simple model of the magnetostriction from which the field-dependent form of the magnetostriction coefficients of the different terms (dH_c/dp and $d\kappa/dp_i$) can be easily obtained. From Abrikosov's analytical solution, which describes very well the high field region, we can deduce the pressure dependencies, which affect the magnetostriction. From [Abr57a]

$$M(H) = -\mu_0 \frac{H_{c2} - H}{\beta_A(2\kappa^2 - 1)}$$

where β_A is the lattice parameter of fluxons, which is usually hexagonal[5] and equal to 1.16. The pressure derivative gives the magnetostriction (2.10) near the upper critical field:

$$\lambda(H) = \frac{dM(H)}{dp} = -\frac{\mu_0}{\beta_A(2\kappa^2 - 1)}\frac{dH_{c2}}{dp} + \frac{4\mu_0\kappa(H_{c2} - H)}{\beta_A(\kappa^2 - 1)}\frac{d\kappa}{dp} \tag{6.5}$$

In the vicinity of the H_{c2} the magnetostriction coefficient λ depends on two pressure derivatives: dH_{c2}/dp, which by definition $H_{c2} = H_c\kappa = H_{c0}g(t)\kappa$ also contains three pressure parameters (dH_{c0}/dp, dT_c/dp, $d\kappa/dp$), and $d\kappa/dp$. So, we can roughly estimate, that the magnetostriction is a sum of three different terms:

$$\lambda(H) = \frac{dM(H)}{dp} \propto A\frac{dH_{c0}}{dp} + B\frac{dT_c}{dp} + C\frac{d\kappa}{dp}, \tag{6.6}$$

where A, B and C are parameters. Assuming that H_c and T_c are somehow coupled, as in BCS superconductors, then only two independent pressure dependencies should be considered: dT_c/dp and $d\kappa/dp$. One can see that there are two main scenarios possible: First, as one applies pressure to the superconductor, both uniaxial or hydrostatic, the critical temperature T_c increases (decreases), which gives rise to an increase (decrease) of the critical field $H_c(T_c)$. It means that the magnetization curve will "stretch", the area under it will also increase (Fig. 6.4). Of course, H_{c1} and H_{c2} increase with increasing T_c, but the relation $H_{c1} = (H_{c2} ln\kappa)/(2\kappa^2)$ still remains fulfilled.

Second, the applied pressure can increase (decrease) the Ginsburg-Landau parameter κ, which also will distort the magnetization curve, but the area remains constant. In this case the upper critical field would increase (decrease) (Fig. 6.5).

Taking the theoretical $M(H)$ curve from one of the aforementioned solutions of GL equation and stretching it 1% in both directions which would model the increase of the critical field H_c due to applied field, then taking the difference $M'(H', p') - M(H, p) \propto dM/dp \equiv \lambda$ results in the first scenario. Or we can calculate the $M(H)$ for two different κ values, find the difference of these two curves and get the theoretical magnetostriciton curve for second one. The main result here is that in the case of the second scenario the obtained magnetostriction curve will cross the field axis.

In order to find a theoretical model for magnetostriction coefficient, we compared three different solutions of GL equations for superconductors, namely Koppe-Willebrand

[5] In his original work Abrikosov investigated the quadratic lattice.

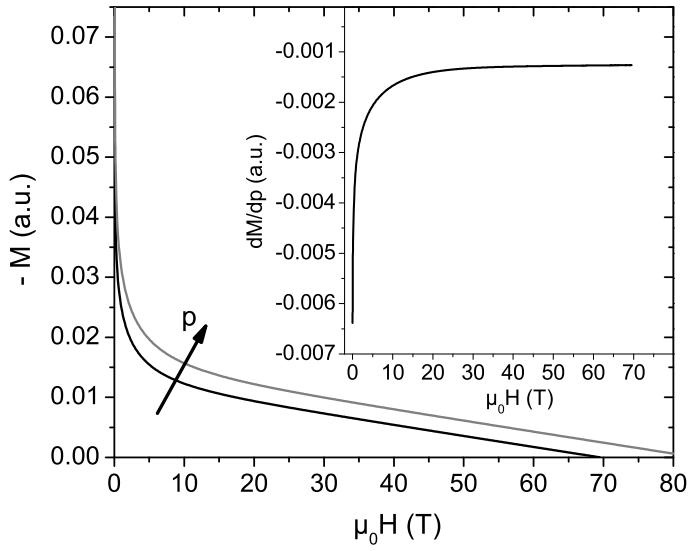

Figure 6.4: Modeling of dM/dp by "stretch", governed by the pressure dependence of the critical field. For the sake of clarity, 20% stretch was taken. *Insert:* The resulting difference between "streched" and starting curves, which is proportional to the dM/dp. Details in text.

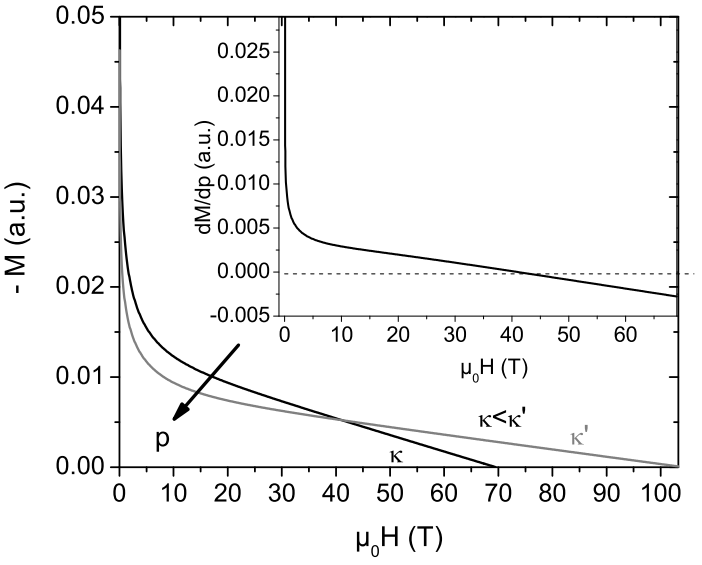

Figure 6.5: Modeling of dM/dp by "stretch", governed by the pressure dependence of the Ginsburg-Landau parameter κ. *Insert:* The resulting difference between "stretched" and starting curves, which is proportional to the dM/dp. Note that the resulting curve cuts the field axis. Details in text.

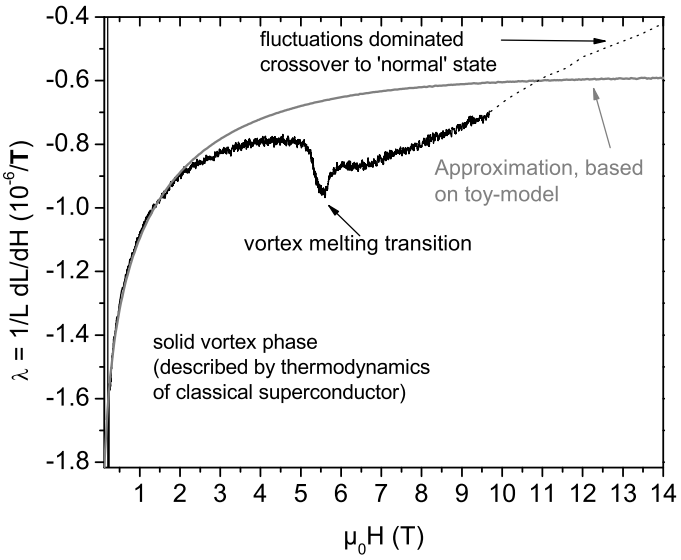

Figure 6.6: Theoretical curve (gray line), obtained from the toy model with the first scenario (assumption $d\kappa/dp \equiv 0$), fitted to the SRLW sample a-axis isothermal magnetostriction coefficient at 79 K (black curve). The theoretical magnetization curve was obtained from the approximate Koppe-Willebrand solution of GL equations. Details in text.

[Kop70], Hao-Clem [Hao91] and Pogosov [Pog00]. All these approximate solutions give the dependence of the magnetization M on the applied magnetic field H, $M(H)$ for different κ, so we compared the dM/dp curves for these two scenarios, and found that only the Koppe-Willebrand approximation[6] gives smooth curves all over, so we will use only this approximation[7].

We have made several fits with these two different scenarios, for example for the magnetostriciton coefficient λ of sample SRLW along the a-axis, 79 K (Fig. 6.6) and found out that second scenario gives worse fits than the first one. We can distinguish three different regions here: first of all, the solid vortex phase, which is well described by thermodynamics (actually, fitted well with our model), the fluctuation-driven vortex melting transition, and finally the fluctuation dominated region, well fitted with the 3D-XY model [Lor02a].

However, in the case of high temperature superconductors we could neither surely distinguish between these two scenarios experimentally, nor rule out the possible appearance of both scenarios as some sum of these two different pressure dependencies, due to the very high upper critical field, unreachable for our current setups (up to 100-200 T). Also, Abrikosov's solution is not valid for the low field region by $H \ll H_{c2}$, so we try to find out the theoretical shape of the magnetostrictive curve comparing the fits with curves of

[6]The final equation in this article is mistyped.

[7]The discrepancy between these approximate solutions comes from difference in used simplifications and trial functions.

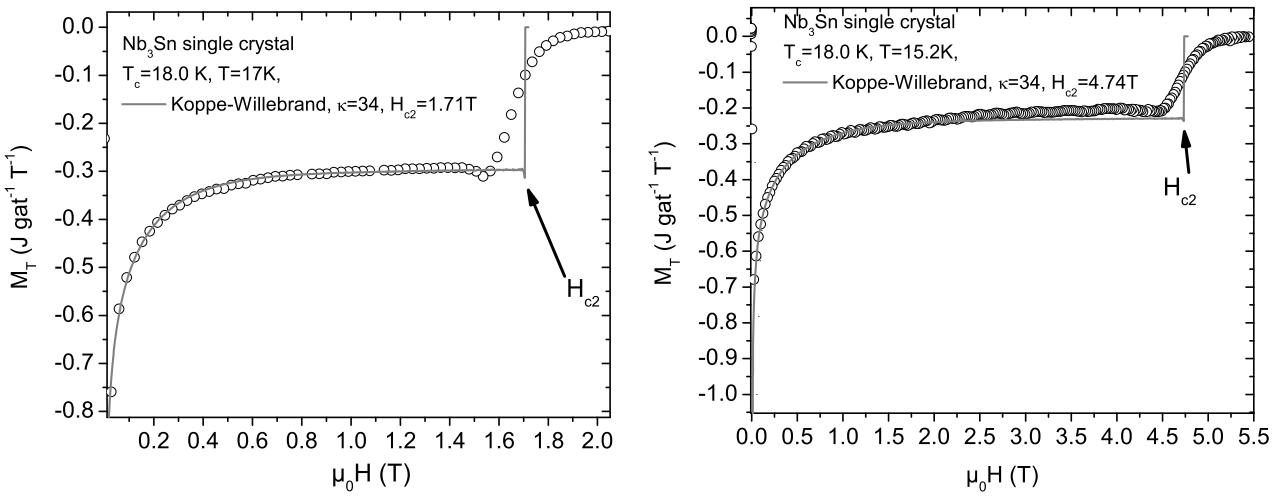

Figure 6.7: Theoretical curves (gray lines), obtained from the toy model with the first scenario (assumption $d\kappa/dp \equiv 0$), fitted to Nb_3Sn isothermal magnetocaloric coefficient (black circles) at 17 K (*left*) and 15.2 K (*right*). The theoretical magnetization curve was obtained from the approximate Koppe-Willebrand solution of GL equations. Details in text.

the magnetocaloric effect, measured on Nb_3Sn[8]. As we already know, the coefficients of magnetostriction and magnetocaloric effects have the same shape, and can be scaled taking into account simple theoretical considerations (Chapter 6.3), so we do an assumption that if one of aforementioned scenarios would be ruled out for MCE, it would be ruled out for the magnetostriction as well.

In order to check our method, we calculated the field dependence of the magnetocaloric effect for Nb_3Sn, which can be compared directly to experiment [Lor06b]. As seen in Fig. 6.7, a very good effect description of M_T with reasonable κ values is obtained for two different temperatures in the framework of the first scenario. No such scaling is possible for the second one, that is why we can exclude the second scenario from our analysis.

6.6 Theoretical calculation of the magnetostriction

To be able to calculate the length change we need several experimental parameters, which we can collect from the literature. As a basis we took the article about precise heat capacity measurement of YBCO by Liang and Loram in [Lia04]. We take Ginzburg-Landau parameter $\kappa = 120$, found in aforementioned article, and with this parameter we calculate the theoretical magnetization curve[9] $M(H)$ from the Koppe-Willebrand approximate solution of the Ginzburg-Landau equations (Section 6.5). The critical field, found by Loram and Liang was $\mu_0 H_{c0} = 1.23$ T. As they used a not fully doped sample, we approximated

[8]We are in debt to Dr. Rolf Lortz, who kindly gave us these data prior to publication.

[9]Here we get a reversible curve from the numerical calculations, all fluctuations and irreversibilities are neglected. We will use the function, describing the shape of this curve, i.e. $f(H_c, \kappa) = -M(H)/(H_c V)$.

$\mu_0 H_{c0}$ with the value 1.5 T due to our higher oxygen content. This value was the only fit parameter we used in our calculations.

The upper critical field at zero temperature is defined as $\mu_0 H_{c2} = \mu_0 \sqrt{2} \kappa H_c$, which is in our case is 254 T. This value is somewhat higher than the result of another specific heat measurement of Wang et al. [Wan01] done for fully doped YBCO (150 ± 102 Tesla).

Another important parameter, which we can find from thermal capacity measurement is the dependence of the thermodynamic critical field on temperature. In case of a classical superconductor, the experimental data give approximately $g \equiv 1 - t^2$, where $t = T/T_c$ is the reduced temperature. To determine this dependence we took a graph of $H_c(T)$ from [Lia04] and found the best fit with $g = 1 - t^3$ (Fig. 6.8).

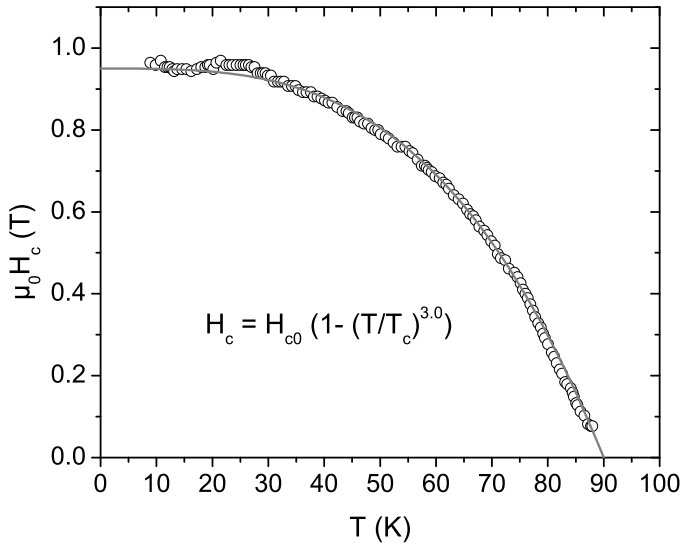

Figure 6.8: Temperature dependence of the thermodynamical critical field. (Taken from [Lia04].)

The compressibility term (first term in equation 6.1) can be calculated directly using the uniaxial compressibilities $k_a = 2.38 * 10^{-12}$ Pa^{-1}, $k_b = 1.93 * 10^{-12}$ Pa^{-1} and $k_c = 4.66 * 10^{-12}$ Pa^{-1} [Lei03], and values of κ and $H_c(T)$. The results are shown in Fig. 6.9 in comparison to the measured signal. As can be seen, this term is quite small and does not play a significant role, but nevertheless is subtracted from the original data for further analysis. The term, proportional to the pressure dependence of the critical temperature, is the largest near the phase transition, and tends toward zero with decreasing temperature.

The pressure dependence of H_{c0} can be obtained directly from the field induced length change at 10 T using Eq. 6.1 and considering $T = 0$ (Fig. 6.9, right). As the signal in c-axis was very small, we approximated the pressure dependence of critical field as zero.

We also calculated the normalized pressure dependencies for the SRLW sample, our data presented in Table 6.2. The always positive sign of $1/H_c dH_c/dp_i$ is worthy of notice, because it does not correlate with sign of dT_c/dp_i, and furthermore its absolute value

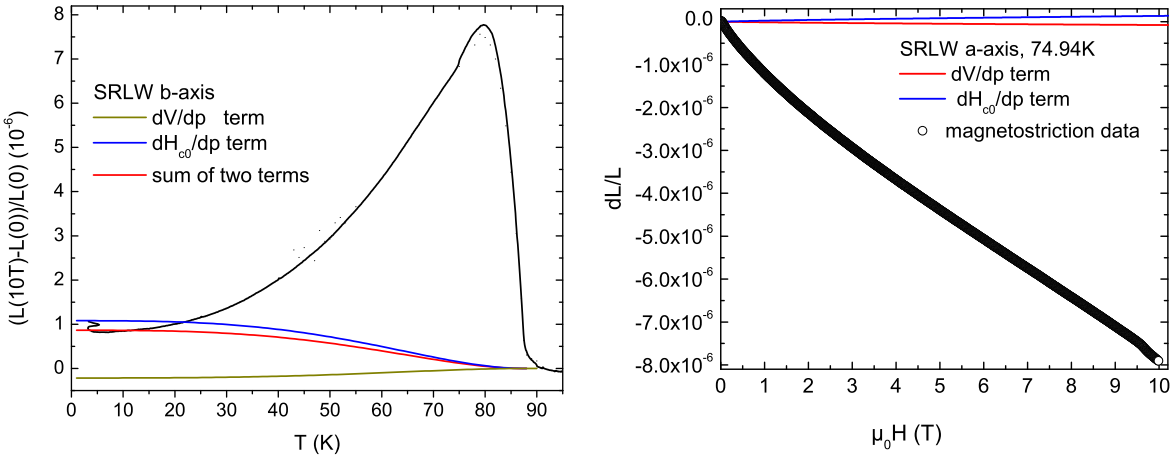

Figure 6.9: *Left:* Calculation of the pressure dependence of critical field from length difference at 10 T, extrapolated to zero Kelvin (b-axis, SRLW sample). *Rigth:* Comparison of the effects of compressibility and pressure dependence of critical field terms with magnetostriction at 74.94 K (a-axis, SRLW sample). The main driving force of the magnetic field induced length change here is the pressure dependence of the critical temperature.

is much smaller. For classical superconductors the signs of these pressure dependencies always match and have the same order of magnitude [Roh60]. This may suggest a different underlying mechanism of pairing.

axis	$\frac{1}{H_{c0}}\frac{\partial H_{c0}}{\partial p_i}$ (Pa^{-1})	$\frac{1}{T_c}\frac{\partial T_c}{\partial p_i}$ (Pa^{-1})
a	$(2.51 \pm 0.3) * 10^{-12}$	$-(3.39 \pm 0.2) * 10^{-11}$
b	$(5.02 \pm 0.6) * 10^{-12}$	$(2.83 \pm 0.2) * 10^{-11}$
c	$(0 \pm 0.2) * 10^{-12}$	$-(0.98 \pm 0.2) * 10^{-11}$

Table 6.2: Normalized uniaxial pressure dependencies of the critical field and critical temperature, calculated for different axes for the SRLW sample.

Our results for the $a-$, $b-$ and $c-$axes are compared to the experimental data in Fig. 6.10. The theoretical curves describe both the field and temperature dependence of the experimental data surprisingly well; strong deviations are seen only above the vortex melting transition, which is not surprising, since this transition seems to mark the onset of strong 3D XY fluctuations [Lor02a]. The magnetostriction obtained from the thermal expansion (black lines) is compared to the calculated values (open circles) in Fig. 6.11. Again, very good agreement is seen between measured and calculated data, except close to T_c, where fluctuations dominate. Fig. 6.11 also shows the total length changes expected at $H_{c2}(T)$, i.e. above 254 T, for all three axes (gray curve).

These curves are valid if the following assumptions are fulfilled:

- the magnetization curve can be described by the Ginsburg-Landau approach, i.e. fluctuations need not to be accounted for;

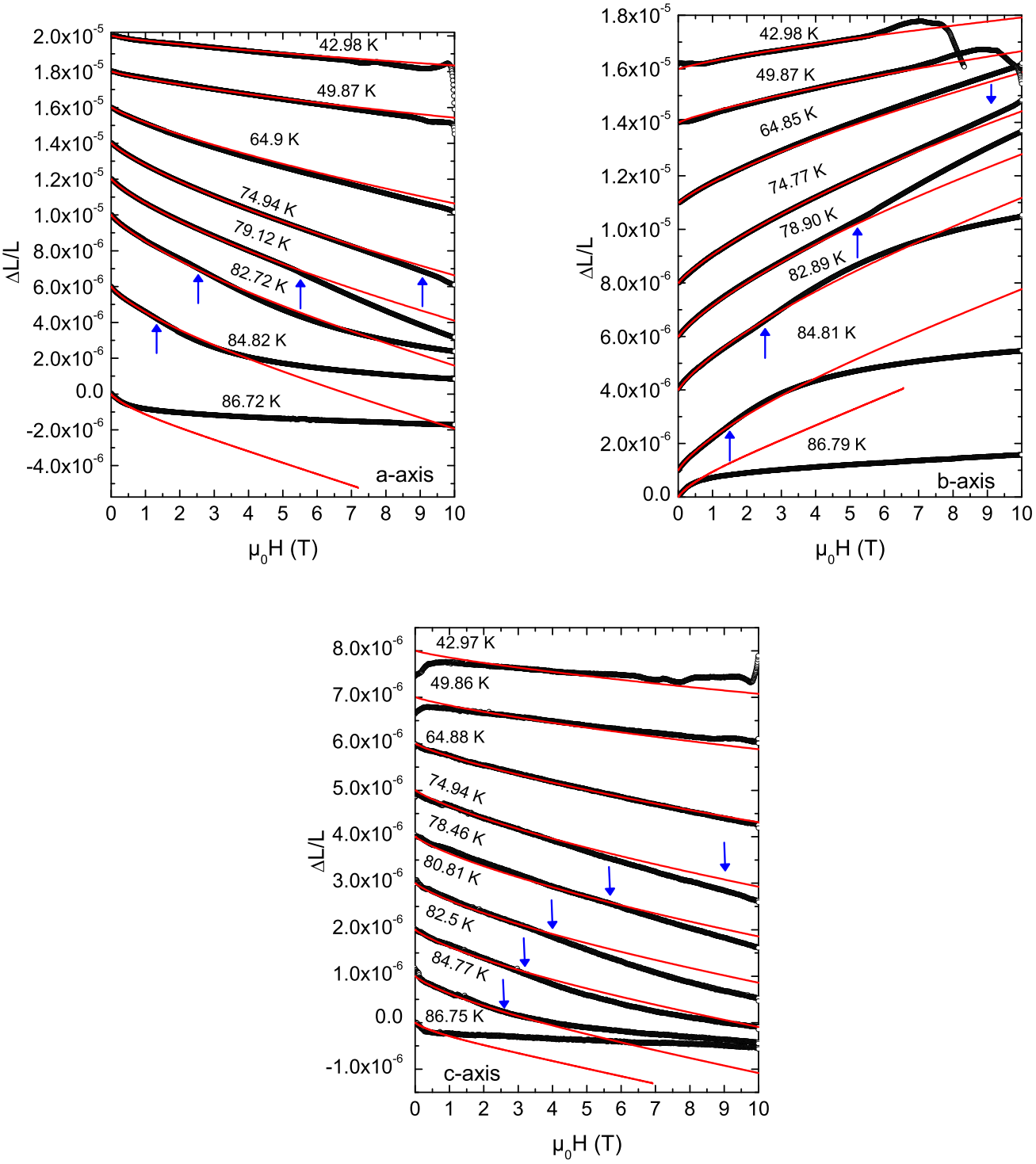

Figure 6.10: Experimental magnetostriction data (black points), fitted by the thermodynamical model (red lines), for a-, b- and c-axes for SRLW sample. The vortex melting transition is marked with blue arrows. For 43 K and 50 K the approximated data from Section 5.2 were used.

- the temperature dependence of the critical field follows $g = 1 - t^{3.2}$ for 85 K $< T <$ T_c and $g = 1 - t^{3.0}$ for $T <$ 85 T;
- there is no temperature and field dependence of the Ginsburg-Landau parameter κ;
- the applied magnetic field $H > H_{c2}$ governs the transition from the superconducting to the normal state, this state is field insensitive.

6.7 3D XY scaling

As we have seen from the last Section, our thermodynamic model can describe the magnetostrictive response of the superconductor up to the field of the melting transition. What can we say about higher fields? The fluctuating behavior of our system has been described in the framework of 3D XY scaling [Lor02a]. Due to this work we scaled our length differences $\Delta L(H)$, defined by Eq. 5.1, for a- and b-axis (Fig. 6.12), taking a field-independent critical temperature $T_c(H) = T_c(0)$ and correlation length critical exponent $\nu = 0.669$. A straight line was subtracted from some measurements along a-axis (1, 2, 6, 8, 9 T) and b-axis (1 T), in order to remove the small background appearing due to thermal cycling of cell. One can see that this scaling is working well in our case for the scaled temperature region between -0.03 and 0.02; the small discrepancy between scaled curves here we attribute to the errors of measurements, which are much smaller for measurements along the b-axis. For scaled temperatures lower then -0.03, i.e. below the melting transition, the data could not be described within the framework of this scaling. This is because there are no fluctuations and the low temperature region is well described as shown in Section 6.6 with thermodynamic model.

Using the scaling found in Fig. 6.12, it is possible to extrapolate the field induced length changes up to higher fields than actually measured, and the results are shown in Fig. 6.13 for fields up to 255 T. (Note that the scaling only works above the peak in $\Delta L(T, H)$; the dashed lines below the peak do not obey this scaling.) 255 T corresponds to the value of the field where the peak in $\Delta L(T, H)$ is shifted to zero temperature and is interpreted as a measure of H_{c2} in this scaling approach. Interestingly, this value is close to the value we obtained from the thermodynamic approach in Section 6.6. This analysis of course assumes that this scaling will continue to such high fields, which may be questionable. Within this scaling approach, the melting transition at $T = 0$ occurs at 133 T.

In Fig. 6.14, left, the total magnetostriction between zero field and H_{c2} is plotted as a function of temperature for both the thermodynamical model from Section 6.6 and the 3D XY scaling; clearly, these extrapolations are very different, especially at $T = 0$, where a large length change is expected from the 3D XY scaling and little length change is expected in the thermodynamical approach. In order to see which extrapolation makes more sense, we have subtracted the appropriate extrapolated curves (Fig. 6.14, left) from the zero-field length changes. The results are shown along with the 10 T data in Fig. 6.14 and 6.15. If the "correct" total magnetostriction is subtracted from the zero field thermal expansion curves, the resulting curve should represent the featureless phonon

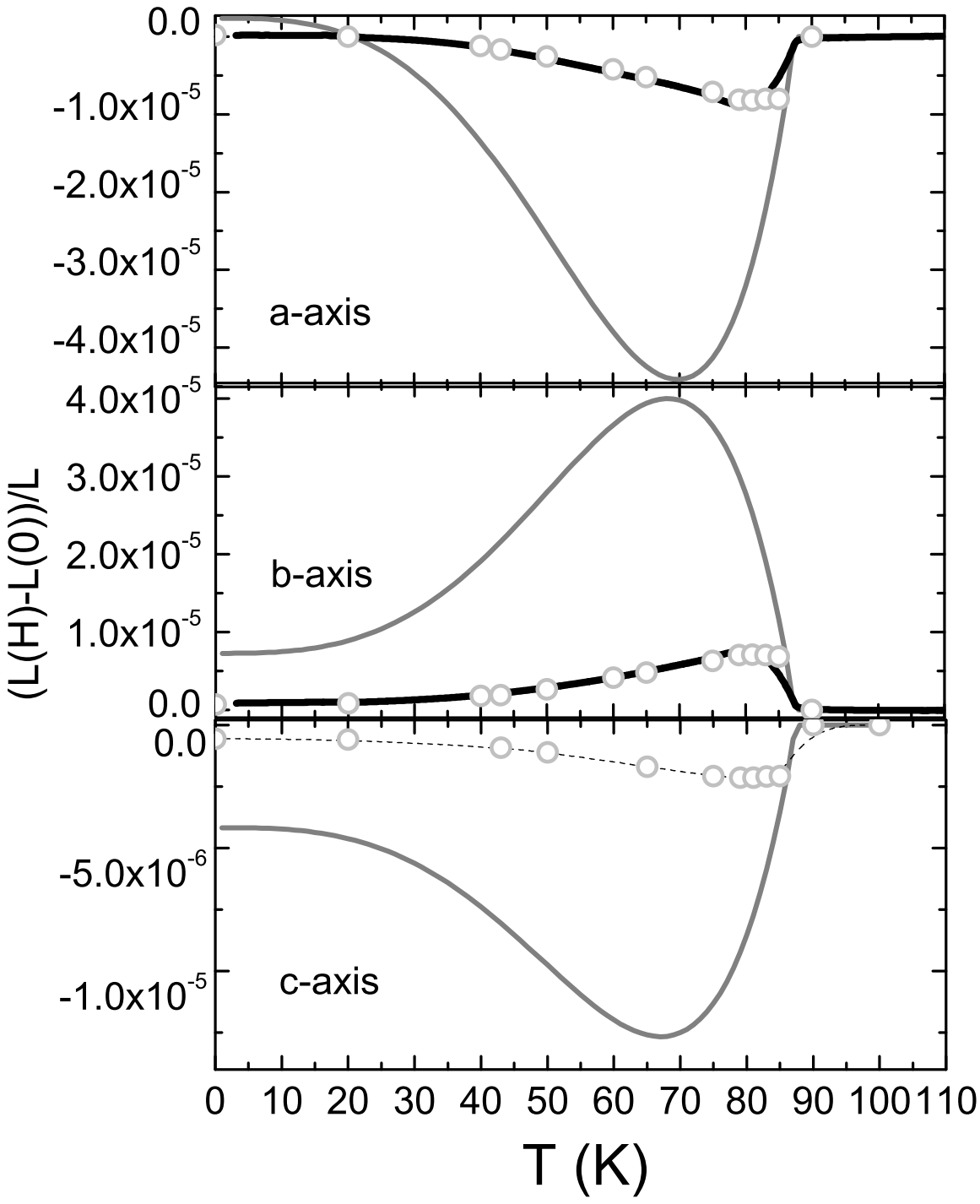

Figure 6.11: Thermodynamical calculations of the length difference between normal, i.e. above $\mu_0 H_c$= 255 T , and superconducting state (gray curve), for *a*-, *b*- and *c*-axes (SRLW sample). Also the measured signal for 10 T (black curve) and calculated magnetostriction for 10 T (gray circles) are presented. The discrepancy between measured and calculated 10 T magnetostriction in the temperature region between 75 and 88 K is caused by fluctuations.

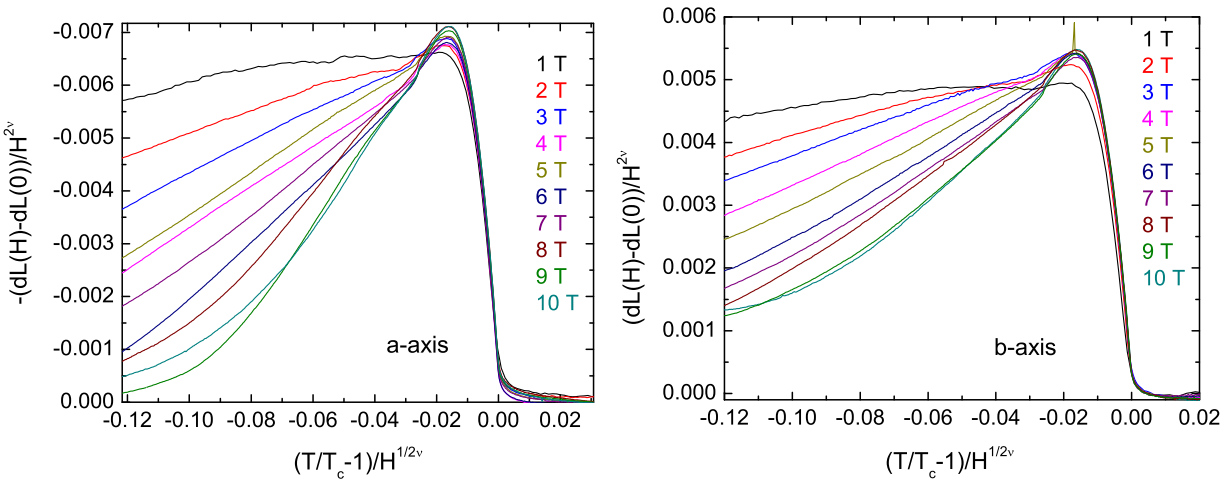

Figure 6.12: 3D XY scaling of the length changes in different fields and zero field for the a- and b-axes of SRLW sample.

and normal electronic background. An inspection of Fig. 6.14 and 6.15 shows that the "background" obtained by subtracting the 3D XY extrapolated magnetostriction appears more reasonable, i.e. these curves do not show any left-over anomalies at T_c.

In order to check how the $L(H) - L(0)$ will change with applied field, we have done a 3D-XY scaling analysis for the different magnetic fields up to 255 T (Fig. 6.13). The dotted lines present the part coming from 10 T measurement for $T < T_{peak}(10\ \mathrm{T})$, which should be investigated in the framework of the thermodynamic model. The scaling is valid under the following assumptions:

- the critical temperature T_c does not depend on magnetic field;
- the 3D XY model is valid for high magnetic field, there is no crossover to Gaussian or Landau-lowest-level fluctuations.

6.8 Upper critical field

What about H_{c2}, which is a crucial parameter used in the thermodynamic model? Indeed, from our magnetostriction measurements not so far from T_c (Fig. 6.10, $T \approx 86.8$ K) one can see that even after reaching H_{c2} the signal does not disappear, it decreases with the same slope, which corresponds to the phase fluctuations expected from the "preformed pair scenario" [Eme95]. This behavior supports the hypothesis that there is no well defined upper critical field in this material, there is only a sharp change with increasing field - the melting transition from vortex solid to vortex liquid, transition from non-dissipative to dissipative state.

One should also bear in mind that there is a discrepancy between different techniques employed to determine the upper critical field: some authors, e.g. [Mac93, Nak98, Obr00], use the "resistive $H_{c2}(T)$", which suppresses the superconductivity, and the electrical resistivity of sample appears again, others (e.g.[Ges98]) the "thermodynamic $H_{c2}(T)$",

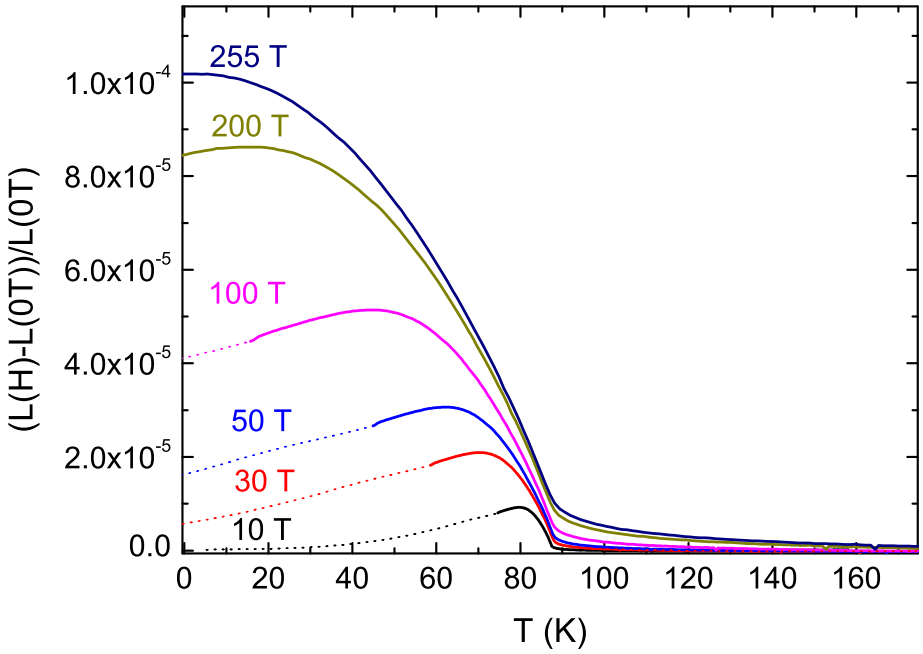

Figure 6.13: Extrapolation to higher fields of the length difference between different fields and zero field using the 3D-XY scaling, shown in Fig. 6.12, a-axis (SRLW sample).

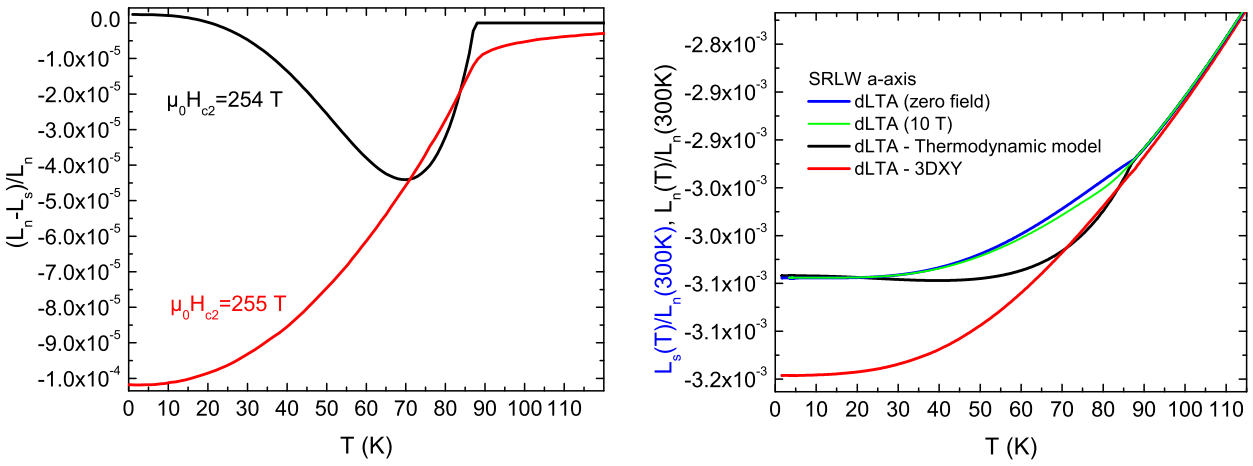

Figure 6.14: *Left:* Comparison of the length difference between normal and superconducting state, obtained from the thermodynamic model (black curve) and 3D XY scaling (red curve) (a-axis, SRLW sample). *Right:* Comparison of normal state length for these two models, obtained from the thermodynamic model (black curve) and 3D XY scaling (red curve) (a-axis, SRLW sample). The blue curve is a zero field thermal expansion measurement, i.e. the length change in superconducting state (a-axis, SRLW sample).

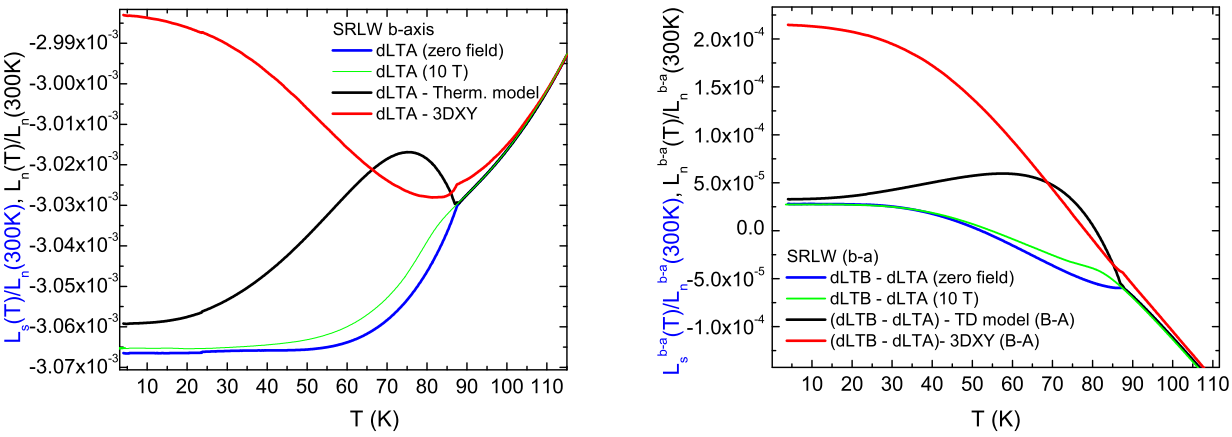

Figure 6.15: Comparison of normal state length for these two models, obtained from the thermodynamic model (black curve) and 3D XY scaling (red curve). The blue curve is a zero field thermal expansion measurement, i.e. the length change in superconducting state (SRLW sample). *Left:* b-axis. *Right:* Difference between b- and a-axes.

which is gathered from specific heat, magnetization and thermal expansion measurements. The "resistive" transition in our case is ascribed to the vortex melting transition, $H_m(T)$, when the system changes from vortex solid to vortex liquid. The other, "thermodynamic", transition is the scale at which the bulk pairing vanishes and gives the broadened phase ordering transition, H_{c2}^{3DXY}.

The paramagnetic limit (Clogston-Chandrasekhar) [Clo62] also can constrain the upper critical field. This effect is governed by the energy win of the spin system, if the spins align along the applied magnetic field. The Cooper pairs will break up at some limiting field B_P, at which the Zeeman energy $\sqrt{2}\mu_B B_P$ exceeds the energy gap Δ_0, μ_B is the Bohr magneton. From BCS theory [Bar57] for a $d_{x^2-y^2}$ wave superconductor (weak coupling) [Yan97]:

$$1.75 k_B T_c = 0.56 \mu_B B_P. \tag{6.7}$$

So, the paramagnetic limit B_P and the critical temperature are coupled via:

$$B_P = T_c \cdot 2.32(\mathrm{T/K}) \tag{6.8}$$

For the SRLW sample $B_P = 203$ T; but this estimation is very rough, because in the case of preformed pairs one should use T^* instead of T_c, which will increase B_P.

From our measurements we got the following $H-T$ phase diagram (Fig. 6.16, left): the solid vortex phase is separated by the melting line from the vortex liquid phase, which is limited by $T_{peak}(H)$ line. Both of these lines are well described by 3D XY scaling.

The thermodynamic critical field and the upper critical field correspond as $H_{c2} = \kappa\sqrt{2}H_c$. So we can expect that if one of them follows 3D XY scaling, the other one will do the same, in case of constant κ, that is why we tried to use 3D XY scaling for the critical field. From our calculations we know which H_c gives us good coincidence between calculated and measured magnetostriction curves. In order to use 3D XY scaling instead of semiclassical $1-t^3$, the values of $H_c(T)$ should be more or less be equal. In Figure

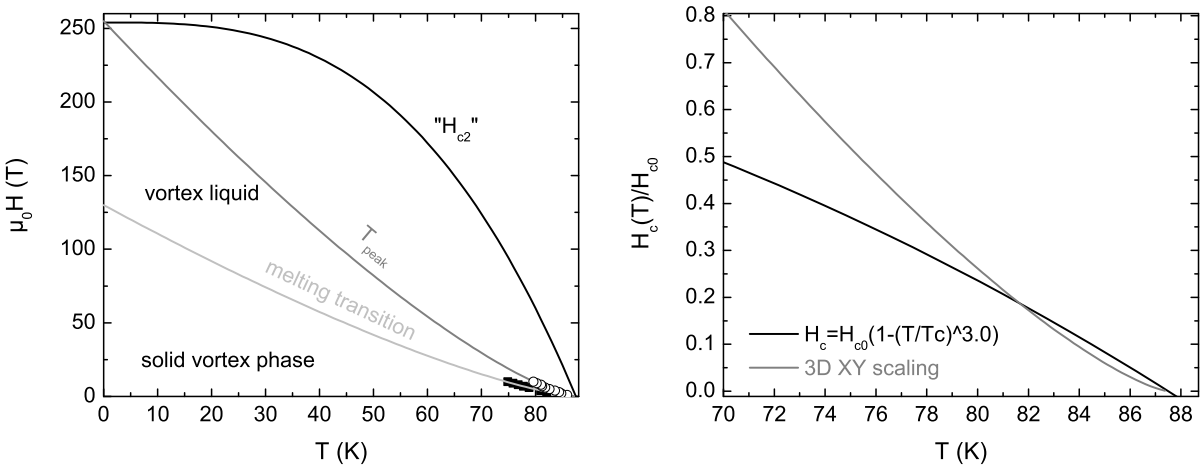

Figure 6.16: *Left:* Proposed $H-T$ diagram for the SRLW sample. The melting transition (black squares), measured in thermal expansion measurements in field is fitted with 3D XY scaling (gray curve). The T_{peak} (black circles) is also fitted by 3D XY scaling, giving $\mu_0 H_{c2}^{3DXY} = 255$ T. *Right:* Comparison of critical field scaling, given by different approaches: $g = 1 - t^3$ (black line) and 3D XY scaling (gray curve).

6.16 (right) we present such a fit. 3D XY scaling gives too high values of the critical field already around 75K, which is rather well described using $1 - t^3$. Considering the lower value for 3D XY H_{c0} will not give a good scalings either. This may suggest that in case of a constant κ, H_c would not follow this scaling, it behaves rather classically.

Let consider a isothermal magnetostriction measurement in the reversible region: Up to the melting transition $H_m(T)$, the vortices build up a solid vortex phase, which is well described by the thermodynamic model, similar to the behavior of classical superconductors. H_{c2} here is a limiting parameter used in calculations. Already lower than $H_m(T)$ a "pre-melting" of vortices appears, the vortex lattice transforms to the vortex liquid in a first order phase transition. The system now follows the 3D XY scaling up to the broadened transition at $H_{peak}(T) < H_{c2}$, at higher field only a small number of fluctuations exists. In this scenario H_{c2} is merely a thermodynamic value, similar to the critical field H_c in type-II superconductors, which plays the role of an energy scale, there is no transition or crossover at this field.

We calculated the 10 T magnetostriction for the temperature range between 0 and 40 K with the thermodynamic theory, using the semiclassical temperature dependence of H_c, and obtained well coinciding results with the measurement. This constitutes a proof that the thermodynamic approach can be used also at low temperatures and H_{c2} still a meaningful parameter here.

6.9 Pressure dependence of electronic specific heat

The BCS coupling constant x is defined as [Car90]:

$$x = \frac{\gamma^* T_c^2}{\mu_0 H_{c0}^2} \tag{6.9}$$

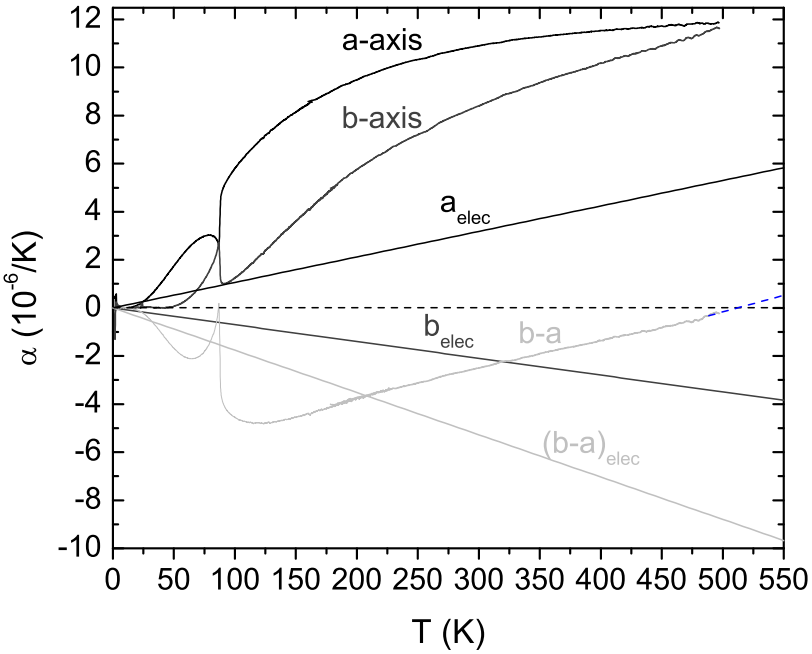

Figure 6.17: Comparison of the measured total expansivities (a-, b-axis, and difference between them ($b-a$)) with the electronic expansivities (a_{elec}, b_{elec} and $(b-a)_{elec}$) calculated using Eq. 6.10. The high temperature data were taken from [Nag01].

The value of x for d-wave superconductor in weak coupling limit is 3.7. Taking values, experimentally found from our calculations (T_c= 87.5 K, $\mu_0 H_{c0}$= 1.5 T) and from literature [Wan01] (γ^*= 150 J/(K^2 m^3)), we find for our sample x=0.64, which lies in strong coupling region. If one assumes that x is not pressure dependent, one can find from Eq. 6.9:

$$\frac{dH_{c0}}{dp} = \frac{1}{x}\left(\frac{dT_c}{dp}\sqrt{\gamma^*} + \frac{1}{2}\frac{T_c}{\sqrt{\gamma^*}}\frac{\gamma^*}{dp}\right) \tag{6.10}$$

Using our results from Section 6.6 we can calculate the following scaled pressure dependencies of the electronic specific heat coefficient using Eq.6.10:

$$\frac{1}{\gamma^*}\frac{d\gamma^*}{dp_a} = 7.07 \cdot 10^{-2}\mathrm{GPa}^{-1},$$

$$\frac{1}{\gamma^*}\frac{d\gamma^*}{dp_b} = -4.66 \cdot 10^{-2}\mathrm{GPa}^{-1}.$$

For a Fermi liquid the electronic thermal expansion is equal to:

$$\alpha^{elec}(T) = \frac{1}{\gamma^*}\frac{d\gamma^*}{dp_i}\gamma^* T,$$

from which we find:

$$\frac{\alpha_a^{elec}}{T} = 1.06 \cdot 10^{-8}\mathrm{K}^{-2}$$

$$\frac{\alpha_b^{elec}}{T} = -0.67 \cdot 10^{-8}\mathrm{K}^{-2}$$

The measured expansivity is the sum of the electronic and phononic contributions. By inspection of Fig. 6.17, it appears implausible that the actual electronic contributions are as calculated. This is especially evident in the curve for α_{b-a}^{elec}, in which most of the phonon contribution should vanish at higher temperatures; here it looks as a possible electronic contribution has a positive slope, whereas the calculated one has a large negative slope. This apparent discrepancy may be due to a pressure dependent coupling constant x or a possible inapplicability of the thermodynamical model leading to equation 6.10.

6.10 Conclusions

The theoretical model to describe our data was discussed, the parameters needed were found in the literature. The thermal expansion in field was found as a suitable approach complementary to the magnetostriction method, in order to obtain a thermodynamic signal in the irreversible region. The uniaxial pressure dependencies of the critical temperature, were calculated from the Ehrenfest relation for our samples. They are the main driving force of the length change, other pressure dependencies play a less significant role. The pressure dependence of the Ginsburg-Landau parameter κ was found to be negligible by applying a simple toy model. Theoretical magnetostriction curves were calculated, up to field of melting transition these curves fit well our measurements in the whole temperature range of interest for all three axes.

dT_c/dp_i is positive for stress along the b-axis, and negative for a- and c-axes. The uniaxial pressure dependencies of the thermodynamic critical field, which are complicated to measure directly, were estimated from our measurements. They were found to be positive for a- and b-axes, which contradicts the behavior expected for classical superconductors, where dT_c/dp_i and dH_c/dp_i have the same sign. We attribute this to the different pairing mechanism in comparison to the classical superconductors.

We determined the uniaxial pressure dependencies of the melting transition from the Clausius-Clapeyron relation, combining magnetocaloric and magnetostriction measurements. These values coincide with ones obtained from other experiments [Lor02b].

3D XY scaling was used to approximate the $L_n - L_s$ curve, which differs from the results of the thermodynamic model. The estimated upper critical field $\mu_0 H_{c2}^{3DXY} = 255$ T is equal to that used in our thermodynamic calculations. The reason for two different possible length changes in temperature is caused by different approaches to calculate them. The thermodynamic one shows only the possible picture in fluctuation-free classical case.

At $T \approx T_c$ the values of expected H_{c2} are smaller then our maximal magnetic field, but we did not detect any sign of transition from superconducting to normal state. However, the possibility of a crossover to the field region, where H_{c2} can be detected experimentally at lower temperatures where the fluctuations play a less important role can not be excluded.

Chapter 7

Summary

The anisotropic magnetostriction and thermal expansion of fully oxygenated untwinned $YBa_2Cu_3O_7$ single crystals have been studied for magnetic fields $H||c$ up to 10 T along all three crystallographic directions. In order to obtain reliable data of the magnetostriction, which can be just a few Angstroms in magnitude, important improvements were made both in the hardware of the dilatometer and in the data analysis. Due to the high crystal quality, the measurements are reversible over a large part of the $H-T$ region studied, making a thermodynamical analysis of the data possible. By carefully measuring the thermal expansion in a restricted temperature interval, it was also possible to obtain a thermodynamic signal in the irreversible low temperature region. Complementary magnetization, specific heat and magnetocaloric measurements on the same crystals were made.

The magnetostriction of a classical superconductor is related to the pressure dependencies of T_c, H_{c0}, κ and of the Sommerfeld constant, and an analysis of the reversible magnetostriction using a classical model without thermal fluctuations was made in order to obtain these pressure dependencies for $YBa_2Cu_3O_7$. It was found that this thermodynamical model describes the magnetostriction data very well up to the vortex melting transition, which marks the onset of strong fluctuations, and that $1/T_c \cdot dT_c/dp_i$ is much larger than $1/H_{c0} \cdot dH_{c0}/dp_i$ and $1/\kappa \cdot d\kappa/dp_i$. This is quite surprising, since in conventional superconductors, $1/T_c \cdot dT_c/dp_i$ and $1/H_{c0} \cdot dH_{c0}/dp_i$ are closely related. Moreover, there are two disturbing implications of these results. First, $d\gamma/dp_i$, based on the above results, was calculated and shown to be much larger and of opposite sign than expected from thermal expansion measurements up to 500 K. Second, subtracting the total extrapolated magnetostriction between normal and superconducting states from the zero-field thermal expansion data does not lead to the expected smooth normal state background. These discrepancies may indicate that the magnetostriction in $YBa_2Cu_3O_7$ is not fully described by the model based on the thermodynamics of classical superconductors.

An alternative method to describe the magnetostriction based on 3D XY scaling was investigated. Here, the basic idea was to extrapolate the scaling region (roughly above the vortex melting transition) to much higher fields and thus also to lower temperatures. Surprisingly, at very high fields, where the scaling region is moved to zero Kelvin, this scaling resulted in a smooth background, suggesting that this is the more physical approach. In both approaches, the upper critical field was found to be about 250 Tesla at

$T = 0$. At this time, the implications of these two seemingly contradictory results, giving different normal state backgrounds, are unclear.

Finally, the irreversible magnetostriction (43-50 K), which results from flux pinning of the vortices was investigated. There we found several peaks, which scale with field and temperature. They are detected neither in magnetization nor in specific heat measurements. These peaks have no magnetic field sweep rate dependence, they are present also after reinstalling the sample, so we attribute them to possible transitions between different vortex phases. This can be a sign that the vortex phase diagram is more complicated as expected and that the magnetostriction experiments may be a useful technique to explore it.

Chapter 8

Appendix: Measurements in the irreversible state

Three energy scales describe vortex matter: the defect energy E_{def}, i.e. the energy that the system wins if the vortex is pinned, the thermal energy E_{th} which is the measure of kinetic energy of vortices, and the Coulomb repulsion between vortices E_{rep} which prevents the vortices to approach too closely. In contrast to the first two energies, the third does not depend on temperature. There are several scenarios, depending on the relation between these energies and magnetic field. At high temperatures and low defect density one has $E_{def} < E_{th}$, the defects play a minor role, the vortex repulsion tries to build up an Abrikosov-lattice, resulting in a reversible magnetic state. The decreasing temperature will make the difference between E_{def} and E_{th} smaller, the vortex lattice will be more and more distorted, the magnetic hysteresis will rise. The vortex phase diagram is rather complicated [Bla94], and its study was not the main goal of our work.

After we have described the reversible region of the measurements, the origin of the irreversibilities can be assumed to be the flux pinning by the defects, but several questions are still open, such as what kind of structures exist at low temperatures.

8.1 Critical state

Defects in the bulk of the superconductor reduce the amplitude of superconducting order parameter Ψ, which means that the system can gain energy if the magnetic vortex stays on that position, which prevents vortices to move. Such an energy-favorable defect is called "pinning center", and the process itself "pinning".

If there are pinning centers in the bulk of superconductor, a field change will cause the dilation of the sample, but this effect does not correlate with *thermodynamic* magnetostriction, discussed before. Let us check the length change more carefully. At the beginning, in the Meissner-Ochsenfeld state[1] ($H < H_{c1}$) no vortices are present in the bulk of material. Increasing the applied magnetic field to $H \geq H_{c1}$ will produce some magnetic fluxons, which pass through the surface barrier caused by screening currents (ef-

[1]We are neglecting the demagnetization factor which will decrease the field when the first vortex coming in.

fect of Bean-Livingston [Bea64]) into bulk of the sample. The penetration of the fluxons will hindered, this will cause a tension on the surface and thus compress the sample. As the field increases, the number of vortices in the sample rises, but due to pinning they will be located near the surfaces, making some gradient toward the center of the sample (Fig. 8.1, left). The vortices build a so-called critical state [Bea62]. The shape of this gradient is given by field dependence of the critical current J_c. For sake of simplicity we follow Bean's assumption of a field independent J_c, which gives linear gradient. At field B_1 the vortices occupy a part of the sample near the surface, the gradient of magnetic flux is directed toward the center of the crystal, where no vortices appear. Increasing the applied field to B_2 moves the front of vortices toward the middle of the sample. At some field (B_3) the whole sample will be filled by vortices, but the gradient remains - the increasing field makes it shallow and less steep (B_4). What happens when now the field

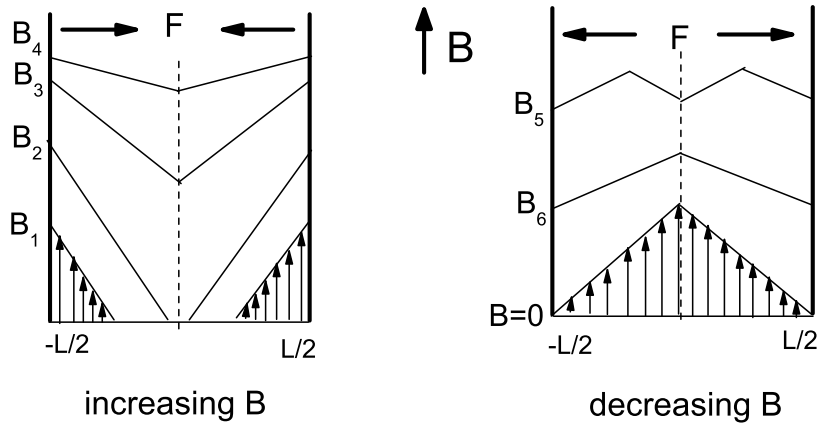

Figure 8.1: The critical state model for an infinite slab of finite thickness L for increasing (*left*) and decreasing (*right*) fields. The arrows show the value and direction of magnetic flux in the sample, lines represent their front.

decreased? The gradient will no longer be linear because the vortices near the surface will escape from the sample first, and now the gradient has opposite sign. At some point the gradient will become linear again (B_6). At zero field this gradient describes the trapped fluxons in the sample. Exactly these trapped fluxons make the magnetic measurements irreversible. The movement of pinned vortices compresses the sample in increasing field, and stretches it in decreasing field.

8.2 How do irreversibilities depend on field sweep rate?

At temperatures not so far from critical we have two different vortex phases depending on field (Fig. 6.6), which are separated by the vortex melting transition. In the low field part there is a solid vortex phase, which is an Abrikosov lattice, distorted by pinning centers which still exist even in samples of very good quality. Here one has a non-dissipative, magnetically irreversible state caused by pinning. After entering the liquid vortex phase

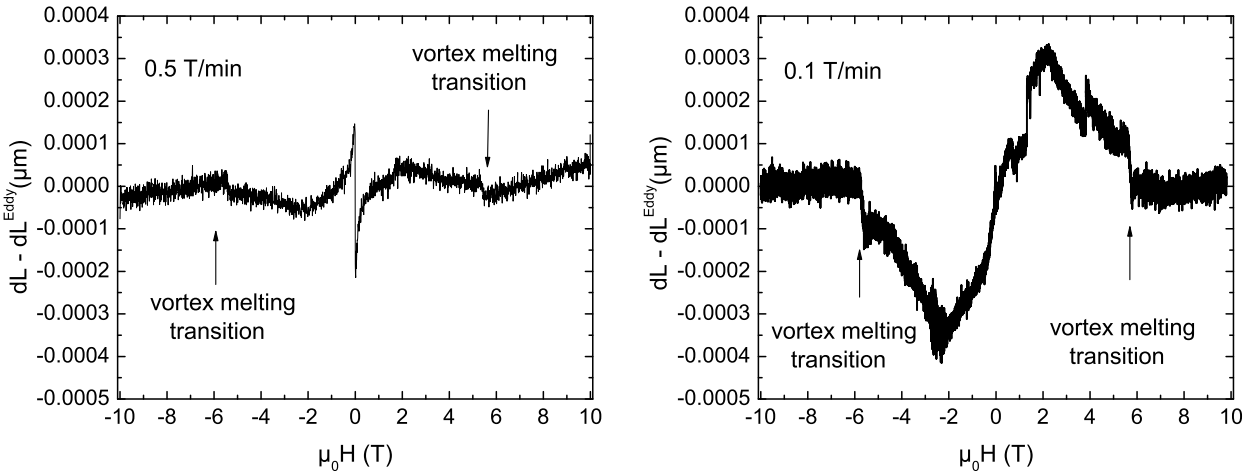

Figure 8.2: Flux pinning induced irreversibilities in magnetostriction. The difference between dL_{irr}, calculated from measurement, and modeled eddy current contribution presented for different magnetic field sweep rates (a-axis, 79 K, SRLW sample). *Left:* 0.5 T/min. *Right:* 0.1 T/min.

upon increasing field across the melting transition, the hysteresis in magnetic measurements completely disappears. The sample is now in a reversible state with dissipative transport properties. In this phase vortices can bend and so better match the pinning centers. These entangled vortices now form a liquid phase.

In order to check the dependence of the irreversibilities on the applied magnetic field sweep rate in both vortex phases, we have done several measurements on SRLW sample. We investigated the a-axis at 79 K, where the smallest possible hysteresis expected (Section 5.5). We took the quantity $(dL \uparrow -dL \downarrow)/2 \equiv dL_{irr}$, as a natural measure of irreversibilities. In the fully reversible state after correction for thermal drift, cell drift and cell background, dL_{irr} is equal to the eddy currents effect, which is reliably modeled from copper and silicon measurements (Subsection 3.4.2). In Fig. 8.2, *left*, a difference between dL_{irr} from measurement and modeled eddy current effect is shown, calculated for 79 K, for a measurement done with 0.5 T/min, which is our usual sweep rate. Easy to see that there are very small deviation from modeled eddy currents, especially for vortex liquid phase ($\mu_0 H > \pm 6$ T). The melting transition is presented with sharp jump. The biggest hysteresis is seen around zero Tesla, which we attribute to the build-up of the critical state.

Let us now check the difference between dL_{irr} and modeled eddy current effect curve, obtained from the 0.1 T/min measurement (Fig. 8.2, *right*). In this case the modeled eddy current effect is smaller due to slower field change, and downscaled 0.5/0.1=5 times, which means that this effect is linearly proportional to the sweep rate. Again, in liquid vortex phase there is almost no difference between calculated from measurement and modeled curves, what we interpret as there are no irreversibilities appear - the sample is in a magnetic reversible state. But in solid vortex phase ($\mu_0 H < \pm 6$ T) there is a big discrepancy appears, which has maxima at $\pm$2T, after the curve is approaching the

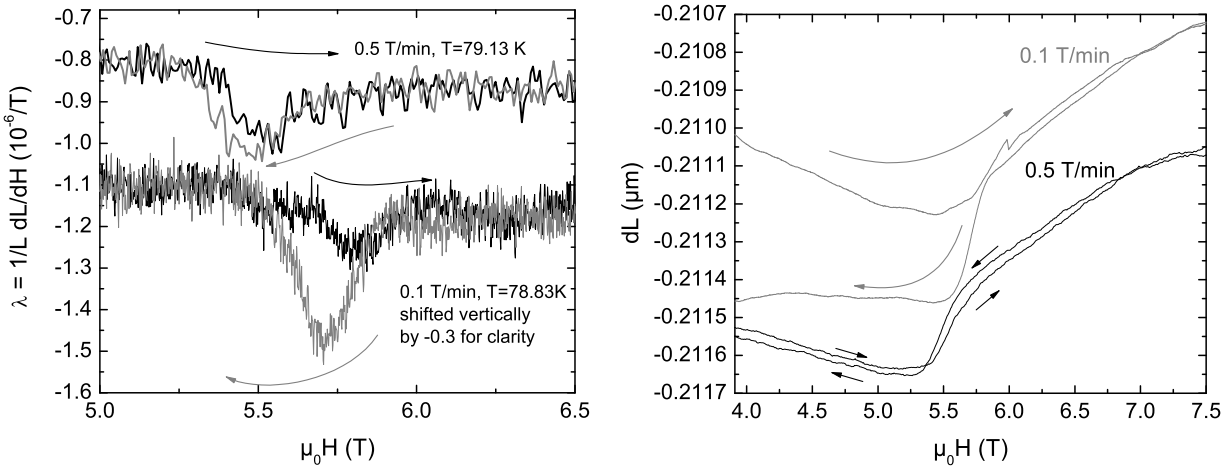

Figure 8.3: *Left:* Irreversibilities in magnetostriction coefficient λ for a-axis, 79 K (0.5 and 0.1 T/min, SRLW sample). *Right:* For sake of clarity a straight line subtracted from magnetostrictive length change $dL(H)$.

modeled one up to phase transition, where the system transform to liquid phase with jump.

Fig. 8.3 presents the magnetostriction coefficients λ for these two measurements. There is an offset for clarity on both graphs. The small discrepancy between peak maxima by different sweep rates comes from temperature difference. Note that due to noisy measurements we had to smooth our data. We took smoothing over 25 and 125 points for 0.5 T/min and 0.1 T/min, respectively, in order to have comparable results. It is important to do a smoothing for the same field "frame" for different sweep rates (in our case 25 points correspond to 0.1 T) in the neighborhood of the melting transition, where a peak in λ appears, because the smoothing makes it shallow. If one compares the increasing and decreasing loops of both measurements, one can see that the peak in the increasing part always appear at higher fields as in the decreasing part. The reason for this is the build-up of the critical state.

In order to present the difference between hystereses we also subtracted a straight line from length changes of these $dL(H)$ curves, our results are shown in Fig. 8.3, right. Again, there is an offset for clarity. There is almost no difference in the vortex liquid state. The small discrepancy between up and down loops (less than 0.5 Å) is attributed to the error of measurement and data treatment.

The difference between magnetic sweep rates can be understood in the following way: The kinetic energy E_{th} of the vortices is proportional to the chosen sweep rate. The bigger the kinetic energy of the vortex, the smaller the probability of pinning, i.e. the high sweep rate "deactivates" the pinning.

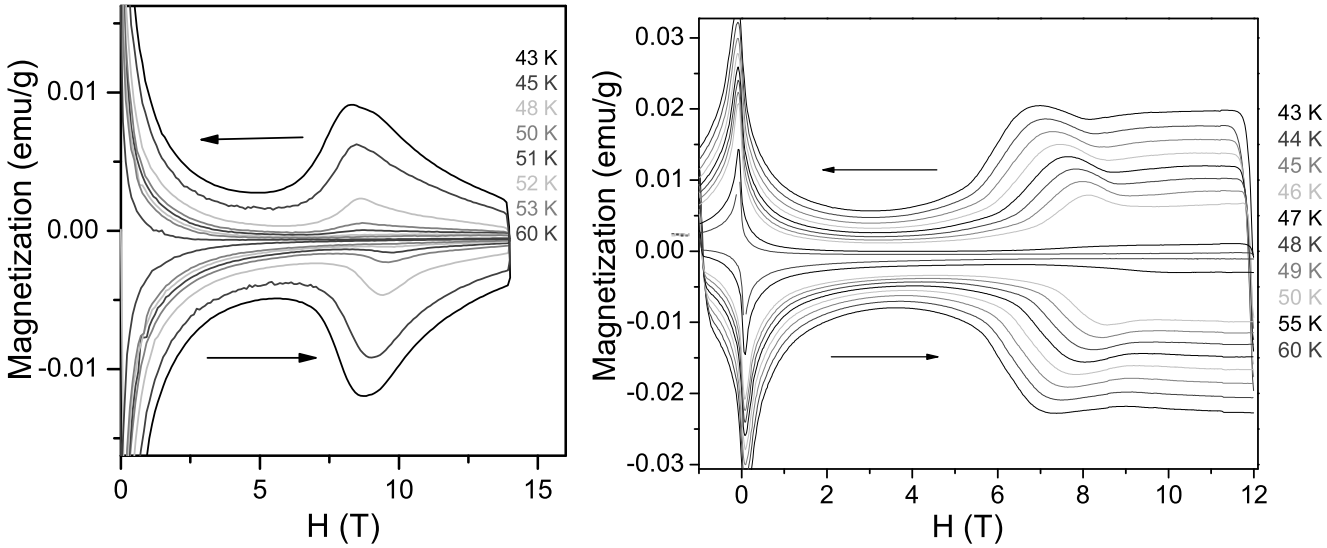

Figure 8.4: Magnetization measurements for SRLW (*left*) and SRL Genf (*right*) samples for different temperatures.

8.3 Comparison of samples

As we saw before, our two samples, SRLW and SRL Genf have almost the same critical temperature T_c (87.5 and 88 K), almost the same oxygen content (δ=0.001 and δ=0.005, respectively) and the same thermodynamical properties, as the jump in thermal expansion at T_c, the pressure dependencies T_c and so on. With small deviations, which can be attributed to measurement error due to different linear sizes of samples, there are two crystals with the same characteristics in reversible region - but what happens in irreversible one?

The first - and quickest - possibility to obtain valuable information on this question was the magnetization measurements for different temperatures. We have done a wide range of experiments at different temperatures, the most surprising part start around 60 K and lower, when the magnetization curves become very different (Fig. 8.4). The SRL Genf sample behaves rather in the expected way, with a "fishtail", where after a "hump" (around 7 T at 43 K) goes almost linear increase of the signal, symmetric in increasing and decreasing field [Nis00]. In contrary, in SRLW crystal, after "hump" (around 8 T at 60 K) the signal decreasing without any sign of similarity with usual "fishtail" behavior. It means that the pinning forces decreased with increasing field - the sample becomes more reversible, which is rather unexpected. It would be the case near H_{c2}, as it was detected in classical dirty-limit type-II superconductors [Cam72], but for our crystal at 50 K the estimated $H_{c2}^{3DXY} \approx 100$ T and $H_{c2}^{TD} \approx 200$ T, that is why this scenario is rather impossible. After this the interest for making magnetostriction measurement at these temperatures only raised due to fact, that the irreversibilities in this kind of experiment play small role, at least, in reversible region. (To compare, see Fig. 4.3.)

In Fig. 8.5 one can see the comparison of the *a*- and *b*-axis measurement for the SRLW sample for temperatures 43, 45 and 48 K. Now the shape of the curves - after all corrections

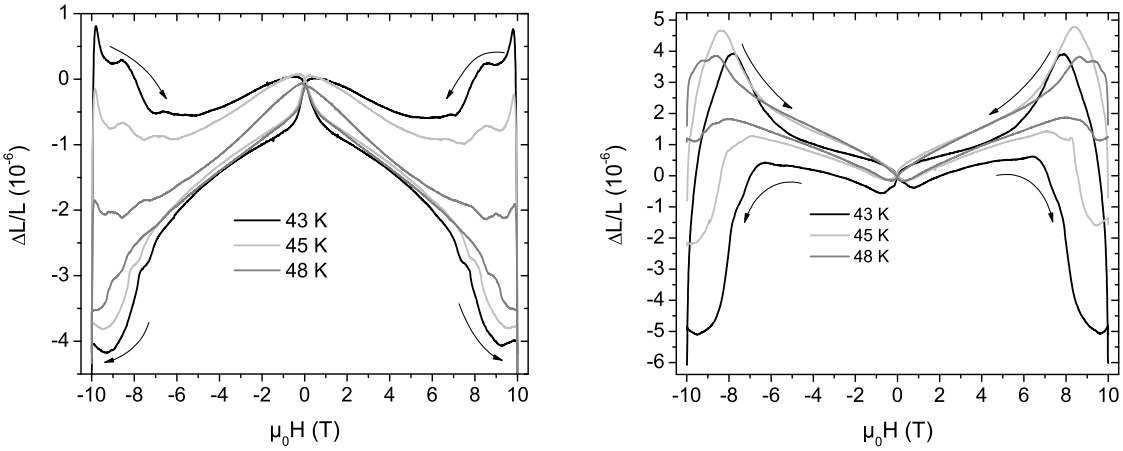

Figure 8.5: Irreversibilities in a- and b-axis measurements (SRLW sample).

- still remains very different. First of all, the "turn" of the curves has the opposite sign - when one measure magnetostriction in the reversible region, the magnetic field loop 0 T $\rightarrow$ +10 T $\rightarrow$ 0 T $\rightarrow$ -10 T $\rightarrow$ 0 T results a clockwise loop of the length change, caused by eddy current effects. Now we have an anticlockwise curve, which means that the irreversibilities have an opposite effect, and also they have much higher value than those due to eddy currents. We also tried to find out the thermodynamical signal by fitting the mean value of increasing and decreasing loop after doing all corrections, as described in Section 5.2, but we could not scale the obtained "thermodynamic" curves with the pressure dependence of the critical temperature, even taking into account the dH_{c0}/dp and dV/dp terms. Apparently, the signal of the thermodynamic part is overwhelmed by flux pinning[2].

All these peculiarities are well reproducible, there are only some discrepancies between very first and second measurements in the same field and same temperature due to the build-up of the critical state after zero field cooling. This effect is similar to the build-up of the remanent magnetization in ferromagnets from virgin state.

Let us compare the a- and b-axis curves for 43 K. After a more or less smooth change of the length up to 6.5 T, peculiarity is found in both axes, then the curve continuing further with a different slope. After another peculiarity around 9 T, the curve goes in the opposite direction up to 10 T, which is the limit of our magnetic field. When the field is decreasing, we have a big jump in the region between 10 and 9.5 T, which is assumed to be associated with the destruction of the critical state. One can see that these peculiarities, "peaks", appear also in the decreasing part of the curve, again around 9 and 6.5 T.

To check these features more carefully, we plot the magnetostriction coefficient λ for these two axis in Fig. 8.6. In the field increasing part the response along the different axes is similar, the peaks and valleys appear at the same fields, which is the sign for the similarity of the driving force of these changes. The peak in increasing field around 8 T

[2]Note, that it is true only for magnetostriction measurements. Thermal expansion experiments in field were found less pinning-dependent and the thermodynamic model from Section 6.6 still well describe them down to zero Kelvin.

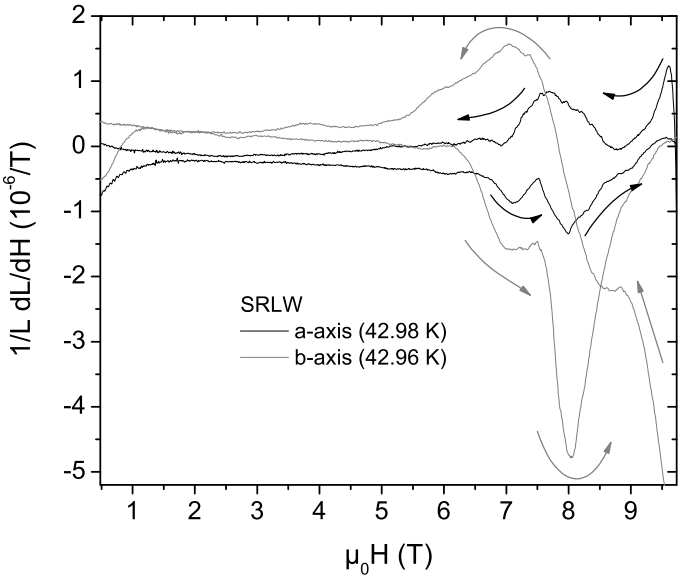

Figure 8.6: Comparison of the peaks at 43 K for the a- and b-axis of the SRLW sample. The arrows show the direction of the change of the applied magnetic field (sweep rate 0.5 T/min).

corresponds to the "hump" have seen in magnetization measurement (Fig. 8.4, left). It is the only one peculiarity in λ seen also in magnetization experiment. In decreasing the field, some differences can be seen, i.e. the destroying of the critical state happens more quickly in a-axis (only 0.5 Tesla in comparison with more than 1 T in b-direction). The peak, seen at 8 T in a-axis, seems to be shifted to 7 T in b-axis. Overall, the effects are much bigger for the b-direction.

The area under the hysteresis loop is a natural measure to describe the value of the irreversibilities. The calculation of the $\int_0^B dLdH$ was done for the loops for positive and for negative fields. Although there is a very small discrepancy between the loops in positive and negative fields for the same measurement - overall, these loops are symmetric. Results of such calculations are presented in Fig. 8.7. There is a rather steep increase of the area, and hence of the pinning forces, with decreasing temperature. As the pinning forces increased more than twice between 48 and 43 K, we did not make any magnetostriction experiment at lower temperature due to fear to destroy the sample, as mentioned in Section 3.6.

We have also done several measurements for the SRL Genf-A sample in order to compare the differences between irreversible properties depending on the sample. The shape of the length change (Fig. 8.8) is more or less similar: in the low field region there is a monotonic increase of the signal and the hysteresis is bigger in the SRL Genf-A sample. We attribute this difference in hysteresis to the slightly lower content of oxygen in the latter crystal where every oxygen vacancy is a pinning center.

At the end of the sweep near 10 T in SRL Genf-A crystal there is an increasing slope in comparison with SRLW, where after the jump at 9 T the slope is negative. This behavior is similar to the results, obtained in magnetization measurements (Fig. 8.4): the SRL

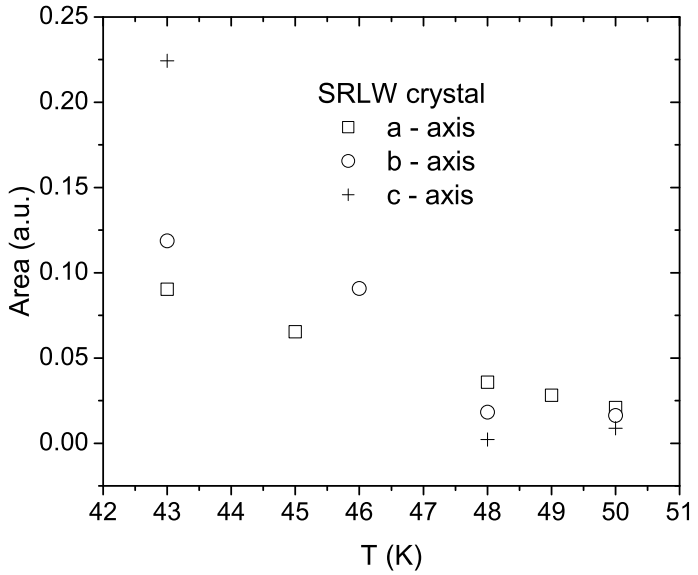

Figure 8.7: Calculated area of the hysteresis loop of the SRLW sample low temperature magnetostriction curves for three axes.

Genf sample has the usual 'fishtail' behavior, while the SRLW tends have less hysteresis with increasing field, which is a sign for decreasing pinning forces at higher field or some kind of thermodynamic transition. The peculiarities in decreasing field are even more similar than in increasing field, the peak, which appears in SRLW around 8.5 T seems to happen at 7 T for SRL Genf sample, which we take as a proof of equality of the underlying mechanism.

Several measurements with different sweep rates of magnetic field for SRL Genf-A in *c*-direction were done in order to check the change of the peaks (Fig. 8.9). Almost no difference between 1 and 0.5 T/min sweep rates is seen, neither the shape of curve nor its area changes. Also, the 0.1 T/min shows no new behavior, only at 8 T in the decreasing part are the peaks a bit smoother. Perhaps, some kind of relaxation appears here. In comparison with the sweep rate dependence in the reversible region (Section 8.2) we attribute the independence of the signal from the sweep rate to the much bigger E_{def} compared to the kinetic energy of vortices at this temperature, even the highest sweep rate does not increase enough the E_{th} to distort the pinning mechanics.

Also we did an experiment on the similarity of the critical state at different fields (Fig. 8.10, *left*). We swept the field with 0.5 T/min in steps, waiting some minutes between them, starting from ten Tesla: 10 T → 9 T → 10 T → 8 T → 9 T → 7 T → 8 T → 6 T → 7 T → 5 T. This quasi-static measurement procedure gives us the possibility to check the critical state affects the length change. One can see, that the height of peaks, caused by destruction and build-up of the critical state, slightly decreased from 10 T to 7 T. At 6 T it is much smaller. Below 6 T the irreversibilities become very small, on the calculated $(dL \uparrow -dL \downarrow)/2$ curve (Fig. 8.10, *left*) this field corresponds to a jump, caused by rapidly increasing pinning forces; between 0 and 6 T this curve (black) nicely follows the modeled eddy current contribution (blue line). In the usual measurement from zero

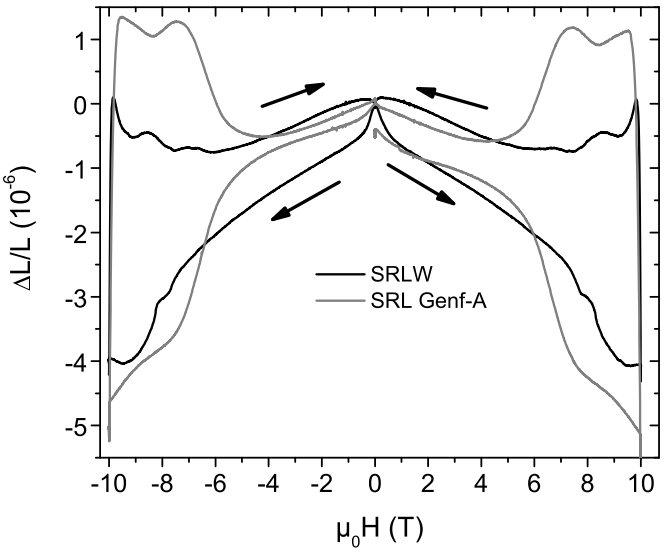

Figure 8.8: Different shape of length change for the SRLW sample ($T = 44.88$ K) and SRL Genf-A ($T = 45.00$ K) crystals. The arrows show the direction of magnetic field sweep.

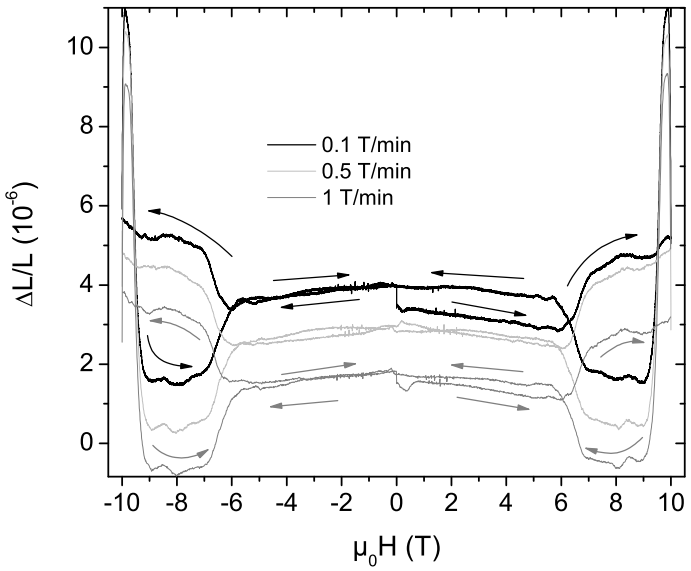

Figure 8.9: Comparison of different sweep rates (0.1, 0.5 and 1 T/min) of magnetic field for the SRL Genf-A sample in c-direction ($T = 44.89$ K). The arrows show the direction of magnetic field sweep. Vertical offset for clarity.

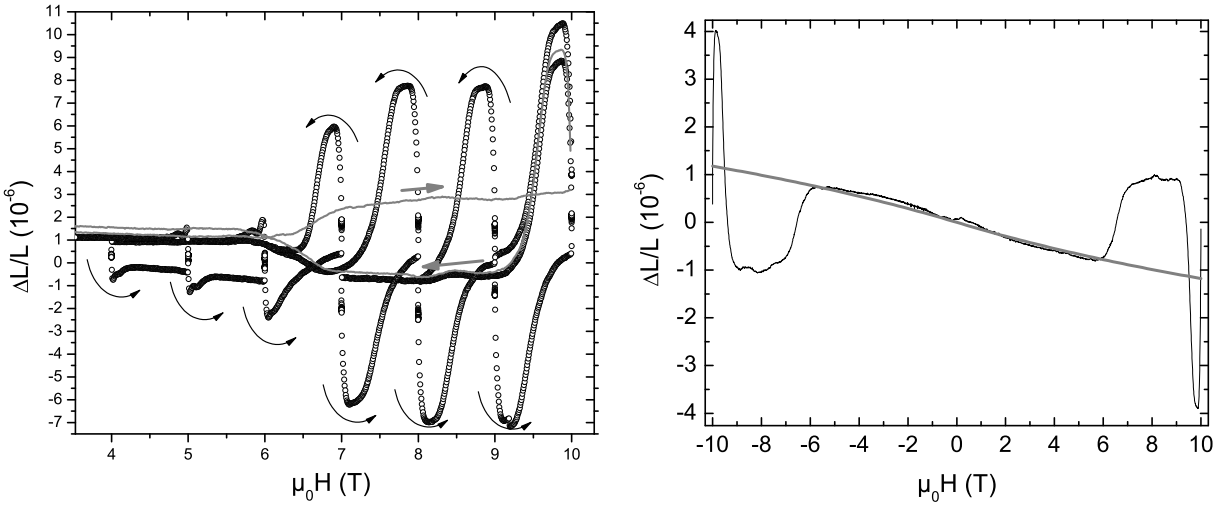

Figure 8.10: Study of the critical state (T = 44.89 K, c-axis, SRL Genf-A sample). *Left:* The magnetostrictive signal for 1 T/min constant sweep rate (gray line) and steps, taken with 0.5 T/min (black circles). The arrows show the direction of magnetic field sweep. *Right:* The calculated irreversibilities (black line) and the modeled eddy currents contribution (gray line) for 1 T/min constant sweep rate measurement. There is almost no critical state caused irreversibilities in magnetic field $\mu_0 H < \pm$ 6 T. See details in text.

to 10 Tesla and back, there is an opening of the hysteresis around 6 T, which suggests that at lower fields only negligible pinning is present. But the measurement loop 6 T $\rightarrow$ 5 T $\rightarrow$ 6 T $\rightarrow$ 4 T $\rightarrow$ 5 T $\rightarrow$ 0 T also shows this build-up and destruction of critical state behavior, but on a smaller scale, which we attribute to the presence of pinning at lower field, which "deactivated" due to high sweep rate. This difference between measurements in constantly swept magnetic field and almost static measurement supports our argument about sweep rate dependent pinning, as discussed in Section 8.2.

8.4 Dependence of the measured signal on the angle to the field

How do pinning forces depend on the angle to the magnetic field? Several measurements with angle of about 5° between the c-axis and applied magnetic field were done, both in the reversible and irreversible state. We examined the b-axis due to the high signal in this direction and more irreversibilities, in comparison to the a-axis. The sample was not re-installed during the adjusting the angle to the magnetic field, which guaranteed the good reproducibility of our results for all two positions. The thermodynamic signal change due to this angle is proportional to the $\sin(5°) \approx 0$. In the reversible region at 79 K (Fig. 8.11, *left*) there is only a minor change in the shape of the magnetostriction coefficient up to 1 T. We attribute this change to the decreasing pinning force in the 5° tilted experiment.

In the irreversible region, pinning plays a vital role in the length change in magnetic

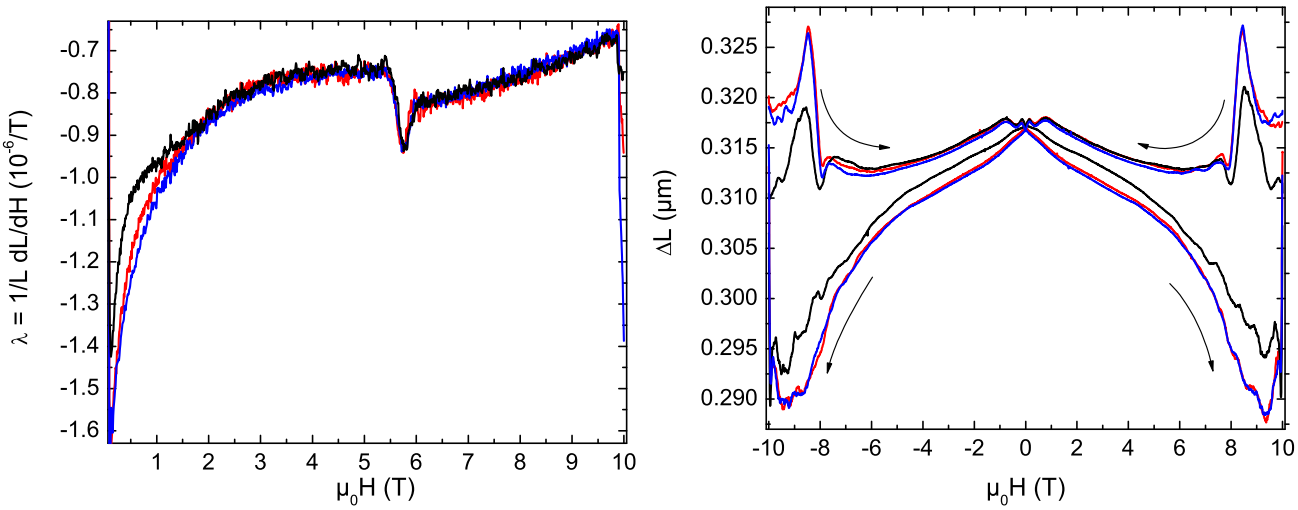

Figure 8.11: Magnetostriction measurements with 5° angle between c-axis and magnetic field (black curves), b-axis, SRLW. The red and blue curves represents the $H||c$ case. *Left:* Magnetostriction coefficient λ, 79 K. *Right:* Absolute length change in magnetic field at 46 K.

field, so the expected effect is much higher then in the aforementioned measurement. Indeed, the area of hysteresis in the tilted position decreased by more than 44% (from a 0.088 to 0.049 a.u., calculated as for Figure 8.7), but the peaks happen at the some fields as for normal measurement.

8.5 Reproducibility with time

As we have samples with small oxygen deficit in a structure that tends to accumulate it from atmosphere with time, we can expect some changes in the behavior of the crystals as time goes by. The gradient of oxygen concentration in the bulk is a reason for the pinning of the magnetic fluxons, the change of this gradient would change the shape of length change curve; also the surface of crystals degrades with time, which again might affect the length change. We took special care of the samples, they always were stored in exsiccator or in the cryostat in vacuum around liquid nitrogen temperature. To check the possible degradation we did a set of measurements on the SRLW sample along the b-direction, where the change of the oxygenization level expected to play the biggest role, 11 months after the end of a previous set. There is no difference between two measurements at 79 K where the thermodynamic magnetostriction response is the biggest. The reversible properties of the sample did not change appreciably over this time. Measurements along the a-axis showed that the reversible properties still remains the same. The change of the critical temperature T_c and the temperature of the melting transition, T_m, which is coupled to T_c [Lor02a], were found to be 45-55 mK smaller in the new measurements suggesting that the oxygen content had slightly increased.

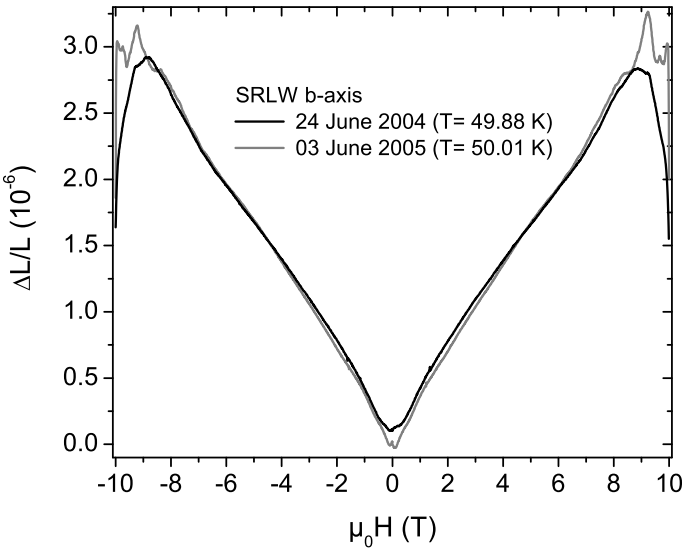

Figure 8.12: Comparison of the averaged signal after 11 months ($T = 50$ K, b-axis, SRLW sample). The parts, where no irreversibilities present ($1 < \mu_0 H < 8$ T), are similar for both measurements. Details in text.

Several measurements at low temperatures ($T \leq 65$ K) were done. There is no remarkable difference between 65 K measurements, which fits well to the assumption of the unchanged reversible properties. The mean signal $dL_{ms}(H) = (dL \uparrow (H) + dL \downarrow (H))/2$ for two 50 K measurements are compared in Fig. 8.12. The first difference comes already at low fields, which we attribute to the possible additional pinning near the degraded surface. There is always some small hysteresis around zero. Then the curves are almost the same, the small discrepancies could be explained by a small difference in temperature of the measurement and another installation of the sample. Around 9 T the sample approaches the irreversible region, where the signal from different measurements does not have the same peculiarities. The results of $T = 43$ K measurements along a- and b-axes plotted in Fig. 8.13. The shape of the length change curve is rather different, the area under the hysteresis loop had increased in 16%, also the pecularities have definitely changed, but the some similarities can also be found, e.g., along the a-axis, with increasing field, around 7 T and 9 T, and decreasing field around 8 T etc.

8.6 Geometrical aspects in magnetostriction

If the pinning-induced (irreversible) magnetostriction overwhelms the thermodynamic (reversible) one, non-uniform stress can be generated in the sample [Joh98, Joh99a, Joh99b]. This stress can produce a convex distortion even of the ideally flat sample, the sample touches the fixators only over the rim, only the signal from this small area of the crystal will be detected, the treatment of this data will be misleading.

Even in very flat samples one expects that the sample touches the fixators only in a few small areas (Fig. 5.12). These spots will change upon taking the sample out and

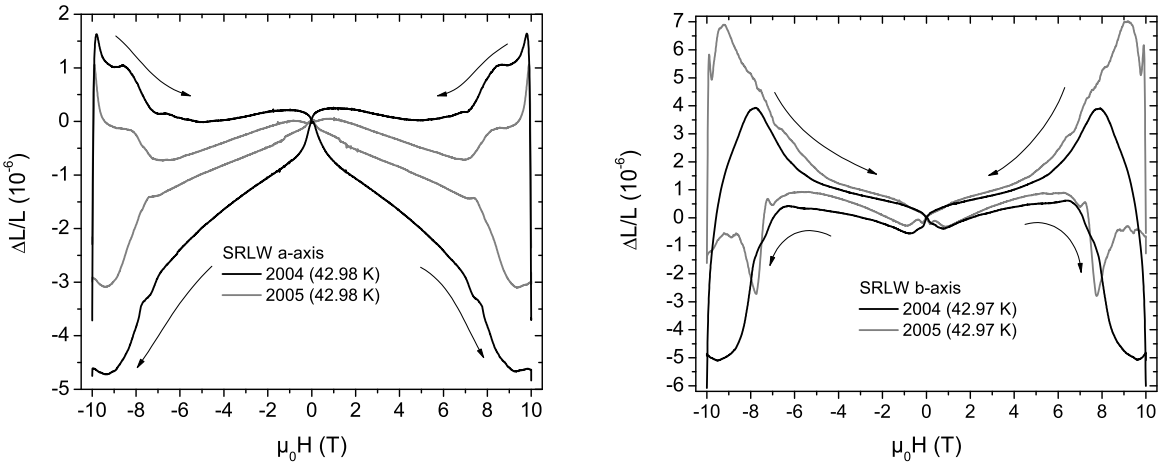

Figure 8.13: Comparison of the 43 K magnetostriciton measurements after 11 months, *a*- and *b*-axis, SRLW sample.

remounting it again. In the reversible state the sample behaves homogeneously, the stress distribution in the interior is uniform - there is no difference in the measured signal between different installations. Near the peak region the critical current density has a maximum, which is directly coupled to the maximum of the pinning force density, which will result a distortion of the sample. Increasing field will move the leading edge of the critical state to the center of the crystal, the movement of this distortion over these spots will be detected as peaks in length change [Schl02].

In our case this issue could not explain the complicated flux induced magnetostriction, while the same peaks where found along different axes (Fig. 8.6) and at different sample installations (Fig. 8.13). However, the importance of this effect has to be concluded in correct data treatment.

8.7 Conclusions

We presented our measurements in the irreversible region, where the pinning forces start to play a role. The magnetization measurements showed a different behavior of the sample in this region, since the SRL Genf crystal shows the "fishtail", while in the SRLW sample the pinning forces above peak region decreased in increasing magnetic field.

Our samples were found to have almost no oxygen variation over 11 months of measurement time, the thermodynamic signal is well reproducible. There are some changes in irreversible magnetostriction, we attribute them to the slight variation of oxygen content over time.

Even at temperatures not so far from T_c it is possible to find flux-induced irreversibilities at slow enough sweep rates. Increasing this sweep rate quickly returns the sample into the reversible state. We attribute this behavior to the increase of the kinetic energy of the vortices with increasing sweep rate of the magnetic field.

There are several fine features in the field-induced length change in the irreversible

region, which were not seen in magnetization measurements. These peaks appear for all three axes at the same positions, in decreasing temperature they shift toward low field in a similar fashion, but do not depend on sweep rate. Due to more or less reproducible character of these pecularities after remounting of the sample, the sample dependent geometric issues only (Subsection 8.6) could not explain the properties of these peaks. We attribute these peaks to the possible transition in vortex matter, i.e. between hexagonal and quadratic vortex lattice.

Bibliography

[Abr57a] A.A. Abrikosov, *Journal of Physics and Chemistry of Solids* **2**, p.199 (1957)

[Abr57b] A.A. Abrikosov, *Soviet Physics - Journal of Experimental and Theoretical Physics* **5**, p.1174 (1957)

[Adk87] C.J. Adkins, *An Introduction to Thermal Physics*, Cambridge University Press (1987)

[And62] K. Andres et al., *IBM Journal* **6**, p.84 (1962)

[Avr01] N. Avraham et al., *Nature* **411**, p.451 (2001)

[Bar57] J. Bardeen, L. N. Cooper, and J. R. Schrieffer, *Physical Review* **108**, p.1175 (1957)

[Bea62] C.P. Bean, *Physical Review Letters* **8**, p.250 (1962)

[Bea64] C.P. Bean and J.D. Livingston, *Physical Review Letters* **12**, p.250 (1964)

[Bed86] J.G. Bednorz and K.A. Mueller, *Zeitschrift für Physik B* **64**, p. 189 (1986)

[Bla94] G. Blatter et al., *Review of Modern Physics* **66**, p.1125 (1994)

[Bra70] G. Brändli, *Physik der kondensierten Materie* **11**, p.93 (1970); G. Brändli, *Physik der kondensierten Materie* **11**, p.111 (1970)

[Bra73] G. Brändli and R. Griessen,*Cryogenics* **13**, p.299 (1973)

[Bra99] B.L. Brandt et al., *Review of Scientific Instruments* **70**, p.104 (1999)

[Bro04] S.P. Brown et al., *Physical Review Letters* **92**, p.067004 (2004)

[Buc04] W. Buckel and R. Kleiner, *Supraleitung*, Wiley-VCH (2004)

[Cam72] A. M. Campbell and J. E. Evetts, *Advances in Physics* **21**, p.327 (1972)

[Car90] J. P. Carbotte, *Review of Modern Physics* **62**, p.1027 (1990)

[Car99] E. W. Carlson et al., *Physical Review Letters* **83**, p.612 (1999)

[Clo62] A.M. Clogston, *Physical Review Letters* **9**, p.266 (1962)

[Ehr33] P. Ehrenfest, *Proc. Amsterdam Acad.* **36**, p.153 (1933)

[Eme95] V.J. Emery and S.A. Kivelson, *Nature* **374**, p.434 (1995)

[Ere99] V.V. Eremenko et al., *Low Temperature Physics* **25**, p.225 (1999)

[Fie05] W.H. Fietz et al., *Superconductors Science and Technology* **18**, p.332 (2005)

[Gao94] L. Gao et al, *Physical Review B* **50**, p.4260 (1991)

[Ges98] V.B. Geshkenbein et al., *Physical Review Letters* **80**, p.5778 (1998)

[Gin50] V.L. Ginzburg and L.D. Landau, *Zhurnal Experimentalnoj i Teoreticheskoj Fiziki* **20**, p.1064 (1950)

[Hao91] Z. Hao, J. R. Clem, M. W. Elfresh et al., *Physical Review B* **43**, p.2844 (1991)

[Hei98] G. Heine and W. Lang, *Cryogenics* **38**, p.377 (1998)

[Hong91] D.J.L. Hong et al., *Journal of the American Ceramic Society* **74**, p.1751 (1991)

[Iku93] H. Ikuta et al., *Physical Review Letters* **70**, p.2166 (1993)

[Joh98] T.H. Johansen, *Physical Review Letters* **80**, p.4757 (1998)

[Joh99a] T.H. Johansen, *Physical Review B* **59**, p.9690 (1999)

[Joh99b] T.H. Johansen, *Physical Review B* **60**, p.11187 (1999)

[Kop70] H. Koppe and J. Willebrand, *Journal of Low Temperature Physics* **2**, p.499 (1970)

[Kro77] F.R. Kroeger and C.A. Swenson, *Journal of Applied Physics* **48**, p.853 (1977)

[Kru97] Ch. Krüger at al., *Journal of Solid State Chemistry* **134**, p.356 (1997)

[Kwo92] W.K. Kwok et al, *Physical Review Letters* **69**, p.3370 (1992)

[Lan91] M. Lang, PhD thesis, University of Darmstadt (1991)

[Lei03] H. Leibrock, PhD thesis, University of Karlsruhe (2003)

[Lia04] W.Y. Liang and J.W. Loram, *Physica C* **404**, p.230 (2004)

[Lor02a] R. Lortz, PhD thesis, University of Karlsruhe (2002)

[Lor02b] R. Lortz et al., *Physical Review Letters* **90**, p.237002 (2002)

[Lor03] R. Lortz et al., *Physical Review Letters* **91**, p.207001 (2003)

[Lor06a] R. Lortz et al., *Physical Review B*, **73**, p.024512 (2006)

[Lor06b] R. Lortz et al., to be published (2006)

[Lyo77] K.G. Lyon et al., *Journal of Applied Physics* **48**, p.243 (1977)

[Mac93] A.P. Mackenzie et al., *Physical Review Letters* **71**, p.1238 (1993)

[Mei91] C. Meingast et al., *Physical Review Letters* **67**, p.1634 (1991)

[Mei96] C. Meingast, A. Junod and E. Walker, *Physica C* **272**, p.106 (1996)

[Mei01] C. Meingast et al., *Physical Review Letters* **86**, p.1606 (2001)

[Nag00] P. Nagel et al., *Physical Review Letters* **85**, p.2376 (2000)

[Nag01] P. Nagel, PhD thesis, University of Karlsruhe (2001)

[Nak98] H. Nakagawa et al., *Journal of Physics: Condensed Matter* **10**, p.11571 (1998)

[Nis00] T. Nishizaki and N.Kobayashi, *Superconductors Science and Technology* **13**, p.1 (2000)

[Obr00] J.L.O'Brien et al., *Physical Review B* **61**, p.1584 (2000)

[Pan87] C. S. Pande et al., *Physical Review B* **36**, p.5669 (1987)

[Par69] A. L. Fetter and P. C. Hohenberg, *Theory of type II superconductors*, in *Superconductivity*, edited by R. D. Parks, Marcel Dekker Inc (1969)

[Pas98] V. Pasler et al., *Physical Review Letters* **81**, p.1094 (1998)

[Pas00] V. Pasler, PhD thesis, University of Karlsruhe (2000)

[Pic97] W.E. Pickett, *Physical Review Letters* **78**, p.1960 (1997)

[Pla02] T. Plackowski et al., *Review of Scientific Instruments* **73**, p.2755 (2002)

[Pog00] V.V. Pogosov, A. L. Rakhmanov and K. I. Kugel, *Journal Experimental and Theoretical Physics* **91**, p.588 (2000)

[Pot83] R. Pott and R. Schefzyk, *Journal of Physics E: Scientific Instruments* **16**, p.444 (1983)

[Roh60] H. Rohrer, *Helvetica Physica Acta* **33**, p.675 (1960)

[Ros99] B. Rosenstein and A. Knigavko, *Physical Review Letters* **83**, p.844 (1999)

[Ryk96] A. I. Rykov et al., in *Advances in Superconductivity VIII*, edited by H. Hayakawa and Y. Enomoto (Springer-Verlag,Tokyo, 1996), p.341

[Saf92] H. Safar et al., *Physical Review Letters* **69**, p.824 (1992)

[Saf94] H. Safar et al., *Physical Review Letters* **72**, p.1272 (1994)

[Sch89] H. Schmid et al., *Physica C* **157**, p.555 (1989)

[Schi97] A. Schilling et al., *Physical Review Letters* **78**, p.4833 (1997)

[Schi00] A. Schilling et al., *Physical Review B* **61**, p.3592 (2000)

[Schl99] S.I. Schlachter et al., *Journal of Low Temperature Physics* **117**, p.922 (1999)

[Schl02] R. Schleser, PhD thesis, University of Konstanz (2002)

[Sho65] D. Shoenberg, *Superconductivity*, Cambridge University Press (1965)

[Tin75] M. Tinkham, *Introduction to the superconductivity*, McGraw-Hill (1975)

[Ull90] S. Ullah and A.T. Dorsey, *Physical Review Letters* **65**, p.2066 (1990)

[Var99] A.A.Varlamov et al., *Advances in Physics* **48**, p.655 (1999)

[Wan01] Y. Wang et al., *Physical Review B* **63**, p.094508 (2001)

[Wei03] K.-P. Weiss, PhD thesis, University of Karlsruhe (2003)

[Wel92] U. Welp. et al., *Physical Review Letters* **69**, p.2130 (1992)

[Wel94] U. Welp. et al., *Journal of Superconductivity* **7**, p.159 (1994)

[Wel96] U. Welp. et al., *Physical Review Letters* **76**, p.4809 (1996)

[Wu87] M.K. Wu et al., *Physical Review Letters* **58**, p.908 (1987)

[Yan97] Kun Yang and S. L. Sondhi, *Physical Review B* **57**, p.8566 (1998)

Danksagung

Zum Schluß will ich mich bei all denen bedanken, die zum Gelingen dieser Arbeit beigetragen haben.

Ich möchte mich bei Herrn Prof. Dr. H. von Löhneysen bedanken, der durch seinen persönlichen Einsatz diese Arbeit möglich gemacht hat und auch für Korrekturen und zahlreichen Verbesserungsvorschläge. Herrn Prof. Dr. E. Dormann danke ich für die Übernahme des Korreferates.

Ich möchte mich bei Dr. Christoph Meingast bedanken, in dessen Arbeitsgruppe ich diese Arbeit anfertigen durfte, und der mir mit vielen konstruktiven Diskussionen und Anregungen sehr geholfen hat. Ohne seine ständigen Bemühungen konnte diese Arbeit nicht so schnell gefertigt werden. Ausserdem möchte ich mich für seine Geduld und seine zahlreichen Verbesserungsvorschläge bedanken.

Herrn Dr. Kai Grube danke ich für die unzählbaren Hinweise und ständige Hilfe sowohl im technischen als auch im wissenschaflichen Bereich. Auch möchte ich mich bei meinem Vorgänger Dr. Rolf Lortz bedanken; mit seiner Hilfe am Anfang meiner Arbeit ist vieles leichter geworden. Nach seinem Umzug zur Universität Genf hat er meine Arbeit mit Ideen und Daten unterstützt.

Für die zahlreichen Magnetisierungsmessungen möchte ich mich bei Herrn Dr. M. Uhlarz und Herrn Dr. H. Küpfer bedanken. I would like to thank Dr. W. Knafo for his help in measurements and for correction of the beta-version of this thesis. Frau Steffi Drobnik danke ich für die Hilfe sowohl im technischen Bereich als auch mit der Rechtschreibung verschiedener römisch-germanischer Sprachen. Auch möchte ich mich bei Frau Sandra Drotziger für ihre Hilfe bei meinem Vortrag in der Universität Karlsruhe bedanken. Beiden wünsche ich gutes Gelingen für ihre Doktorarbeiten.

I would like to thank Dr. A. Rykov and Dr. S. Tajima for preparation of the excellent samples. Without these perfect single crystals this work would have remained a dream.

Bedanken möchte ich mich auch bei allen Mitarbeitern des Instituts für Festkörperphysik, für die angenehme Zusammenarbeit und die freundliche Unterstützung. Ausserdem bedanke ich mich bei Frau E. Maass für Hilfe in administrativen Dingen, Dr. R. Hott für immer kompetente theoretische Hilfe auf dem Gebiet der Supraleitung, Herrn R. Brandt und Herrn B. Burbulla für das immer frische flüssige Helium. Den Mitarbeitern der Werkstätten unter der Leitung von Herrn M. Schlenker und Herrn O. Walz danke ich für die sorgfälige Ausführung der Aufträge, besonders bei Reparaturen unserer Kryostaten.

Herrn Prof. Dr. R. Kleiner von der Universität Tübingen und seiner Arbeitsgruppe möchte ich danken für ihre freundlicher Unterstützung bei meiner Entscheidung, eine Doktorarbeit zu machen.

I would like to send many thanks to Dr. V. V. Bunda from Uzhgorod National University, who strongly influenced my decision to make my diploma thesis about high temperature superconductors and helped me in the very beginning of my scientific career. Also I appreciate the help of the coworkers of the Institute for Solid State Physics and Chemistry, Uzhgorod National University.

Köszönöm az ATOMKI Hideglabor munkatársainak, Dr. Mészáros Sándornak, Dr. Vad Kálmannak és Dr. Hakl Józsefnek, hogy támogatták tanulmányaimat és így nagy mértékben elosegítették eme munka elokészítését. Külön köszönöm a családomnak és barátaimnak, hogy a kezdetektol bíztattak és mindvégig mellettem álltak, a többéves külföldi munkámat könnyebbé téve. Nélkülük nem készült volna el ez a disszertáció.